UNIVERSITY OF THESSALY

POLYTECHNIC SCHOOL

DEPARTMENT OF MECHANICAL & INDUSTRIAL ENGINEERING

M.Sc. Thesis

RAREFIED GAS FLOW BETWEEN MOVING PLATES WITH HEAT TRANSFER

by

SERAFEIM G. MISDANITIS

Mechanical Engineer

University of Thessaly, 2005

A Master's Report Submitted for the Partial Fulfilment of the Requirements for the Post Graduate Degree

Volos, February 2009

Εγκρίθηκε από τα Μέλη της Πενταμελούς Εξεταστικής Επιτροπής:

Πρώτος Εξεταστής (Επιβλέπων)	Δρ. Βαλουγεώργης Δημήτριος Αναπληρωτής Καθηγητής, Τμήμα Μηχανολόγων Μηχανικών Βιομηχανίας, Πανεπιστήμιο Θεσσαλίας
Δεύτερος Εξεταστής	Δρ. Μποντόζογλου Βασίλειος Καθηγητής, Τμήμα Μηχανολόγων Μηχανικών Βιομηχανίας Πανεπιστήμιο Θεσσαλίας.
Τρίτος Εξεταστής	Δρ. Μαθιουλάκης Δημήτριος Αναπληρωτής Καθηγητής, Τμήμα Μηχανολόγων Μηχανικών Εθνικό Μετσόβειο Πολυτεχνείο
Τέταρτος Εξεταστής	Δρ. Πελεκάσης Νικόλαος Αναπληρωτής Καθηγητής, Τμήμα Μηχανολόγων Μηχανικών Βιομηχανίας, Πανεπιστήμιο Θεσσαλίας
Πέμπτος Εξεταστής	Δρ. Λιακόπουλος Αντώνιος Καθηγητής, Τμήμα Πολιτικών Μηχανικών Πανεπιστήμιο Θεσσαλίας.

Acknowledgements

First of all, I would like to express my respect and gratitude to my supervisor Associate Professor Dimitris Valougeorgis. Without his constant support and mentorship, this dissertation would not have been completed. His patience and significant assistance, provided throughout the course of our cooperation, are the two key factors that contributed to the completion of this thesis. I am also grateful to the other members of the Committee, Professors Bontozoglou Vasilios, Mathioulakis Dimitrios, Pelekasis Nikolaos and Liakopoulos Antonios, for their careful reading and valuable suggestions. I would also like to express my gratitude to Dr. Steryios Naris, Dr. Stelios Varoutis and my colleague Sarantis Pantazis for their valuable support and assistance throughout my graduate work. Last, but not least, I would like to thank Christine Mastrogiannidou and Yiannis Moutsinas for their helpful discussions and advice.

Above all, I am grateful to my parents, Georgios and Eleni Misdanitis and my brother Yiannis for their love and support for all these years.

The support provided by the National Program of controlled thermonuclear fusion: Association EURATOM - Hellenic Republic is gratefully acknowledged.

February, 2009

Serafeim G. Misdanitis

RAREFIED GAS FLOW BETWEEN MOVING PLATES WITH HEAT TRANSFER

SERAFEIM G. MISDANITIS

University of Thessaly, Department of Mechanical and Industrial Engineering, 2009

Abstract

The state of a single-species monatomic gas under rarefied conditions remains a fundamental research problem with important applications. The most powerful approaches to handle this type of flows is the Direct Simulation Monte Carlo method and the kinetic theory. Here, we apply the latter one.

In particular, we apply the non-linear Bhatnagar-Gross-Krook (BGK) and Shakhov (S) kinetic model equations, subject to Maxwell diffuse boundary conditions, to solve the one dimensional compressible Couette flow problem coupled with heat transfer. The intermolecular collisions are modeled by the inverse power law model. The computational scheme is based on finite differencing in the physical space and on the discrete velocity method in the molecular velocity space..

The numerical solution is valid in the whole range of the Knudsen number. Its accuracy has been tested in several ways including the recovery of the corresponding analytical solutions at the free molecular and hydrodynamic regimes and the successful comparison with previous results. In all cases excellent agreement has been demonstrated. In addition, a detailed comparison between the simple BGK model with the more sophisticated Shakhov model, clearly indicates that the BGK model remains a reliable choice at least for engineering purposes. Also, the application of the hard sphere and Maxwell molecular models for intermolecular interaction shows that the intermolecular potential model does not significantly influence the flow properties and characteristics.

Results for the bulk quantities of velocity, temperature, vertical and horizontal heat flux, density, pressure and shear stress have been presented in terms of the three

dimensionless parameters describing the flow configuration, namely the rarefaction parameter, the temperature ratio and the relative velocity of the plates.

Several interesting issues related to the combined momentum and heat transfer effects have been studied. It has been found that the velocity slip and the temperature jump are larger at the hot plate compared to the ones at the cold plate. Moreover, the pressure distribution is a function of the spatial variable in the transition regime. This is also due to the rarefaction of the flow. Even more, the flow is characterized by the presence of an horizontal axial heat flux, which increases as the rarefaction of the gas is increased and which is present only when both velocity and temperature gradients exist in the flow. This is a non-equilibrium cross effect and it vanishes at the hydrodynamic limit.

NOMENCLATURE

c_i dimensionless molecular velocity vector

f distribution function

f^0 absolute Maxwellian

f^M the local Maxwellian

g distribution function, dimensionless

H characteristic length

h_i perturbed distribution functions

k Boltzmann constant, $[J/K]$

Kn Knudsen number, dimensionless

m mean molecular mass, $[kg]$

Ma Mach number, dimensionless

n_0 equilibrium number density $[number\ \text{of particles}/m^3]$

P pressure of the gas, $[Pa]$

P_{ij} stress tensor, $[Pa]$

P_0 equilibrium pressure, $[Pa]$

$\boldsymbol{q}$ heat flux vector, dimensionless

$\hat{\boldsymbol{q}}$ heat flux vector, $[W/m^2]$

R gas constant, $[J/(kg\ K)]$

Re Reynolds number, dimensionless

T temperature of the gas, $[K]$

T_0 equilibrium temperature, $[K]$

T_1 temperature of the lower wall, $[K]$

T_2 temperature of the upper wall, $[K]$

u_0 Maxwellian equilibrium velocity $[m/\sec]$

$\boldsymbol{u}$ macroscopic velocity vector, dimensionless

$\hat{\boldsymbol{u}}$ macroscopic velocity vector, $[m/\sec]$

U_0 velocity at the walls, dimensionless

$\hat{U}$ velocity at the walls, $[m/\sec]$

ν collision frequency, $\left[\sec^{-1}\right]$

$\langle \upsilon \rangle$. mean thermal velocity, $[m/\sec]$

υ_0 most probable molecular velocity, $[m/\sec]$

x, y coordinates, dimensionless

$\hat{x}, \hat{y}, \hat{z}$ coordinates, $[m]$

Greek

α accommodation coefficient, dimensionless

β temperature parameter at the walls, dimensionless

γ ratio of specific heats, dimensionless

δ gas rarefaction parameter, dimensionless

θ mean intermolecular spacing, $[m]$

λ_0 mean free path of the mixture molecules, $[m]$

μ viscosity of the gas, $[Pa \sec]$

$\bar{\xi}$ average molecular velocity, $[m/\sec]$

$\boldsymbol{\xi}_i$ molecular velocity vector, $[m/\sec]$

ρ number density, dimensionless

ρ_1 parameter at the lower wall needed for the evaluation of the boundary conditions

ρ_2 parameter at the upper wall needed for the evaluation of the boundary conditions

σ molecular diameter, $[m]$

σ_D diffusion slip coefficient, dimensionless

σ_{ij} stress tensor, dimensionless

$\hat{\sigma}_{ij}$ stress tensor, $\left[Pa = N / m^2 \right]$

σ_P viscous slip coefficient, dimensionless

σ_T thermal slip coefficient, dimensionless

τ temperature of the gas, dimensionless

ω intermolecular model, dimensionless

Dedicated to my parents

Georgios and Eleni Misdanitis

Contents

1

Introduction

1.1 Introduction

The ability of mankind to develop and manufacture tools to deal with daily needs was something that characterized the early stages of evolution. This has led people to develop a "self-centered" theory regarding the size of these devices, within a range of two orders of magnitude bigger or smaller than its size (Figure 1.1). However, there were many efforts for the construction of buildings and equipment outside this range. A typical example is, in the one hand, the competition for the construction of the highest building and, on the other hand, the construction of small-sized mechanisms by the watchmakers. The need to reduce the size, weight and energy savings coupled with increased needs for credibility and proper functioning of conventional-sized machines led humans shift to the microcosm. The invention of the microscope brought this need even closer to reality. Smaller and smaller in size devices continued to be manufactured reaching to a peak with the construction of integrated circuits (10nm).

Only few people envisioned from the very beginning the evolution of technology in such small dimensions [Feynman, 1977]. Yet, today's technology comes to confirm them. Micro-and nano-devices with dimensions less than 100mm are now a reality. This evolution of technology with applications in micro fluid-dynamics [Gad-el Hak, 2002] in vacuum devices [Umrath, 1998; Reese & Gallis, 2003], in micro- (MEMS) and nano-electro-mechanical systems (NEMS) [Reese & Gallis, 2003; Ho & Tai, 1998] and in devices used at high altitudes and in space technology [Ho & Tai, 1998; Karniadakis & Beskok, 2000] (> 50 Km) raised the need for better and more detailed understanding of the phenomena that are developed in such conditions.

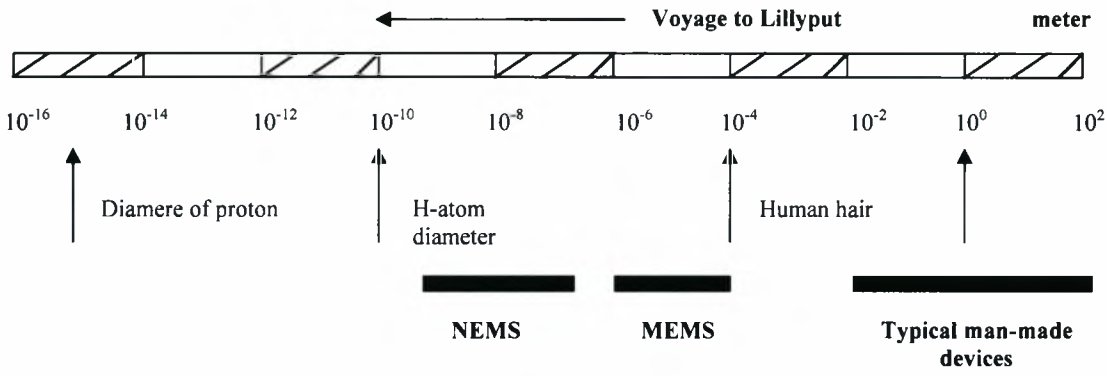

Figure 1.1: *Travelling to the microcosm [Gad-el Hak, 2002].*

The development of such devices has opened up an entirely new field of research where the behaviour of flows far from equilibrium conditions is very important. The traditional methods of dealing respective problems (Euler equations and Navier-Stokes [White, 2002]) do not apply, since the theory of continuous medium collapses.

To deal with these cases, several approaches are used depending on the application under study. The different methodologies for flow modelling are shown in Figure 1.2. To deal with the new phenomena occurring within the flows, slip boundary conditions [Karniadakis & Beskok, 2000] of first or higher order are applied to the already known Euler and Navier-Stokes equations, or new advanced equations are developed such as Burnett, super Burnett and others. However, the results in many cases are not satisfactory leading to the need of modelling the flow in molecular level, where the approaches are either deterministic, through the application of molecular dynamics (MD), or probabilistic, through the implementation of the Boltzmann equation or the DSMC method. Given the vast computational effort required by the MD method, the statistical study and the development and application of relative methodologies have attracted a lot of attention.

The probabilistic approach is based on a statistical study of the behaviour of particles that consist the fluid and the macroscopic properties arise as secondary quantities. Part of this effort focuses on determining the distribution function, which obeys the well-known Boltzmann equation and through which all the macroscopic

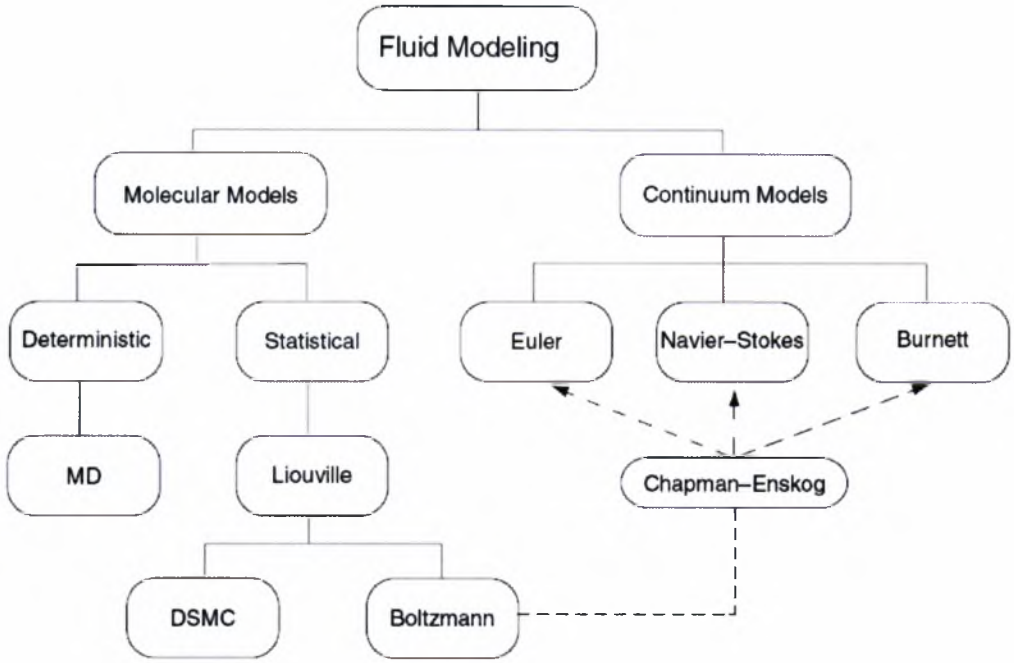

Figure 1.2: *Molecular and continuum flow models [Gad-el Hak, 2002].*

quantities can be evaluated [Boltzmann, 1995; Ferziger & Kaper, 1972; Huang, 1987; Cercignani, 1975; 1988; 1969; Chapman & Cowling, 1952; Kogan, 1969]. The Boltzmann equation is based on the kinetic theory of gases used to describe transport phenomena, with emphasis on dilute gas systems. Like all methods, so the statistical approach through the Boltzmann equation is characterized by its respective advantages and disadvantages. However, the solution of this equation, though painful, is widely used today and leads to a good approach for a larger number of problems with satisfactory results.

1.2 Knudsen number and gas rarefaction

Rarefied gas flows are mainly found in small devices and low-pressure applications. The characteristic number that determines the degree of rarefaction and the area in which continuum model equations are valid is the number Knudsen (Kn), which is defined by the relationship [Karniadakis & Beskok, 2000]

$$Kn = \frac{\lambda}{L} = \sqrt{\frac{\gamma\pi}{2}}\frac{Ma}{Re} \tag{1.1}$$

where L is a characteristic dimension of the problem, λ the mean free path of the particles, γ the ratio of specific heats, Ma the Mach number and Re the Reynolds number. The mean free path is defined as the average distance travelled by molecules between collisions and can be expressed mathematically by multiplying the average molecular velocity $\bar{\xi}$ to the mean free time, i.e.

$$\lambda = \bar{\xi}\tau . \tag{1.2}$$

The average molecular velocity is given by [Karniadakis & Beskok, 2000]

$$\bar{\xi} = \sqrt{\frac{3k_B T}{m}} = \sqrt{3RT} . \tag{1.3}$$

where k_B is the Boltzmann constant $\left(k_B = 1.3805 \times 10^{-23} J/K\right)$, m the molecular mass and R the specific gas constant. If ν is the collision frequency, which is determined by dividing the number of collisions N that occur in time unit to the total number of molecules n in a unit volume, then the mean free time between collisions equals

$$\tau = \frac{1}{\nu} = \frac{n}{\mathrm{N}} . \tag{1.4}$$

The mean free path cannot be measured directly and may be calculated on the basis of measured macroscopic quantities in accordance to the relationship [Sharipov & Seleznev, 1998]

$$\lambda = \frac{\sqrt{\pi}\mu}{2P}\upsilon_0 \tag{1.5}$$

where P is the local pressure, μ the dynamic viscosity at local temperature T, and

$$\upsilon_0 = \sqrt{\frac{2k_B T}{m}} = \sqrt{2RT} . \tag{1.6}$$

the most probable molecular velocity. The quantity υ_0 is often used to non-dimensionalise the molecular velocity. Another molecular velocity of some interest is the mean thermal velocity $\langle \upsilon \rangle = \frac{2}{\sqrt{\pi}}\upsilon_0$.

Also, the gas rarefaction parameter δ is frequently used, which is linked to the Knudsen number as follows [Sharipov & Seleznev, 1998]:

$$\delta \equiv \frac{\sqrt{\pi}}{2}\frac{L}{\lambda} = \frac{\sqrt{\pi}}{2}\frac{1}{Kn} = \frac{LP}{\mu}\sqrt{\frac{m}{2k_BT}} = \frac{LP}{\mu\upsilon_0} \tag{1.7}$$

The *Kn* number (or rarefaction parameter δ) is characteristic for any problem and its value characterizes the flow of gas. The local value of the Knudsen number in a particular flow determines the degree of rarefaction and the degree of validity of the continuum model. The different Knudsen number regimes are determined empirically and they are therefore only approximate for a particular flow geometry and they have been specified in the pioneering experiments conducted by Knudsen in 1909. In the limit of zero Knudsen number, the mean free path is zero, i.e. for $P \neq 0$ the viscosity is zero and then the Navier–Stokes equations reduce to the inviscid Euler equations. The equivalent molecular viewpoint is described by the local Maxwellian distribution. As *Kn* increases, rarefaction effects become more important, and eventually the Navier–Stokes equations break down. The different Knudsen number regimes are depicted in Figure 1.3, and can be summarized as follows:

i. $Kn = 0, (\delta \to \infty)$: **Hydrodynamic Limit**, in which the Euler equations are valid.

ii. $Kn < 10^{-3}$ $(\delta > 10^3)$: **Hydrodynamic Regime**, in which the Navier- Stokes equations coupled with no-slip boundary conditions are valid.

iii. $10^{-3} \le Kn < 10^{-1} (10^3 \le \delta \le 10)$: **Slip regime**, in which the Navier-Stokes equations coupled with no-slip boundary conditions are valid.

iv. $10^{-1} \le Kn \le 10 (10 \le \delta \le 10^{-1})$: **Transition regime**, in which the Boltzmann equation is valid. It is noted that the validity of the Boltzmann equation is extended well outside the transition regime.

v. $Kn > 10 (\delta < 10^{-1})$: **Free molecular regime**, in which there are no collisions between the molecules.

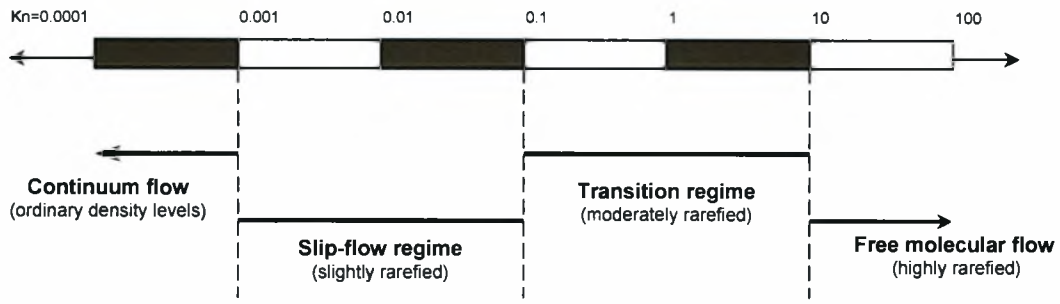

Figure 1.3: *Knudsen number regimes [Gad-el Hak, 2002].*

The logarithmic chart shown in Figure 1.4 [Bird, 1994] presents the limits of various theories. On the horizontal axis the number density n/n_o (or the mass density ρ/ρ_o) varies from 10^{-10} up to 10^2, while on the vertical axis the characteristic dimension L of the problem varies from 10^{-8} (m) up to 10^2. The reference densities ρ_o and n_o are computed at standard conditions. Additional quantities that are used are the Knudsen number (Kn), the average spacing θ between molecules and the average molecular diameter σ. In the context of a double logarithmic plot of L versus ρ/ρ_o the three limits may be defined by straight lines, as shown in Figure 1.4. The dilute gas assumption requires that $\theta/\sigma >> 1$ and $\theta/\sigma = 7$ has been chosen as the limit. Since both θ and σ are independent of L, the line is vertical and a scale for θ/σ has been set along the upper edge of Figure 1.4. The validity of the continuum approach has been identified with the validity of the Navier-Stokes equations. This requires that the Knudsen number should be small compared with unity, and Kn=0.1 has been chosen as the limit. So, the dilute gas approximation is valid for $\theta/\sigma < 7$, the continuum approach for $Kn < 0.1$ and the neglect of statistical fluctuations for $L/\theta > 100$.

The lines describing the three limits very nearly intersect at a single point. This result would not be substantially altered by any reasonable changes in the typical dimensions and the criteria that define the limits. As density or characteristic dimension is reduced in a dilute gas, the Navier–Stokes model breaks down before the level of statistical fluctuations becomes significant. In a dense gas, on the other hand, significant fluctuations may be present even when the Navier–Stokes model is still valid. For

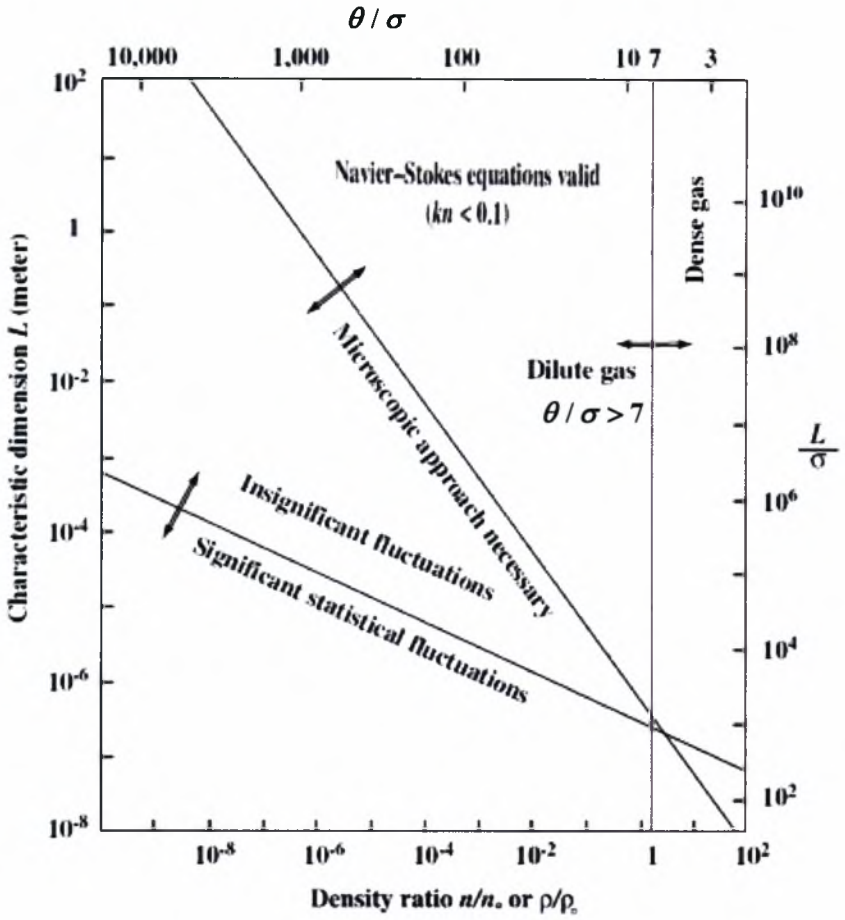

Figure 1.4: *Effective limits of different flow models [Bird, 1994].*

example, the theory of Brownian motion is partially based on these equations although the phenomenon is, itself, a manifestation of significant statistical fluctuations. It is noted that kinetic theory may provide a unified solution in the whole range of the *Kn* number.

1.3 Scope of the present work

In the present work we investigate some transport phenomena far from equilibrium. We apply classical kinetic model equations to investigate the rarefied gas flow between two parallel plates maintained at different temperatures and moving with different velocities.

Our objective is to determine the macroscopic distributions in the whole range of the Knudsen number in terms of arbitrary large relative velocity and the temperature ratio of the two plates. This is accomplished by using non-linear kinetic equations. In particular, the flow is modeled by implementing the nonlinear BGK [Bhatnagar, Gross, Krook, 1945; Welander, 1954] and Shakhov [Shakhov, 1947; Sharipov & Seleznev, 1998] kinetic equations coupled to Maxwell diffuse boundary conditions [Maxwell, 1879]. It is pointed out that this is one of the first efforts of our group work with non equilibrium transport phenomena to implement non-linear kinetic equations. Through the present work, the developed numerical scheme is validated by solving this relatively simple flow configuration, investigating at the same time some very interesting phenomena which appear as the Knudsen number is increased. The contents of this thesis are as follows:

In the 2nd Chapter a literature review of the kinetic theory and kinetic models developed to approximate the flows is presented. Also, available research work solving the specific problem under consideration is discussed. Chapter 3 includes the problem description and the corresponding kinetic equations based on the implemented BGK and Shakhov models. In Chapter 4 the implementation of various projection procedures to reduce the computational effort is described. The numerical scheme is described in Chapter 5. Analytical results for both the free molecular and the hydrodynamic regimes are provided in Chapter 6. Also, basic conservation principles and flow properties valid for the whole range of the Knudsen number are derived. Chapter 7 provides extensive computational results. In particular, comparisons between the two kinetic models, the corresponding analytical solutions for both the free molecular and the hydrodynamic regimes and the intermolecular potential for the whole range of the Knudsen number are presented. Finally, in Chapter 8, a brief outline of the present work, followed by some concluding remarks and the description of the future work is presented.

2

Literature Review

2.1 Basic concepts on kinetic theory

One of the most important theories which counts more than a century of life, is the kinetic theory of Maxwell and Boltzmann related to dilute gases. A particle at the time t is characterized by its position vector $\boldsymbol{r}=(x,y,z)$ and its molecular velocity vector $\boldsymbol{\xi}=(\xi_x,\xi_y,\xi_z)$, $\boldsymbol{\xi}\in(-\infty\ ,\ \infty)$. The basic unknown is the function f, which is called distribution function of the particles and it is defined so that the quantity $f(\boldsymbol{r},\boldsymbol{\xi},t)d^3\boldsymbol{r}d^3\boldsymbol{\xi}$ is the expected number of particles contained in the volume $d^3\boldsymbol{r}$ around $\boldsymbol{r}$ with molecular velocity in $d^3\boldsymbol{\xi}$ around $\boldsymbol{\xi}$ at the time t. The distribution function f satisfies the Boltzmann transport equation

$$\frac{\partial f}{\partial t}+\boldsymbol{\xi}\cdot\frac{\partial f}{\partial \boldsymbol{r}}=J(f,f^*). \tag{2.1}$$

The left hand side of Eq. (2.1), represents the material derivative, is linear and it is treated with techniques from partial differential equations. The right-hand side of Eq. (2.1) represents the balance between molecules «lost» or «gained» during the binary molecular collisions. The term $J(f,f^*)$ is the nonlinear collision integral that describes the net effect of populating and depopulating particles through collisions on the distribution function. The collision integral is the source of difficulty in obtaining analytical or even numerical solutions of the Boltzmann equation. This term depends on the model of intermolecular potential, which is the way the particles interact during the collisions.

Equation (2.1) is therefore a non-linear integro-differential equation and describes the evolution of the distribution function in a state far from equilibrium thermodynamics. In the case where we have absolute thermodynamic equilibrium, the distribution function

takes the form of the famous Maxwell equilibrium distribution, which is the solution of Eq. (2.1), without changes in time and space. The absolute Maxwellian is given by the relationship

$$f^0 = n_0 \left(\frac{m}{2\pi k_B T_0} \right)^{3/2} \exp\left(-\frac{m(\xi - u_0)^2}{2k_B T_0} \right) \tag{2.2}$$

where n_0 the number density, T_0 the temperature and u_0 the macroscopic velocity vector, which is usually zero since we refer to absolute thermodynamic equilibrium conditions.

The macroscopic properties of the gas, with practical interest, calculated from the moments of distribution function are:

Number density

$$n(\mathbf{r},t) = \int f(\mathbf{r},\xi,t) d^3\xi , \tag{2.3}$$

Velocity

$$\boldsymbol{u}(\boldsymbol{r},t) = \frac{1}{n(\boldsymbol{r},t)} \int \xi f(\boldsymbol{r},\xi,t) d^3\xi \tag{2.4}$$

Stress tensor

$$P_{ij}(\boldsymbol{r},t) = m \int (\xi_i - \boldsymbol{u}_i) \cdot (\xi_j - \boldsymbol{u}_j) f(\boldsymbol{r},\xi,t) d^3\xi , \tag{2.5}$$

Pressure

$$P(\boldsymbol{r},t) = \frac{m}{3} \int (\xi - \boldsymbol{u})^2 f(\boldsymbol{r},\xi,t) d^3\xi , \tag{2.6}$$

Temperature

$$T(\boldsymbol{r}) = \frac{1}{3n(\boldsymbol{r},t)k} \int (\xi - \boldsymbol{u})^2 f(\boldsymbol{r},\xi,t) d^3\xi \tag{2.7}$$

Heat flux

$$\boldsymbol{q}(\boldsymbol{r}) = \frac{m}{2} \iiint (\xi - \boldsymbol{u})^2 (\xi - \boldsymbol{u}) f(\boldsymbol{r},\xi,t) d^3\xi , \tag{2.8}$$

Here, $k = 1.3806503 \times 10^{-23}\ m^2 kg\ s^{-2}\ K^{-1}$ is the Boltzmann constant and $R = k/m$ is the gas constant with molecular mass m. The mass density of the gas is computed via the equation $\varrho = mn$, while density, pressure and temperature are related by the equation $P = nkT$.

To simplify the solution of the Boltzmann equation, the collision term is approximated by introducing simplified collision models.

2.2 The BGK and Shakhov models

One of the first models presented was the BGK model (Bhatnagar-Gross-Krook) [Bhatnagar, Gross, Krook, 1945; Welander, 1954], described by

$$\frac{\partial f}{\partial t}+\boldsymbol{\xi}\cdot\frac{\partial f}{\partial \boldsymbol{r}}=v\left\{f^{M}\left(n,T,\boldsymbol{u}\right)-f\left(t,\boldsymbol{r},\boldsymbol{\xi}\right)\right\} \tag{2.9}$$

where f the distribution function, f^{M} the local Maxwellian and v the collision frequency. The local equilibrium distribution f^{M}, is expressed as

$$f^{M}=n\left(\frac{m}{2\pi k_{B}T}\right)^{3/2}\exp\left(-\frac{m(\boldsymbol{\xi}-\boldsymbol{u})^{2}}{2k_{B}T}\right). \tag{2.10}$$

This model constitutes the simplest possible approach of the collision term, but also the basis on which other more advanced subsequent models have been developed. It is used extensively for a single component flow until today, yielding satisfactory results in the case of isothermal flows.

An improved version, was presented in 1974 by Shakhov, known as the S model [Shakhov, 1947; Sharipov & Seleznev, 1998]. The S model is described by the equation

$$\frac{\partial f}{\partial t}+\boldsymbol{\xi}\cdot\frac{\partial f}{\partial \boldsymbol{r}}=\frac{P}{\mu}\left\{f_{loc}^{eq}\left[1+\frac{2m}{15n(k_{B}T)^{2}}\boldsymbol{q}\bullet(\boldsymbol{\xi}-\boldsymbol{u})\left(\frac{m(\boldsymbol{\xi}-\boldsymbol{u})^{2}}{2k_{B}T}-\frac{5}{2}\right)\right]-f\right\}. \tag{2.11}$$

The diversification of the BGK model presented in the distribution equilibrium which now includes the heat flux terms, making possible the export of results with sufficient precision for non-isothermal flows. The Shakhov model is capable to estimate simultaneously both the transport coefficients of viscosity and thermal conductivity correctly, yielding the correct Prandtl number of 2/3, while the BGK yields the wrong Prandtl number of 1.

2.3 Boundary conditions

In determining the boundaries, our main concern is the correlation between the distribution function of particles emitted from the wall (f^+) and that of particles arriving to the wall (f^-). In general, this behaviour can be expressed mathematically as [Cercignani, 1988]

$$f^+ = -\int \frac{\xi' \cdot \boldsymbol{n}}{\xi \cdot \boldsymbol{n}} W(\xi, \xi') f^-(\xi') d^3\xi'. \tag{2.12}$$

where $W(\xi,\xi')$ is the so called scattering kernel describing the type of interaction. In most cases we assume that the particles departing from the wall may be described by a Maxwellian based on the wall temperature [Cercignani, 1975]. This hypothesis was first described by Maxwell and referred to as diffuse scattering boundary condition (Figure 2.1) [Cercignani, 1975]. However, the results are not always consistent with the corresponding experimental. To deal with this phenomenon, it was considered necessary to amend the diffusion boundary conditions. Under this amendment, a percentage α of particles, reflects on the wall and continues with the same and symmetrical speed in a plane perpendicular to the wall. The coefficient α is called tangential momentum accommodation coefficient and represents the percentage of particles that are absorbed by the wall and reemitted according to the wall properties, while $1-\alpha$ is the percentage of particles reflected from the wall without interacting with it. This factor is a characteristic feature of the gas-wall interaction and is obtained from experimental data [Cercignani, 1975]. Then the kernel, which describes the diffuse-specular reflection, takes the form

$$W(\xi' \to \xi) = (1-\alpha)\delta(\xi' - \xi + 2\boldsymbol{n}[\xi' \cdot \boldsymbol{n}]) + \alpha \frac{m^2 \xi' \cdot \boldsymbol{n}}{2\pi (k_B T_w)^2} e^{-\frac{m\xi^2}{2k_B T_w}}. \tag{2.13}$$

It was also described by Maxwell [Maxwell, 1879] and is known as specular-diffuse reflection (Figure 2.1).

The Maxwell boundary conditions are rather simple and commonly used, while the computed results are consistent in most cases with the corresponding experimental. Nevertheless, the Maxwell gas-wall interaction is not complete from physical aspect of view and there are problems where significant errors have been observed. In such cases

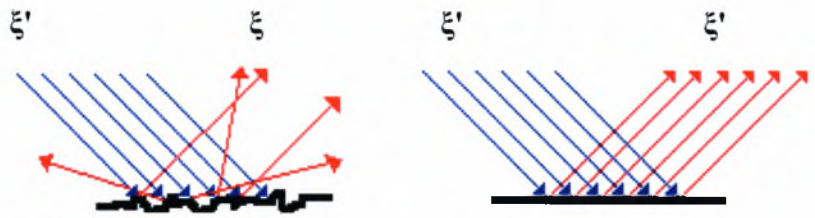

Figure 2.1: *Diffuse scattering (left) and specular diffuse (right).*

more complex boundary conditions are used, (Cercignani-Lampis [Sharipov, 2002; 2003]), which offer better accuracy.

2.4 Nonlinear Couette flow with heat transfer

The gas flow between parallel plates maintained in relative motion and at different temperatures may be considered as a prototype problem for more complicated flow patterns with many applications in the MEMS industry. When the flow is in the slip regime then the problem may be solved based on the Navier-Stokes-Fourier equations subject to slip and jump boundary conditions [Karniadakis & Beskok, 2002]. However, when the flow is far form equilibrium, well inside the transition regime, which is the case in several microfluidic devices and systems, then this approach is not adequate to provide reliable results. In these cases the problem may be tackled in a very efficient manner based on kinetic theory [Cercignani, 1988].

In kinetic theory of gases this specific problem, namely the nonlinear Couette flow with heat transfer, has been examined by several researchers [Ziering, 1960; Huang & Hartley, 1968; Srivastava, 1971]. In addition, exact analysis of the this problem described by the nonlinear BGK model equation has been provided [Brey et al., 1987; Santos et al.,1989; Kim et al., 1989]. The imposed boundary conditions produce combined momentum and heat transport phenomena and their investigation provides some insight into the behavior of more complex non-equilibrium systems. One of the most interesting issues is the presence of a heat flux parallel to the plates, induced by the shear flow [Tij & Santos, 1995]. This is a cross effect, which is absent in the hydrodynamic limit. In most cases the implemented techniques include the moment-hierarchy method applied to the

Boltzmann equation or to kinetic model equations or alternatively the DSMC method [Tij & Santos, 1995; Garzo & Haro, 1994; Reitebuch & Weiss, 1999; Marques et al., 2000; Gallis et al., 2006].

Although a lot of work has been performed on this problem still there are some open issues of some interest. In the present work we investigate and comment on some of them by providing an accurate, detailed and complete numerical solution. In addition, by comparing with existing results we validate and benchmark our fresh-built non-linear kinetic code.

3

Problem description and formulation

3.1 Flow configuration

A monoatomic gas is confined between two infinite parallel plates at $\hat{y} = \mp H/2$, which are moving with constant velocities $\mp\hat{U}_0$, while they are maintained at constant temperatures T_1 and T_2 respectively. Then, the temperature ratio is defined as $T_1/T_2 = (1+\beta)/(1-\beta)$, where $\beta = \Delta T/2T_0$, $\Delta T = T_1 - T_0 > 0$ with $T_0 = (T_1+T_2)/2$ denoting a reference temperature (Figure 3.1). The hot plate, denoted by 1, is in the bottom and it is moving to the left, while the cold plate, denoted by 2, is in the top and it is moving to the right (Figure 3.1). The flow domain is considered as fully developed in the $\hat{x}$ direction and unbounded in the $\hat{z}$ direction. The only component of the macroscopic velocity, which is non-zero, is the velocity in the $\hat{x}$ direction of the flow and it is a function of $\hat{y}$.

When the flow is in the hydrodynamic limit $\left(Kn \le 10^{-3}\right)$, analytical solutions may be deduced both for incompressible and compressible flow. These solutions may be found in several fluid mechanics textbooks [White, 2002]. In this limit the incompressible solution is trivial, while the compressible one is more complicated and requires the introduction of an intermolecular model to relate the transport coefficients to temperature variation. The solution of the problem becomes considerably more complicated when the flow is in the transition and free molecular regimes. In this area, a kinetic approach or the DSMC algorithm are required. Here, we implement the former one. For small relative velocity and temperature differences of the wall plates, linearization of the kinetic equation is allowed. Then the problem is decoupled into the so called "Couette Flow" and "Heat Transfer" problems between parallel plates. Over the years, these problems have been

solved using various analytical and numerical solutions. For arbitrary large relative velocities and temperature differences the non-linear kinetic equation must be implemented and then the problem may be solved only in a computational manner.

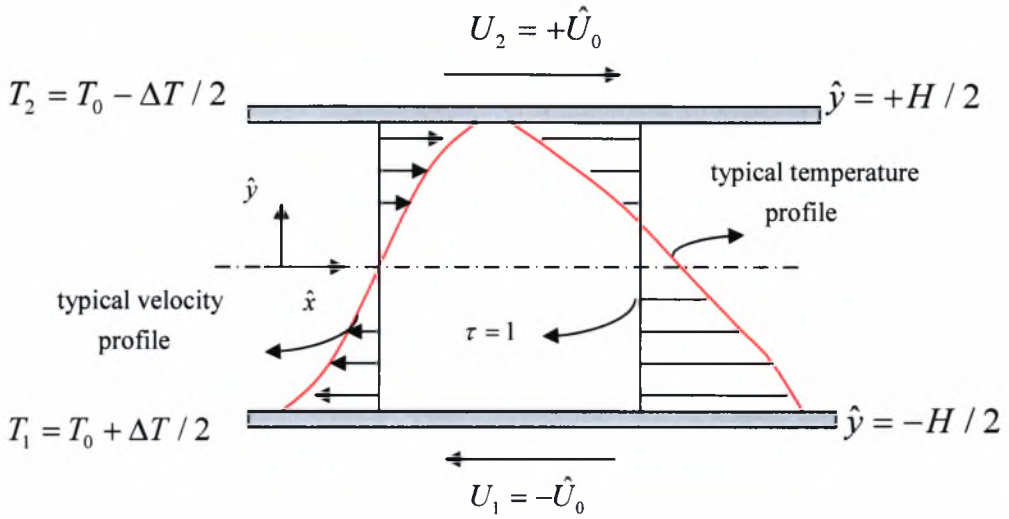

Figure 3.1: *Flow configuration and qualitative velocity profile.*

3.2 Governing equations

For the simulation of the problem both the BGK (Bhatnagar-Gross-Krook) and S (Shakhov) models are used. The BGK model reads [Bhatnagar, Gross, Krook, 1945; Welander, 1954]

$$\frac{\partial f}{\partial t} + \xi_y \frac{\partial f}{\partial \hat{y}} = \frac{P}{\mu}\left\{ f^M\left(n, T, \boldsymbol{u}\right) - f\left(t, \hat{y}, \boldsymbol{\xi}\right)\right\} \tag{3.1}$$

where $f = f\left(y, \boldsymbol{\xi}\right)$ is the distribution function, y is the spatial coordinate vertical to the plates and $\boldsymbol{\xi} = \left(\xi_x, \xi_y, \xi_z\right)$ is the molecular velocity vector, P is the local pressure and μ the gas viscosity at local temperature T. Also, f^M denotes the local Maxwellian described by the equation

$$f^M = n\left(\frac{m}{2\pi k_B T}\right)^{3/2} \exp\left(-\frac{m(\boldsymbol{\xi} - \boldsymbol{u})^2}{2k_B T}\right) \tag{3.2}$$

where

$$n(\hat{y}) = \iiint f d\xi_x d\xi_y d\xi_z \tag{3.3}$$

$$\hat{u}_x(\hat{y}) = \hat{u}(\hat{y}) = \frac{1}{n} \iiint \xi f d\xi_x d\xi_y d\xi_z \tag{3.4}$$

$$T(\hat{y}) = \frac{m}{3nk_B} \iiint (\xi - \hat{u})^2 f d\xi_x d\xi_y d\xi_z \tag{3.5}$$

are the macroscopic (bulk) distributions of local number density, velocity and temperature respectively. The pressure between the plates is given by

$$P(\hat{y}) = nkT = \frac{m}{3} \iiint (\xi - \hat{u})^2 f d\xi_x d\xi_y d\xi_z \,. \tag{3.6}$$

Finally, m denotes the molecular mass of the gas and k_B the Boltzmann constant. This model represents the simplest possible approach of the Boltzmann collision integral, but also the basis on which most subsequent models have developed.

Such a more advanced model is the Shakhov model, first introduced in 1974 [Shakhov, 1947; Sharipov & Seleznev, 1998] which reads

$$\frac{\partial f}{\partial t} + \xi_y \frac{\partial f}{\partial \hat{y}} = \frac{P}{\mu} \left\{ f^M \left[1 + \frac{2m}{15n(k_B T)^2} \hat{\boldsymbol{q}} \cdot (\boldsymbol{\xi} - \boldsymbol{u}) \left(\frac{m(\boldsymbol{\xi} - \hat{\boldsymbol{u}})^2}{2k_B T} - \frac{5}{2} \right) \right] - f \right\} \tag{3.7}$$

where f again is the distribution function and f^M the local Maxwellian given by Eq. (3.2). The bulk quantities of density, velocity, temperature and pressure are given by Eqs. (3.3-3.6), while the heat flux vector is given by

$$\hat{\boldsymbol{q}}(\hat{y}) = \frac{m}{2} \iiint (\xi - \hat{u})(\xi - \hat{u})^2 f d\xi_x d\xi_y d\xi_z \tag{3.8}$$

The Shakhov model provides the correct Prandtl number for monoatomic gases and it is a suitable model for non-isothermal problems as the present one.

Taking into account that the flow is fully developed and one dimensional, the initial BGK model equation Eq. (3.1) is simplified to

$$\xi_y \frac{\partial f}{\partial \hat{y}} = \frac{P}{\mu} \left\{ f^M(n, T, \boldsymbol{u}) - f(t, \boldsymbol{r}, \boldsymbol{\xi}) \right\} \tag{3.9}$$

Similar the Shakhov model is reduced to

$$\xi_y \frac{\partial f}{\partial \hat{y}} = \frac{P}{\mu} \left\{ f^M \left[1 + \frac{2m}{15n(k_B T)^2} q_x (\xi_x - \hat{u}_x) + q_y \xi_y \left(\frac{m(\boldsymbol{\xi} - \hat{\boldsymbol{u}})^2}{2k_B T} - \frac{5}{2} \right) \right] - f \right\} \tag{3.10}$$

The extra terms, namely q_x and q_y, included in this kinetic model described by

$$\hat{q}_x(\hat{y}) = \frac{m}{2}\int\int\int(\xi-\hat{u})^2(\xi_x-\hat{u}_x)fd\xi_x d\xi_y d\xi_z \tag{3.11}$$

$$\hat{q}_y(\hat{y}) = \frac{m}{2}\int\int\int(\xi-\hat{u})^2\xi_y fd\xi_x d\xi_y d\xi_z \tag{3.12}$$

refer to the axial and normal heat fluxes of the flow respectively. A macroscopic quantity of practical interest for the flow, apart from the ones described by Eqs. (3.3-3.6, 3.11, 3.12), is the shear stress

$$\hat{\sigma}_{xy}(\hat{y}) = m\int\int\int(\xi_x-\hat{u}_x)\xi_y fd\xi_x d\xi_y d\xi_z . \tag{3.13a}$$

and the normal stresses

$$\hat{\sigma}_{xx}(\hat{y}) = m\int\int\int(\xi_x-\hat{u}_x)^2 fd\xi_x d\xi_y d\xi_z . \tag{3.13b}$$

$$\hat{\sigma}_{yy}(\hat{y}) = m\int\int\int\xi_y^2 fd\xi_x d\xi_y d\xi_z . \tag{3.13c}$$

$$\hat{\sigma}_{zz}(\hat{y}) = m\int\int\int\xi_z^2 fd\xi_x d\xi_y d\xi_z . \tag{3.13d}$$

In the following sections it will be shown that the shear stress $\hat{\sigma}_{xy}(\hat{y})$ is always constant, i.e. $\hat{\sigma}_{xy}(\hat{y}) = c_0$.

At this stage it is convenient to introduce the non-dimensional quantities

$$y = \frac{\hat{y}}{H},\ \boldsymbol{c} = \frac{\boldsymbol{\xi}}{\upsilon_0} \tag{3.14a}$$

$$g = \frac{f\upsilon_0^3}{n_0} \tag{3.14b}$$

$$\rho = \frac{n}{n_0},\ u = \frac{\hat{u}}{\upsilon_0},\ \tau = \frac{T}{T_0},\ \boldsymbol{q} = \frac{\hat{\boldsymbol{q}}}{P_0\upsilon_0} \text{ and } \sigma_{xy} = \frac{\hat{\sigma}_{xy}}{2P_0} \tag{3.14c}$$

where $-1/2 \le y \le 1/2$ is the dimensionless spatial variable, $\boldsymbol{c} = (c_x, c_y, c_z)$ is the dimensionless molecular velocity vector, $\upsilon_0 = \sqrt{2k_BT_0/m}$ is the most probable molecular velocity, $g = g(y,\boldsymbol{c})$ is the reduced distribution function, ρ, u, τ, q and σ_{xy} are the dimensionless number density, velocity, temperature, heat flux and shear stress respectively, while $P_0 = n_0k_BT_0$ is a reference pressure and n_0 a reference density.

Even more, we define the reference rarefaction parameter

$$\delta_0 = \frac{P_0 H}{\mu_0 \upsilon_0} = \frac{\sqrt{\pi}}{2}\frac{1}{Kn_0} \tag{3.15}$$

which is proportional to the inverse reference Knudsen number, while μ_0 is the gas viscosity at temperature T_0. At this point we have to define also the local rarefaction parameter defined by

$$\delta = \frac{PH}{\mu\upsilon}. \tag{3.16}$$

In order to relate the local rarefaction parameter to the reference one we have

$$\frac{\delta}{\delta_0} = \frac{P\mu_0\upsilon_0}{P_0\mu\upsilon} = \frac{n}{n_0}\frac{T}{T_0}\left(\frac{T_0}{T}\right)^{\omega}\left(\frac{T_0}{T}\right)^{1/2} = \frac{n}{n_0}\left(\frac{T}{T_0}\right)^{1/2-\omega} = \rho\tau^{1/2-\omega}. \tag{3.17}$$

For the derivation of Eq. (3.17) we have assumed that viscosity is proportional to temperature according to the inverse power law

$$\frac{\mu}{\mu_0} = \left(\frac{T}{T_0}\right)^{\omega}. \tag{3.18}$$

The parameter ω describes the molecular model being implemented. For the hard sphere intermolecular model $\omega = 1/2$, while for the Maxwell intermolecular model $\omega = 1$.

Then, we non-dimensionalize Eqs. (3.9) and (3.10) accordingly, to yield

$$c_y\frac{\partial g}{\partial y} = \frac{PH}{\mu\upsilon_0}\left(g^M - g\right) = \frac{P}{P_0}\frac{\mu_0}{\mu}\frac{P_0 H}{\mu_0\upsilon_0}\left(g^M - g\right) = \delta_0\rho\tau^{1-\omega}\left(g^M - g\right) \tag{3.19}$$

and

$$c_y\frac{\partial g}{\partial y} = -\delta_0\rho\tau^{1-\omega}\left\{g - g^M\left[1 + \frac{4}{15}\frac{q_x\left(c_x - u_x\right) + q_y c_y}{\rho\tau^2}\left(\frac{\left(c_x - u_x\right)^2 + c_y^2 + c_z^2}{\tau} - \frac{5}{2}\right)\right]\right\} \tag{3.20}$$

where

$$g^M = \frac{\rho}{\left(\pi\tau\right)^{3/2}}\exp\left[-\frac{\left(c-u\right)^2}{\tau}\right]. \tag{3.21}$$

The corresponding moments of the distribution function for the computation of the non-dimensional macroscopic quantities are described by the equations

$$\rho = \int\int\int g dc_x dc_y dc_z \tag{3.22a}$$

$$u_x = \frac{1}{\rho}\iiint c_x g dc_x dc_y dc_z \tag{3.22b}$$

$$u_y = \frac{1}{\rho}\iiint c_x g dc_x dc_y dc_z \tag{3.22c}$$

$$\tau = \frac{2}{3\rho}\iiint (\mathbf{c}-\mathbf{u})^2 g dc_x dc_y dc_z \tag{3.22d}$$

$$q_x = \iiint (\mathbf{c}-\mathbf{u})^2 (c_x - u_x) g dc_x dc_y dc_z \tag{3.22e}$$

$$q_y = \iiint (\mathbf{c}-\mathbf{u})^2 c_y g dc_x dc_y dc_z \tag{3.22f}$$

$$\sigma_{xy} = \iiint (c_x - u_x) c_y g dc_x dc_y dc_z \tag{3.22g}$$

$$\sigma_{xx} = \iiint (c_x - u_x)^2 g dc_x dc_y dc_z \tag{3.22h}$$

$$\sigma_{yy} = \iiint c_y^2 g dc_x dc_y dc_z \tag{3.22i}$$

$$\sigma_{zz} = \iiint c_z^2 g dc_x dc_y dc_z \tag{3.22j}$$

which refer to the density, x and y velocity components, temperature, x and y heat fluxes, shear stress and three normal stresses respectively.

3.3 Boundary conditions

For the closure of the problem we have to define the boundary conditions. The interaction between the particles and the walls is modeled according to Maxwell diffuse boundary conditions [Maxwell, 1879]:

$$f_1^+\left(-\frac{H}{2},\boldsymbol{\xi}\right) = n_1\left(\frac{m}{2\pi k_B T_1}\right)^{3/2} \exp\left(-\frac{m(\boldsymbol{\xi}-\boldsymbol{u})^2}{2k_B T_1}\right), \text{ for } \xi_y > 0 \tag{3.23}$$

and

$$f_2^+\left(\frac{H}{2},\boldsymbol{\xi}\right) = n_2\left(\frac{m}{2\pi k_B T_2}\right)^{3/2} \exp\left(-\frac{m(\boldsymbol{\xi}-\boldsymbol{u})^2}{2k_B T_2}\right), \text{ for } \xi_y < 0 \tag{3.24}$$

In Eqs. (3.23) and (3.24), the subscript $i = 1,2$ denotes the quantities at the lower and the upper wall respectively, f_i^+ denote departing particle distributions at the corresponding wall and n_i are two parameters to be specified by the condition of no gas penetration at each wall. At this point we should remind that the temperature ratio is defined as

$T_1/T_2=(1+\beta)/(1-\beta)$, where $\beta=\Delta T/2T_0$, $\Delta T=T_1-T_0>0$ with $T_0=(T_1+T_2)/2$ denoting a reference temperature. By introducing the dimensionless quantities the corresponding boundary conditions become

$$g^+\left(-\frac{1}{2},\boldsymbol{c}\right)=g_1^+=\frac{\rho_1}{\left[\pi(1+\beta)\right]^{3/2}}\exp\left(-\frac{\left[(c_x+U_0)^2+c_y^2+c_z^2\right]}{(1+\beta)}\right),\qquad c_y>0 \tag{3.25}$$

and

$$g^+\left(\frac{1}{2},\boldsymbol{c}\right)=g_2^+=\frac{\rho_2}{\left[\pi(1-\beta)\right]^{3/2}}\exp\left(-\frac{\left[(c_x-U_0)^2+c_y^2+c_z^2\right]}{(1-\beta)}\right),\qquad c_y<0 \tag{3.26}$$

The variables $\rho_i(\mp 1/2)$, $i=1,2$ are two parameters to be specified by the condition of no penetration at each wall. According to this condition, the normal velocity at the upper and lower wall is equal to zero. For the case of the lower wall we deduce

$$u_y\left(-\frac{1}{2}\right)=0\Rightarrow\frac{1}{\rho}\int_{-\infty}^{+\infty}\int_{-\infty}^{+\infty}\int_{-\infty}^{+\infty}c_y g\left(-\frac{1}{2},\boldsymbol{c}\right)dc_x dc_y dc_z=0\Rightarrow$$

$$\Rightarrow\underbrace{\frac{1}{\rho}\int_{-\infty}^{0}\int_{-\infty}^{+\infty}\int_{-\infty}^{+\infty}c_y g\left(-\frac{1}{2},\boldsymbol{c}\right)dc_x dc_z dc_y}_{arriving}+\underbrace{\frac{1}{\rho}\int_{0}^{+\infty}\int_{-\infty}^{+\infty}\int_{-\infty}^{+\infty}c_y g\left(-\frac{1}{2},\boldsymbol{c}\right)dc_x dc_z dc_y}_{departing}=0 \tag{3.27}$$

According to Eq. (3.25) the quantity $g^+\left(-\frac{1}{2},\boldsymbol{c}\right)$ for the departing molecules is already known. By introducing this information into Eq. (3.27) we deduce

$$\underbrace{\frac{1}{\rho}\int_{-\infty}^{0}\int_{-\infty}^{+\infty}\int_{-\infty}^{+\infty}c_y g\left(-\frac{1}{2},\boldsymbol{c}\right)dc_x dc_z dc_y}_{arriving}+\underbrace{\frac{\rho_1}{\rho\left[\pi(1+\beta)\right]^{3/2}}\int_{0}^{+\infty}\int_{-\infty}^{+\infty}\int_{-\infty}^{+\infty}c_y\exp\left(-\frac{\left[(c_x+U_0)^2+c_y^2+c_z^2\right]}{(1+\beta)}\right)dc_x dc_z dc_y}_{departing}=0\Rightarrow$$

$$\rho_1=-2\frac{\sqrt{\pi}}{\sqrt{(1+\beta)}}\int_{-\infty}^{0}\int_{-\infty}^{+\infty}\int_{-\infty}^{+\infty}c_y g\left(-\frac{1}{2},\boldsymbol{c}\right)dc_x dc_z dc_y\Rightarrow$$

$$\rho_1=2\frac{\sqrt{\pi}}{\sqrt{(1+\beta)}}\int_{0}^{+\infty}\int_{-\infty}^{+\infty}\int_{-\infty}^{+\infty}c_y' g\left(-\frac{1}{2},\boldsymbol{c}\right)dc_x dc_z dc_y',\qquad c_y'>0. \tag{3.28}$$

In order to compute the corresponding parameter for the case of the upper wall we follow the exact procedure as described above, i.e.,

$$u_y\left(\frac{1}{2}\right)=0 \Rightarrow \frac{1}{\rho}\int_{-\infty}^{+\infty}\int_{-\infty}^{+\infty}\int_{-\infty}^{+\infty} c_y g\left(\frac{1}{2},\boldsymbol{c}\right)dc_x dc_y dc_z = 0 \Rightarrow$$

$$\Rightarrow \underbrace{\frac{1}{\rho}\int_{-\infty}^{0}\int_{-\infty}^{+\infty}\int_{-\infty}^{+\infty} c_y g\left(\frac{1}{2},\boldsymbol{c}\right)dc_x dc_z dc_y}_{departing} + \underbrace{\frac{1}{\rho}\int_{0}^{+\infty}\int_{-\infty}^{+\infty}\int_{-\infty}^{+\infty} c_y g\left(\frac{1}{2},\boldsymbol{c}\right)dc_x dc_z dc_y}_{arriving} = 0 \ . \qquad (3.29)$$

According to Eq. (3.26) the quantity $g\left(\frac{1}{2},\boldsymbol{c}\right)$ for the departing molecules is already known. By introducing this information into Eq. (3.29) we deduce

$$\frac{\rho_2}{\rho\left[\pi(1+\beta)\right]^{3/2}}\underbrace{\int_{-\infty}^{0}\int_{-\infty}^{+\infty}\int_{-\infty}^{+\infty} c_y \exp\left(-\frac{\left[(c_x-U_0)^2+c_y^2+c_z^2\right]}{(1+\beta)}\right)dc_x dc_z dc_y}_{departing} + \underbrace{\frac{1}{\rho}\int_{0}^{+\infty}\int_{-\infty}^{+\infty}\int_{-\infty}^{+\infty} c_y g\left(\frac{1}{2},\boldsymbol{c}\right)dc_x dc_z dc_y}_{arriving} = 0 \Rightarrow$$

$$\rho_2 = 2\frac{\sqrt{\pi}}{\sqrt{(1+\beta)}}\int_{0}^{+\infty}\int_{-\infty}^{+\infty}\int_{-\infty}^{+\infty} c_y g\left(\frac{1}{2},\boldsymbol{c}\right)dc_x dc_z dc_y \ , \qquad c_y > 0 \qquad (3.30)$$

The problem is described by the kinetic Eqs. (3.19) and (3.20), coupled by the moments Eqs. (3.22a-3.22i) and subject to boundary conditions described by the Eqs. (3.28) and (3.30). It is seen that the problem is specified in terms of three dimensionless parameters, namely the reference rarefaction parameter δ_0, the temperature ratio β and the velocity U_0.

4

Projection procedure

4.1 Introduction

The projection procedure has been extensively used over the years in solving flow and heat transfer problems using kinetic equations. The main idea is to eliminate, depending upon the problem geometry and physics, one or two components of the molecular velocity vector and as a result to reduce significantly the required computational effort. This can be achieved through a formal mathematical procedure. The governing equations are integrated accordingly over the space of the appropriate component of the molecular velocity yielding a reduced set of equations, which do not include the component of the molecular velocity upon which the integration has been performed. It is important to note that this procedure is not invertible. Therefore, some information, which however is not significant, may be lost. This mathematical procedure is explicitly provided for the specific problem under consideration for both the BGK and Shakhov models.

4.2 Elimination of the z component of the molecular velocity

In order to proceed with the projection procedure we introduce the corresponding reduced distribution functions which read

$$Y\left(y,c_x,c_y\right)=\int_{-\infty}^{+\infty} g\left(y,c_x,c_y,c_z\right)dc_z \tag{4.1}$$

and

$$\Phi\left(y,c_x,c_y\right)=\int_{-\infty}^{+\infty} c_z^2 g\left(y,c_x,c_y,c_z\right)dc_z \tag{4.2}$$

We integrate Eqs. (3.19) and (3.20) by c_z in the interval $(-\infty,\infty)$. After some routine mathematical manipulation we yield

$$c_y \frac{\partial Y}{\partial y} = \delta_0 \rho \tau^{1-\omega}\left(Y^M - Y\right) \tag{4.3}$$

and

$$c_y \frac{\partial Y}{\partial y} = \delta_0 \rho \tau^{1-\omega}\left(Y^M \left\{ 1 + \frac{4}{15} \frac{\left[q_x\left(c_x - u_x\right) + q_y c_y\right]}{\rho \tau^2} \left[\frac{\left(c_x - u_x\right)^2 + c_y^2}{\tau} - 2 \right] \right\} - Y \right). \tag{4.4}$$

For the next reduced moment, we multiply Eqs. (3.19) and (3.20) by c_z^2 and integrate by c_z in the interval $(-\infty,\infty)$. By following the exact steps as in the former case we deduce

$$c_y \frac{\partial \Phi}{\partial y} = \delta_0 \rho \tau^{1-\omega}\left(\Phi^M - \Phi\right) \tag{4.5}$$

for the BGK model and

$$c_y \frac{\partial \Phi}{\partial y} = -\delta_0 \rho \tau^{1-\omega}\left(\Phi - \Phi^M \left\{ 1 + \frac{4}{15} \frac{\left[q_x\left(c_x - u_x\right) + q_y c_y\right]}{\rho \tau^2} \left[\frac{\left(c_x - u_x\right)^2 + c_y^2}{\tau} - 1 \right] \right\} \right) \tag{4.6}$$

for the S model respectively, where Y^M and Φ^M the non-dimensional Maxwellian distributions given by

$$Y^M = \frac{\rho}{\pi\tau} \exp\left(- \frac{\left(c_x - u_x\right)^2 + c_y^2}{\tau} \right) \tag{4.7}$$

and

$$\Phi^M = \frac{\rho}{2\pi} \exp\left(- \frac{\left(c_x - u_x\right)^2 + c_y^2}{\tau} \right) = Y^M \frac{\tau}{2} \tag{4.8}$$

respectively. The macroscopic quantities in terms of $Y\left(y, c_x, c_y\right)$ and $\Phi\left(y, c_x, c_y\right)$ after applying the projection procedure for both models are

$$\rho(y) = \int_{-\infty}^{+\infty}\int_{-\infty}^{+\infty} Y dc_x dc_y \tag{4.9a}$$

$$u_x(y) = \frac{1}{\rho} \int_{-\infty}^{+\infty}\int_{-\infty}^{+\infty} c_x Y dc_x dc_y \tag{4.9b}$$

$$u_y(y)=\frac{1}{\rho}\int_{-\infty}^{+\infty}\int_{-\infty}^{+\infty}c_y Y dc_x dc_y=0 \tag{4.9c}$$

$$\tau(y)=\frac{2}{3\rho}\int_{-\infty}^{+\infty}\int_{-\infty}^{+\infty}\left\{\left[c_x^2+c_y^2\right]Y+\Phi\right\}dc_x dc_y-\frac{2}{3}u_x^2. \tag{4.9d}$$

$$q_x(y)=\int_{-\infty}^{+\infty}\int_{-\infty}^{+\infty}\left\{\left[c_x^3-3u_x c_x^2+c_y^2 c_x-u_x c_y^2\right]Y+\left[c_x-u_x\right]\Phi\right\}dc_x dc_y+2u_x^3\rho \tag{4.9e}$$

$$q_y(y)=\int_{-\infty}^{+\infty}\int_{-\infty}^{+\infty}\left\{\left[\left(c_x^2+c_y^2\right)c_y-2u_x c_x c_y\right]Y+c_y\Phi\right\}dc_x dc_y \tag{4.9f}$$

$$\sigma_{xy}(y)=\int_{-\infty}^{+\infty}\int_{-\infty}^{+\infty}\left(c_x-u_x\right)c_y Y dc_x dc_y=\int_{-\infty}^{+\infty}\int_{-\infty}^{+\infty}c_x c_y Y dc_x dc_y \tag{4.9g}$$

$$\sigma_{xx}(y)=\int_{-\infty}^{+\infty}\int_{-\infty}^{+\infty}c_x^2 Y dc_x dc_y-u_x^2\rho \tag{4.9h}$$

$$\sigma_{yy}(y)=\int_{-\infty}^{+\infty}\int_{-\infty}^{+\infty}c_y^2 Y dc_x dc_y \tag{4.9i}$$

$$\sigma_{zz}(y)=\int_{-\infty}^{+\infty}\int_{-\infty}^{+\infty}c_z^2 Y dc_x dc_y \tag{4.9j}$$

For the definition of the boundary conditions describing the problem under consideration we apply the same mathematical projection to Eqs. (3.29) and (3.30) respectively. For the lower wall at $y=-1/2$ we yield

$$Y\left(-\frac{1}{2},c_x,c_y\right)=\frac{\rho_1}{\pi(1+\beta)}\exp\left(-\frac{\left(c_x+U_0\right)^2+c_y^2}{(1+\beta)}\right),\qquad c_y>0 \tag{4.10}$$

and

$$\Phi\left(-\frac{1}{2},c_x,c_y\right)=\frac{\rho_1}{2\pi}\exp\left(-\frac{\left(c_x+U_0\right)^2+c_y^2}{(1+\beta)}\right),\qquad c_y>0 \tag{4.11}$$

For the upper wall at $y=1/2$ we yield

$$Y\left(\frac{1}{2},c_x,-c_y\right)=\frac{\rho_2}{\pi(1-\beta)}\exp\left(-\frac{\left(c_x-U_0\right)^2+c_y^2}{(1-\beta)}\right),\qquad c_y>0 \tag{4.12}$$

and

$$\Phi\left(\frac{1}{2},c_x,-c_y\right)=\frac{\rho_2}{2\pi}\exp\left(-\frac{\left(c_x-U_0\right)^2+c_y^2}{\left(1-\beta\right)}\right),\qquad c_y>0 \tag{4.13}$$

The variables $\rho_i\left(\mp 1/2\right)$, i=1,2, are two parameters to be specified by the condition of no penetration at each wall. According to this condition, the normal velocity at the upper and lower wall is equal to zero. At the lower wall we deduce

$$u_y\left(-\frac{1}{2}\right)=0\Rightarrow\frac{1}{\rho}\int_{-\infty}^{+\infty}\int_{-\infty}^{+\infty}\int_{-\infty}^{+\infty}c_y g\left(-\frac{1}{2},c_x,c_y,c_z\right)dc_x dc_y dc_z=0\Rightarrow\int_{-\infty}^{+\infty}\int_{-\infty}^{+\infty}c_y Y\left(y,c_x,c_y\right)dc_x dc_y=0\Rightarrow$$

$$\Rightarrow\underbrace{\int_{-\infty}^{+\infty}\int_{-\infty}^{0}c_y Y\left(-\frac{1}{2},c_x,c_y\right)dc_y dc_x}_{arriving}+\underbrace{\int_{-\infty}^{+\infty}\int_{0}^{+\infty}c_y Y\left(-\frac{1}{2},c_x,c_y\right)dc_y dc_x}_{departing}=0. \tag{4.14}$$

According to Eq. (4.12) the quantity $Y\left(-1/2,c_x,c_y\right)$ for the departing molecules is already known. By introducing this information into Eq. (4.14) and we deduce

$$\underbrace{\int_{-\infty}^{+\infty}\int_{-\infty}^{0}c_y Y\left(-\frac{1}{2},c_x,c_y\right)dc_y dc_x}_{arriving}+\frac{\rho_1}{\pi(1+\beta)}\underbrace{\int_{-\infty}^{+\infty}\int_{0}^{+\infty}c_y\exp\left(-\frac{\left(c_x+U_0\right)^2+c_y^2}{1\div\beta}\right)dc_y dc_x}_{departing}=0\Rightarrow$$

$$\rho_1=-2\frac{\sqrt{\pi}}{\sqrt{(1+\beta)}}\int_{-\infty}^{+\infty}\int_{-\infty}^{0}c_y Y\left(-\frac{1}{2},c_x,c_y\right)dc_y dc_x\Rightarrow$$

$$\rho_1=2\frac{\sqrt{\pi}}{\sqrt{(1+\beta)}}\int_{-\infty}^{+\infty}\int_{0}^{+\infty}c_y' Y\left(-\frac{1}{2},c_x,-c_y'\right)dc_y' dc_x,\qquad c_y'>0 \tag{4.15}$$

In order to compute the corresponding parameter for the case of the upper wall we follow the exact procedure as described above, i.e.

$$u_y\left(\frac{1}{2}\right)=0\Rightarrow\frac{1}{\rho}\int_{-\infty}^{+\infty}\int_{-\infty}^{+\infty}\int_{-\infty}^{+\infty}c_y g\left(\frac{1}{2},c_x,c_y,c_z\right)dc_x dc_y dc_z=0\Rightarrow\int_{-\infty}^{+\infty}\int_{-\infty}^{+\infty}c_y Y\left(y,c_x,c_y\right)dc_x dc_y=0\Rightarrow$$

$$\Rightarrow\underbrace{\int_{-\infty}^{+\infty}\int_{-\infty}^{0}c_y Y\left(\frac{1}{2},c_x,c_y\right)dc_y dc_x}_{departing}+\underbrace{\int_{-\infty}^{+\infty}\int_{0}^{+\infty}c_y Y\left(\frac{1}{2},c_x,c_y\right)dc_y dc_x}_{arriving}=0 \tag{4.16}$$

The quantity $Y\left(1/2,c_x,c_y\right)$, given by Eq. (4.12) for the departing molecules is substituted into Eq. (4.16) and after some routine manipulations we deduce

$$\frac{\rho_2}{\pi(1-\beta)}\underbrace{\int_{-\infty}^{+\infty}\int_{-\infty}^{0} c_y \exp\left(-\frac{(c_x-U_0)^2+c_y^2}{1-\beta}\right)dc_y dc_x}_{departing}+\underbrace{\int_{-\infty}^{+\infty}\int_{0}^{+\infty} c_y Y\left(\frac{1}{2},c_x,c_y\right)dc_y dc_x}_{arriving}=0\Rightarrow$$

$$\rho_2=2\frac{\sqrt{\pi}}{\sqrt{(1-\beta)}}\int_{-\infty}^{+\infty}\int_{0}^{+\infty} c_y Y\left(\frac{1}{2},c_x,c_y\right)dc_y dc_x, \qquad c_y>0 \tag{4.17}$$

Thus, initially we have one integro-differential equation for f which is a function of four independent variables. All bulk quantities are given by moments of f. Now, following the above described projection procedure, we obtain a set of two coupled integro-differential equations for the two unknowns Y and Φ. The coupling is present through the bulk quantities, which are given as moments of Y and Φ. It is noted that these reduced distributions depend only on three (instead of four) variables and therefore the computational effort is significantly reduced.

4.3 Elimination of the z and x components of the molecular velocity

For this specific problem it is possible to eliminate two and not only one components of the molecular velocity vector, as presented in Section 4.2. However, in order not to lose information regarding the bulk quantities of the flow which are of theoretical and practical interest, we must obtain additional reduced distribution functions, which will now depend on two independent variables, namely the spatial variable y and the c_y component of the molecular velocity. In order to achieve this, we integrate Eqs. (3.19) and (3.20) in both x and z directions in the interval $(-\infty,\infty)$. To proceed, we introduce the corresponding reduced distribution functions which read

$$Y(y,c_y)=\int_{-\infty}^{+\infty}\int_{-\infty}^{+\infty} g(y,c_x,c_y,c_z)dc_x dc_z \tag{4.18}$$

$$\Phi(y,c_y)=\int_{-\infty}^{+\infty}\int_{-\infty}^{+\infty} c_x g(y,c_x,c_y,c_z)dc_x dc_z \tag{4.19}$$

$$X\left(y,c_y\right)=\int_{-\infty}^{+\infty}\int_{-\infty}^{+\infty}\left[c_x^2+c_z^2\right]g\left(y,c_x,c_y,c_z\right)dc_xdc_z \tag{4.20}$$

$$\Psi\left(y,c_y\right)=\int_{-\infty}^{+\infty}\int_{-\infty}^{+\infty}c_x^2g\left(y,c_x,c_y,c_z\right)dc_xdc_z \tag{4.21}$$

and

$$\Omega\left(y,c_y\right)=\int_{-\infty}^{+\infty}\int_{-\infty}^{+\infty}c_x\left[c_x^2+c_z^2\right]g\left(y,c_x,c_y,c_z\right)dc_xdc_z\,. \tag{4.22}$$

Operate on Eq. (3.19) using the following integral operators:

$$\int\int(\cdot)dc_xdc_z \tag{4.23}$$

$$\int\int(\cdot)c_xdc_xdc_z \tag{4.24}$$

$$\int\int(\cdot)\left(c_x^2+c_z^2\right)dc_xdc_z \tag{4.25}$$

$$\int\int(\cdot)c_x^2dc_xdc_z \tag{4.26}$$

$$\int\int(\cdot)c_x\left(c_x^2+c_z^2\right)dc_xdc_z \tag{4.27}$$

After some mathematical manipulation we find the following system of reduced kinetic equations for the BGK model:

$$c_y\frac{\partial Y}{\partial y}=\delta_0\rho\tau^{1-\omega}\left(Y^M-Y\right) \tag{4.28}$$

$$c_y\frac{\partial \Phi}{\partial y}=\delta_0\rho\tau^{1-\omega}\left(\Phi^M-\Phi\right) \tag{4.29}$$

$$c_y\frac{\partial X}{\partial y}=\delta_0\rho\tau^{1-\omega}\left(X^M-X\right) \tag{4.30}$$

$$c_y\frac{\partial \Psi}{\partial y}=\delta_0\rho\tau^{1-\omega}\left(\Psi^M-\Psi\right) \tag{4.31}$$

$$c_y\frac{\partial \Omega}{\partial y}=\delta_0\rho\tau^{1-\omega}\left(\Omega^M-\Omega\right) \tag{4.32}$$

Operating on a similar manner on Eq. (3.20) we find the corresponding reduced kinetic equations for the case of the S model:

$$c_y\frac{\partial Y}{\partial y}=\delta_0\rho\tau^{1-\omega}\left(Y^M\left[1+\frac{2c_yq_y\left(2c_y^2-3\tau\right)}{15\rho\tau^3}\right]-Y\right) \tag{4.33}$$

$$c_y \frac{\partial \Phi}{\partial y} = \delta_0 \rho \tau^{1-\omega} \left(\Phi^M \left[1 + \frac{4c_y^3 q_y u_x + 2c_y \left(c_y q_x - 3 q_y u_x \right) \tau - q_x \tau^2}{15 \rho u_x \tau^3} \right] - \Phi \right) \tag{4.34}$$

$$c_y \frac{\partial X}{\partial y} = \delta_0 \rho \tau^{1-\omega} \left(X^M \left[1 + \mathcal{K}_X \right] - X \right) \tag{4.35}$$

$$c_y \frac{\partial \Psi}{\partial y} = \delta_0 \rho \tau^{1-\omega} \left(\Psi^M \left[1 + \mathcal{K}_\Psi \right] - \Psi \right) \tag{4.36}$$

$$c_y \frac{\partial \Omega}{\partial y} = \delta_0 \rho \tau^{1-\omega} \left(\Omega^M \left[1 + \mathcal{K}_\Omega \right] - \Omega \right) \tag{4.37}$$

where

$$\mathcal{K}_X = \frac{4c_y^2 q_x u_x \tau - 2 q_x u_x \tau^2 + 4c_y^3 q_y \left(u_x^2 + \tau \right) - 2c_y q_y \tau \left(3u_x^2 + \tau \right)}{15 \rho \left(u_x^2 + \tau \right) \tau^3}$$

$$\mathcal{K}_\Psi = \frac{8c_y^2 q_x u_x \tau - 4 q_x u_x \tau^2 + 4c_y^3 q_y \left(2u_x^2 + \tau \right) - 2c_y q_y \tau \left(6u_x^2 + \tau \right)}{15 \rho \left(2u_x^2 + \tau \right) \tau^3}$$

$$\mathcal{K}_\Omega = \frac{q_x \tau^2 \left(-3u_x^2 + 2\tau \right) + 4c_y^3 q_y u_x \left(u_x^2 + 2\tau \right) + \left(2c_y^2 q_x \tau - 2c_y q_y u_x \tau \right) \left(3u_x^2 + 2\tau \right)}{15 \rho u_x \left(u_x^2 + 2\tau \right) \tau^3}$$

For both the reduced BGK and Shakhov equations, the reduced Maxwellians are:

$$Y^M = \frac{\rho}{\sqrt{\pi \tau}} \exp\left(-\frac{c_y^2}{\tau} \right) \tag{4.38}$$

$$\Phi^M = \frac{\rho}{\sqrt{\pi \tau}} u_x \exp\left(-\frac{c_y^2}{\tau} \right) = Y^M u_x \tag{4.39}$$

$$X^M = \frac{\rho}{\sqrt{\pi \tau}} \left[u_x^2 + \tau \right] \exp\left(-\frac{c_y^2}{\tau} \right) = Y^M \left[u_x^2 + \tau \right] \tag{4.40}$$

$$\Psi^M = \frac{\rho}{2\sqrt{\pi \tau}} \left[2u_x^2 + \tau \right] \exp\left(-\frac{c_y^2}{\tau} \right) = Y^M \frac{\left[2u_x^2 + \tau \right]}{2} \tag{4.41}$$

$$\Omega^M = \frac{\rho}{\sqrt{\pi \tau}} u_x \left[u_x^2 + 2\tau \right] \exp\left(-\frac{c_y^2}{\tau} \right) = \Phi^M \left[u_x^2 + 2\tau \right] \tag{4.42}$$

The reduced expressions for the evaluation of the macroscopic quantities in terms of Y, Φ, X, Ψ and Ω after applying the projection procedure are described by the equations

$$\rho(y) = \int_{-\infty}^{+\infty} Y(y, c_y)\, dc_y \tag{4.43a}$$

$$u_x(y) = \frac{1}{\rho} \int_{-\infty}^{+\infty} \Phi(y, c_y)\, dc_y \tag{4.43b}$$

$$u_y(y) = \frac{1}{\rho} \int_{-\infty}^{+\infty} c_y Y(y, c_y)\, dc_y = 0 \tag{4.43c}$$

$$\tau(y) = \frac{2}{3\rho} \int_{-\infty}^{+\infty} \left[Y c_y^2 + X \right] dc_y - \frac{2}{3} u_x^2(y). \tag{4.43d}$$

$$q_x(y) = \int_{-\infty}^{+\infty} \left(\Omega - 2u_x \Psi + 3u_x^2 \Phi - u_x^3 Y + c_y^2 \Phi - u_x c_y^2 Y - u_x X \right) dc_y \tag{4.43e}$$

$$q_y(y) = \int_{-\infty}^{+\infty} \left(c_y^3 Y + c_y X - 2u_x c_y \Phi \right) dc_y \tag{4.43f}$$

$$\sigma_{xy}(y) = \int_{-\infty}^{+\infty} (\Phi - u_x Y) c_y\, dc_y = \int_{-\infty}^{+\infty} \Phi c_y\, dc_y \tag{4.43g}$$

$$\sigma_{xx}(y) = \int_{-\infty}^{+\infty} \Psi\, dc_y - u_x^2 \rho \tag{4.43h}$$

$$\sigma_{yy}(y) = \int_{-\infty}^{+\infty} c_y^2 Y dc_y \tag{4.43i}$$

$$\sigma_{zz}(y) = \int_{-\infty}^{+\infty} \left[X - \Psi \right] dc_y \tag{4.43j}$$

and refer to density, axial velocity, normal velocity, temperature, axial heat flux, normal heat flux, shear stress and normal stresses in x, y and z directions respectively.

For the definition of the boundary conditions describing the problem under consideration we apply the same mathematical projection to Eqs. (3.28) and (3.30). At the lower wall $(y = -1/2)$ we yield

$$Y\left(-\frac{1}{2}, c_y \right) = \frac{\rho_1}{\sqrt{\pi(1+\beta)}} \exp\left(-\frac{c_y^2}{(1+\beta)} \right), \qquad c_y > 0 \tag{4.44}$$

$$\Phi\left(-\frac{1}{2},c_y\right)=\frac{\rho_1}{\sqrt{\pi(1+\beta)}}(-U_0)\exp\left(-\frac{c_y^2}{(1+\beta)}\right),\qquad c_y>0 \qquad (4.45)$$

$$X\left(-\frac{1}{2},c_y\right)=\frac{\rho_1}{\sqrt{\pi(1+\beta)}}\left[(-U_0)^2+(1+\beta)\right]\exp\left(-\frac{c_y^2}{(1+\beta)}\right),\qquad c_y>0 \qquad (4.46)$$

$$\Psi\left(-\frac{1}{2},c_y\right)=\frac{\rho_1}{2\sqrt{\pi(1+\beta)}}\left[2(-U_0)^2+(1+\beta)\right]\exp\left(-\frac{c_y^2}{(1+\beta)}\right),\qquad c_y>0 \qquad (4.47)$$

$$\Omega\left(-\frac{1}{2},c_y\right)=\frac{\rho_1}{\sqrt{\pi(1+\beta)}}(-U_0)\left[(-U_0)^2+2(1+\beta)\right]\exp\left(-\frac{c_y^2}{(1+\beta)}\right),\ c_y>0. \qquad (4.48)$$

At the upper wall $(y=1/2)$ we yield

$$Y\left(\frac{1}{2},c_y\right)=\frac{\rho_2}{\sqrt{\pi(1-\beta)}}\exp\left(-\frac{c_y^2}{(1-\beta)}\right),\qquad c_y<0 \qquad (4.49)$$

$$\Phi\left(\frac{1}{2},c_y\right)=\frac{\rho_2}{\sqrt{\pi(1-\beta)}}(+U_0)\exp\left(-\frac{c_y^2}{(1-\beta)}\right),\qquad c_y<0 \qquad (4.50)$$

$$X\left(\frac{1}{2},c_y\right)=\frac{\rho_2}{\sqrt{\pi(1-\beta)}}\left[(+U_0)^2+(1-\beta)\right]\exp\left(-\frac{c_y^2}{(1-\beta)}\right),\qquad c_y<0 \qquad (4.51)$$

$$\Psi\left(\frac{1}{2},c_y\right)=\frac{\rho_2}{2\sqrt{\pi(1-\beta)}}\left[2(+U_0)^2+(1-\beta)\right]\exp\left(-\frac{c_y^2}{(1-\beta)}\right),\qquad c_y<0 \qquad (4.52)$$

$$\Omega\left(\frac{1}{2},c_y\right)=\frac{\rho_2}{\sqrt{\pi(1-\beta)}}(+U_0)\left[(+U_0)^2+2(1-\beta)\right]\exp\left(-\frac{c_y^2}{(1-\beta)}\right),\qquad c_y<0 \qquad (4.53)$$

As already mentioned, the variables $\rho_i(\mp 1/2)$, $i=1,2$, are the two parameters to be specified by the condition of no penetration at each wall. For the case of the double projection scheme and for the lower wall we deduce

$$u_y\left(-\frac{1}{2}\right)=0\Rightarrow\frac{1}{\rho}\int_{-\infty}^{+\infty}\int_{-\infty}^{+\infty}\int_{-\infty}^{+\infty}c_y g\left(-\frac{1}{2},c_x,c_y,c_z\right)dc_x dc_z dc_y=0\Rightarrow\frac{1}{\rho}\int_{-\infty}^{+\infty}c_y Y\left(-\frac{1}{2},c_y\right)dc_y=0\Rightarrow$$

$$\Rightarrow\underbrace{\int_{-\infty}^{0}c_y Y\left(-\frac{1}{2},c_y\right)dc_y}_{arriving}+\underbrace{\int_{0}^{+\infty}c_y Y\left(-\frac{1}{2},c_y\right)dc_y}_{departing}=0. \qquad (4.54)$$

The quantity $Y\left(-1/2,c_y\right)$ is substituted by Eq. (4.44) into Eq. (4.54) and we deduce

$$\underbrace{\int_{-\infty}^{0} c_y Y\left(-\frac{1}{2},c_y\right)dc_y}_{arriving}+\frac{\rho_1}{\pi(1+\beta)}\underbrace{\int_{0}^{+\infty} c_y \exp\left(-\frac{c_y^2}{1+\beta}\right)dc_y}_{departing}=0$$

$$\rho_1=-2\frac{\sqrt{\pi}}{\sqrt{1+\beta}}\int_{-\infty}^{0} c_y Y\left(-\frac{1}{2},c_y\right)dc_y \Rightarrow$$

$$\rho_1=2\frac{\sqrt{\pi}}{\sqrt{1+\beta}}\int_{0}^{+\infty} c_y' Y\left(-\frac{1}{2},-c_y'\right)dc_y',\ c_y'>0 \tag{4.55}$$

In order to compute the corresponding parameter for the case of the upper wall we follow the exact procedure as described above to find

$$u_y\left(\frac{1}{2}\right)=0\Rightarrow\frac{1}{\rho}\int_{-\infty}^{+\infty}\int_{-\infty}^{+\infty}\int_{-\infty}^{+\infty} c_y g\left(\frac{1}{2},c_x,c_y,c_z\right)dc_x dc_z dc_y=0\Rightarrow\frac{1}{\rho}\int_{-\infty}^{+\infty} c_y Y\left(\frac{1}{2},c_y\right)dc_y=0\Rightarrow$$

$$\Rightarrow\underbrace{\int_{-\infty}^{0} c_y Y\left(\frac{1}{2},c_y\right)dc_y}_{departing}+\underbrace{\int_{0}^{+\infty} c_y Y\left(\frac{1}{2},c_y\right)dc_y}_{arriving}=0. \tag{4.56}$$

The quantity $Y\left(1/2,c_y\right)$ is substituted by Eq. (4.49) into Eq. (4.56) to find

$$\frac{\rho_2}{\sqrt{\pi(1-\beta)}}\underbrace{\int_{-\infty}^{0} c_y \exp\left(-\frac{c_y^2}{1-\beta}\right)dc_y}_{departing}+\underbrace{\int_{0}^{+\infty} c_y Y\left(\frac{1}{2},c_y\right)dc_y}_{arriving}=0\Rightarrow$$

$$\rho_2=2\frac{\sqrt{\pi}}{\sqrt{1-\beta}}\int_{0}^{+\infty} c_y Y\left(\frac{1}{2},c_y\right)dc_y,\ c_y>0 \tag{4.57}$$

4.4 Some remarks on the projection procedure

The problem may be solved using either the c_z or the c_x and c_z projection procedure. In the first case we have two coupled equations to be solved for the two unknown distribution functions and three independent variables. In the second case, we have five coupled equations to be solved for the five unknown distribution functions and two independent variables. The computational effort for solving the reduced kinetic equations produced by the double projection scheme, is several orders of magnitude less than the corresponding one for solving the reduced equations produced by the single projection scheme. A thorough discussion on this issue is presented in the following section.

5

Numerical Scheme

The implemented computational scheme has been extensively applied to solve linear kinetic equations describing several non-equilibrium systems in a very efficient and accurate manner [Valougeorgis, 1988; Sharipov, 1998; Naris et al, 2004]. Here, it is accordingly extended to the case of non-linear kinetic equations. This is a task, which has been initiated recently in order to solve a wider range of problems and to study non-linear phenomena.

5.1 Iteration procedure

The problems to be solved numerically are described by Eqs. (4.28-4.32) for the BGK model and by Eqs. (4.33-4.37) for the Shakhov model respectively. To solve these equations, an iterative procedure is needed between the kinetic equations and the moments of the distribution function which appear in the expressions of the equilibrium distribution. We demonstrate this iterative process by working only with the reduced BGK kinetic equations produced by the double projection procedure. Then, an identical procedure may be applied to the single projection kinetic equation. The kinetic equations under investigation may be written as

$$c_y \frac{\partial h^{(k+1/2)}}{\partial y} + \delta_0 \rho^{(k)} \tau^{1-\omega^{(k)}} h^{(k+1/2)} = \delta_0 \rho^{(k)} \tau^{1-\omega^{(k)}} h^{M^{(k)}} \tag{5.1}$$

where h may be any of the reduced distribution functions Y, Φ, X, Ψ and Ω, while h^M may be any of the corresponding Maxwellians Y^M, Φ^M, X^M, Ψ^M and Ω^M given by Eqs. (4.38-4.42). The bulk quantities involved in the computations are

$$\rho^{(k+1)} = \int_{-\infty}^{+\infty} Y^{(k+1/2)} dc_y \tag{5.2a}$$

$$u_x^{(k+1)} = \frac{1}{\rho^{(k+1)}} \int_{-\infty}^{+\infty} \Phi^{(k+1/2)} dc_y \tag{5.2b}$$

$$\tau^{(k+1)} = \frac{2}{3\rho^{(k+1)}} \int_{-\infty}^{+\infty} \left[Yc_y^2 + X \right]^{(k+1/2)} dc_y - \frac{2}{3} u_x^{2^{(k+1)}} \tag{5.2c}$$

The indexes *k*, *k+1/2* and *k+1* indicate the steps needed in the iteration process. Initially, assumptions of the macroscopic quantities ρ, u_x, τ as well as of the parameters ρ_1 and ρ_2 are introduced. In all cases independent of β, U_0 and δ_0 the initial guesses are fixed at $\rho = 0.1$, $u_x = 0$ and τ=1. In contrary, parameters at the walls are computed via the corresponding expressions for the free molecular solution, which depend on β and U_0 (see Section 6.1).

Based on these assumptions, the equilibrium distributions h^M are computed. Then, the kinetic equations are solved for the unknown distributions h. In the next step, updated estimates of the macroscopic quantities and the density parameters at the walls are computed based on the moments of the distribution functions h. The iterative procedure is repeated until the termination criterion applied on the macroscopic quantities is satisfied.

The number of iterations needed for convergence in terms of β, U_0 and δ_0 are shown in Table 5.1. It is seen that the number of iterations increases rapidly as δ_0 is increased. This behavior is well known from the corresponding linear results. It is emphasized that in general the weak point of the discrete velocity solver is the large computational time at the hydrodynamic regime. It is also seen that for $\delta_0 \leq 10$ the number of iterations does not depend strongly on β and U_0, while for $\delta_0 = 100$ the number of iterations is increased as β is increased

5.2 Discretization in the physical space

In the physical space, the distance $y \in [-1/2, 1/2]$ is divided in equal intervals (Figure 5.1) and the discretization at each interval $i = 1, 2, ..., I$ is performed by the diamond difference scheme [Lewis & Miller, 1984]. This is a second order central

Table 5.1: *Number of iterations for hard spheres BGK model (ω=0.5) and various values of β and U.*

β	U_0	δ_0				
		0	0.1	1	10	100
0	0.1	2	104	49	410	19241
	0.3	2	104	49	411	19303
	0.5	2	103	49	413	19411
0.1	0	2	107	49	409	21576
	0.1	2	107	49	414	22008
	0.3	2	105	49	434	23278
	0.5	2	104	49	469	24773
0.5	0	2	105	50	436	26671
	0.1	2	107	50	454	27045
	0.3	2	105	50	496	28312
	0.5	2	103	50	538	29966
0.9	0	2	95	53	516	32686
	0.1	2	95	53	525	32941
	0.3	2	94	52	566	34071
	0.5	2	91	50	619	35803

difference scheme, which has been used in solving elliptic integro-differential equations.

A typical example based on Eqs. (4.3) and (4.5) is demonstrated. Let

$$Y\left(y,c_x,c_y\right)\Big|_i = Y\left(y_i,c_x,c_y\right) = Y_i,\ \Phi\left(y,c_x,c_y\right)\Big|_i = \Phi\left(y_i,c_x,c_y\right) = \Phi_i,$$

$$Y^M\left(y,c_x,c_y\right)\Big|_i = Y^M\left(y_i,c_x,c_y\right) = Y_i^M,\ \Phi^M\left(y,c_x,c_y\right)\Big|_i = \Phi^M\left(y_i,c_x,c_y\right) = \Phi_i^M,$$

$$\rho(y) = \rho(y_i) = \rho_i,\ u(y) = u(y_i) = u_i,\ \tau(y) = \tau(y_i) = \tau_i$$

and discretize the kinetic equation at the nodes $i = 1,2,\ldots,I$

$$c_y \left.\frac{\partial Y^{(k+1/2)}}{\partial y}\right|_i + \delta_0 \rho_i^{(k)} \tau_i^{1-\omega^{(k)}} Y_i^{(k+1/2)} = \delta_0 \rho_i^{(k)} \tau_i^{1-\omega^{(k)}} Y_i^{M^{(k)}} \tag{5.3}$$

$$c_y \left.\frac{\partial \Phi^{(k+1/2)}}{\partial y}\right|_i + \delta_0 \rho_i^{(k)} \tau_i^{1-\omega^{(k)}} \Phi_i^{(k+1/2)} = \delta_0 \rho_i^{(k)} \tau_i^{1-\omega^{(k)}} \Phi_i^{M^{(k)}} \tag{5.4}$$

The macroscopic quantities in terms of Y and Φ after applying the projection procedure are

$$\rho_i^{(k+1)} = \int_{-\infty}^{+\infty}\int_{-\infty}^{+\infty} Y^{(k+1/2)}\Big|_i \, dc_x dc_y \tag{5.5a}$$

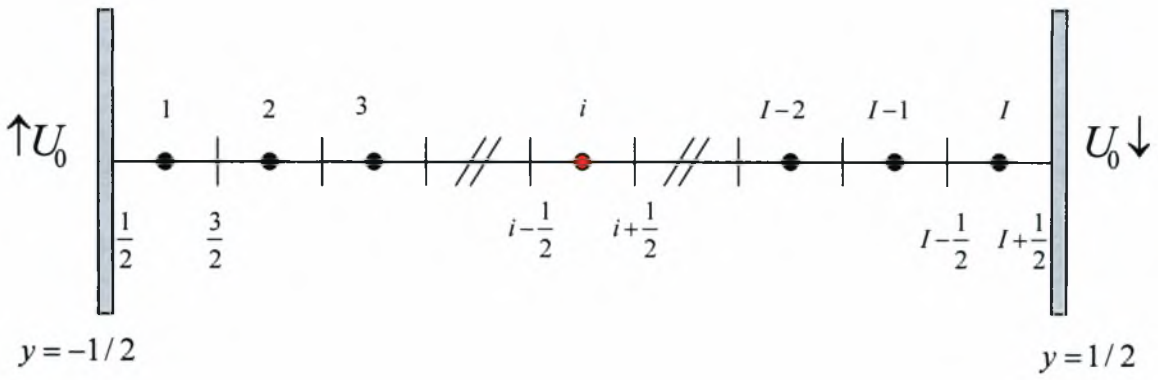

Figure 5.1: *Physical space discretization scheme.*

$$u_{x_i}^{(k+1)} = \frac{1}{\rho_i^{(k+1)}} \int_{-\infty}^{+\infty}\int_{-\infty}^{+\infty} c_x Y_i^{(k+1/2)} dc_x dc_y \tag{5.5b}$$

$$\tau_i^{(k+1)} = \frac{2}{3\rho_i^{(k+1)}} \int_{-\infty}^{+\infty}\int_{-\infty}^{+\infty} \left\{ \left[c_x^2 + c_y^2 \right] Y_i^{(k+1/2)} + \Phi_i^{(k+1/2)} \right\} dc_x dc_y - \frac{2}{3} u_{x_i}^{2^{(k+1)}} \tag{5.5c}$$

By approximating

$$\left.\frac{\partial Y}{\partial y}\right|_i = \frac{1}{h}\left(Y_{i+\frac{1}{2}} - Y_{i-\frac{1}{2}} \right) + O\left[h^2\right] \tag{5.6}$$

$$\left.\frac{\partial \Phi}{\partial y}\right|_i = \frac{1}{h}\left(\Phi_{i+\frac{1}{2}} - \Phi_{i-\frac{1}{2}} \right) + O\left[h^2\right] \tag{5.7}$$

$$Y_i = \frac{1}{2}\left(Y_{i+\frac{1}{2}} + Y_{i-\frac{1}{2}} \right) + O\left[h^2\right] \tag{5.8}$$

$$\Phi_i = \frac{1}{2}\left(\Phi_{i+\frac{1}{2}} + \Phi_{i-\frac{1}{2}} \right) + O\left[h^2\right] \tag{5.9}$$

$$Y_i^M = \frac{1}{2}\left(Y_{i+\frac{1}{2}}^M + Y_{i-\frac{1}{2}}^M \right) + O\left[h^2\right] \tag{5.10}$$

$$\Phi_i^M = \frac{1}{2}\left(\Phi_{i+\frac{1}{2}}^M + \Phi_{i-\frac{1}{2}}^M \right) + O\left[h^2\right] \tag{5.11}$$

$$\rho_i = \frac{1}{2}\left(\rho_{i+\frac{1}{2}} + \rho_{i-\frac{1}{2}}\right) + O\left[h^2\right] \tag{5.12}$$

$$\tau_i = \frac{1}{2}\left(\tau_{i+\frac{1}{2}} + \tau_{i-\frac{1}{2}}\right) + O\left[h^2\right] \tag{5.13}$$

we deduce

$$c_y \frac{Y^{(k+1/2)}_{i+\frac{1}{2}} - Y^{(k+1/2)}_{i-\frac{1}{2}}}{h} + \frac{\delta_0}{8}\left(\rho_{i+\frac{1}{2}} + \rho_{i-\frac{1}{2}}\right)^{(k)}\left(\tau_{i+\frac{1}{2}} + \tau_{i-\frac{1}{2}}\right)^{1-\omega^{(k)}}\left(Y^{(k+1/2)}_{i+\frac{1}{2}} + Y^{(k+1/2)}_{i-\frac{1}{2}}\right) = \frac{\delta_0}{8}\left(\rho_{i+\frac{1}{2}} + \rho_{i-\frac{1}{2}}\right)^{(k)}\left(\tau_{i+\frac{1}{2}} + \tau_{i-\frac{1}{2}}\right)^{1-\omega^{(k)}}\left(Y^{M\,(k)}_{i+\frac{1}{2}} + Y^{M\,(k)}_{i-\frac{1}{2}}\right) \tag{5.14}$$

and

$$c_y \frac{\Phi^{(k+1/2)}_{i+\frac{1}{2}} - \Phi^{(k+1/2)}_{i-\frac{1}{2}}}{h} + \frac{\delta_0}{8}\left(\rho_{i+\frac{1}{2}} + \rho_{i-\frac{1}{2}}\right)^{(k)}\left(\tau_{i+\frac{1}{2}} + \tau_{i-\frac{1}{2}}\right)^{1-\omega^{(k)}}\left(\Phi^{(k+1/2)}_{i+\frac{1}{2}} + \Phi^{(k+1/2)}_{i-\frac{1}{2}}\right) = \frac{\delta_0}{8}\left(\rho_{i+\frac{1}{2}} + \rho_{i-\frac{1}{2}}\right)^{(k)}\left(\tau_{i+\frac{1}{2}} + \tau_{i-\frac{1}{2}}\right)^{1-\omega^{(k)}}\left(\Phi^{M\,(k)}_{i+\frac{1}{2}} + \Phi^{M\,(k)}_{i-\frac{1}{2}}\right) \tag{5.15}$$

The Maxwellians are computed using the macroscopic quantities at the corresponding nodes. The above system of Eqs. (5.14) and (5.15) coupled with the corresponding equations for the evaluation of the macroscopic quantities is solved by following the particle trajectories.

5.3 Discretization in the $\left(c_x, c_y\right)$ space

The set of kinetic equations for the BGK and the Shakhov models are now discretized in the physical space. In the molecular velocity space, the discretization is performed by the discrete velocity method, where the continuum spectrum $c_x, c_y \in \left(-\infty, \infty\right)$ is replaced by a suitable set of discrete velocities p_x^m, p_y^m, $m = 1, 2, ..., M$. We choose p_x^m, p_y^m to be the roots of the Legendre polynomials of order M. Since the initial set of Legendre polynomials is from $\left[-1, 1\right]$, a transformation is necessary in order to compute the correct values in the interval $\left[0, \infty\right)$. This is achieved by introducing the new variable

$$\zeta_x = \frac{1+p_x}{1-p_x} \text{ and } \zeta_y = \frac{1+p_y}{1-p_y} \text{ with } d\zeta_x = \frac{2dp_x}{(1-p_x)^2} \text{ and } d\zeta_y = \frac{2dp_y}{(1-p_y)^2} \tag{5.16}$$

which defines a set of discrete velocities ζ_m, $m = 1,2,\ldots,M$, in $[0,\infty)$. By letting

$$Y\left(y,c_x,c_y\right)\Big|_{i,\zeta_x,\zeta_y} = Y\left(y_i,\zeta_{x_m},\zeta_{y_m}\right) = Y_{i,m,m}$$

and

$$\Phi\left(y,c_x,c_y\right)\Big|_{i,\zeta_x,\zeta_y} = \Phi\left(y_i,\zeta_{x_m},\zeta_{y_m}\right) = \Phi_{i,m,m}$$

Equations (5.14) and (5.15) can be rewritten as

$$\begin{aligned}\zeta_{y_m}\frac{Y^{(k+1/2)}_{i+\frac{1}{2},m,m} - Y^{(k+1/2)}_{i-\frac{1}{2},m,m}}{h} + \frac{\delta_0}{8}\left(\rho_{i+\frac{1}{2}}+\rho_{i-\frac{1}{2}}\right)^{(k)}\left(\tau_{i+\frac{1}{2}}+\tau_{i-\frac{1}{2}}\right)^{1-\omega^{(k)}}\left(Y^{(k+1/2)}_{i+\frac{1}{2},m,m}+Y^{(k+1/2)}_{i-\frac{1}{2},m,m}\right) = \\ = \frac{\delta_0}{8}\left(\rho_{i+\frac{1}{2}}+\rho_{i-\frac{1}{2}}\right)^{(k)}\left(\tau_{i+\frac{1}{2}}+\tau_{i-\frac{1}{2}}\right)^{1-\omega^{(k)}}\left(Y^{M^{(k)}}_{i+\frac{1}{2},m,m}+Y^{M^{(k)}}_{i-\frac{1}{2},m,m}\right)\end{aligned} \tag{5.17}$$

and

$$\begin{aligned}\zeta_{y_m}\frac{\Phi^{(k+1/2)}_{i+\frac{1}{2},m,m} - \Phi^{(k+1/2)}_{i-\frac{1}{2},m,m}}{h} + \frac{\delta_0}{8}\left(\rho_{i+\frac{1}{2}}+\rho_{i-\frac{1}{2}}\right)^{(k)}\left(\tau_{i+\frac{1}{2}}+\tau_{i-\frac{1}{2}}\right)^{1-\omega^{(k)}}\left(\Phi^{(k+1/2)}_{i+\frac{1}{2},m,m}+\Phi^{(k+1/2)}_{i-\frac{1}{2},m,m}\right) = \\ = \frac{\delta_0}{8}\left(\rho_{i+\frac{1}{2}}+\rho_{i-\frac{1}{2}}\right)^{(k)}\left(\tau_{i+\frac{1}{2}}+\tau_{i-\frac{1}{2}}\right)^{1-\omega^{(k)}}\left(\Phi^{M^{(k)}}_{i+\frac{1}{2},m,m}+\Phi^{M^{(k)}}_{i-\frac{1}{2},m,m}\right)\end{aligned} \tag{5.18}$$

In order to simplify Eqs. (5.17) and (5.18) we introduce

$$T0 = \frac{h\delta_0}{8\zeta_{y_m}}\left(\rho_{i+\frac{1}{2}}+\rho_{i-\frac{1}{2}}\right)^{(k)}\left(\tau_{i+\frac{1}{2}}+\tau_{i-\frac{1}{2}}\right)^{1-\omega^{(k)}} \tag{5.19}$$

and then following the particle trajectories we yield the following algebraic equations

For $\zeta_{x_m} > 0$ and $\zeta_{y_m} > 0$:

$$Y^{(k+1/2)}_{i+\frac{1}{2},m,m} = \frac{1}{(1+T0)}\left\{(1-T0)Y^{(k+1/2)}_{i-\frac{1}{2},m,m} + T0\left(Y^{M^{(k)}}_{i+\frac{1}{2},m,m} + Y^{M^{(k)}}_{i-\frac{1}{2},m,m}\right)\right\} \tag{5.20a}$$

$$\Phi^{(k+1/2)}_{i+\frac{1}{2},m,m} = \frac{1}{(1+T0)}\left\{(1-T0)\Phi^{(k+1/2)}_{i-\frac{1}{2},m,m} + T0\left(\Phi^{M^{(k)}}_{i+\frac{1}{2},m,m} + \Phi^{M^{(k)}}_{i-\frac{1}{2},m,m}\right)\right\} \tag{5.20b}$$

$$m = 1,2,\ldots,M \quad i = 1,2,\ldots,I$$

For $\zeta_{x_m} < 0$ and $\zeta_{y_m} > 0$:

$$Y^{(k+1/2)}_{i+\frac{1}{2},m+M,m} = \frac{1}{(1+T0)}\left\{(1-T0)Y^{(k+1/2)}_{i-\frac{1}{2},m+M,m} + T0\left(Y^{M^{(k)}}_{i+\frac{1}{2},m+M,m} + Y^{M^{(k)}}_{i-\frac{1}{2},m+M,m}\right)\right\} \quad (5.21a)$$

$$\Phi^{(k+1/2)}_{i+\frac{1}{2},m+M,m} = \frac{1}{(1+T0)}\left\{(1-T0)\Phi^{(k+1/2)}_{i-\frac{1}{2},m+M,m} + T0\left(\Phi^{M^{(k)}}_{i+\frac{1}{2},m+M,m} + \Phi^{M^{(k)}}_{i-\frac{1}{2},m+M,m}\right)\right\} \quad (5.21b)$$

$$m = 1,2,\ldots,M \quad i = 1,2,\ldots,I$$

For $\zeta_{x_m} > 0$ and $\zeta_{y_m} < 0$:

$$Y^{(k+1/2)}_{i+\frac{1}{2},m,m+M} = \frac{1}{(1-T0)}\left\{(1+T0)Y^{(k+1/2)}_{i-\frac{1}{2},m,m+M} - T0\left(Y^{M^{(k)}}_{i+\frac{1}{2},m,m+M} + Y^{M^{(k)}}_{i-\frac{1}{2},m,m+M}\right)\right\} \quad (5.22a)$$

$$\Phi^{(k+1/2)}_{i+\frac{1}{2},m,m+M} = \frac{1}{(1-T0)}\left\{(1+T0)\Phi^{(k+1/2)}_{i-\frac{1}{2},m,m+M} - T0\left(\Phi^{M^{(k)}}_{i+\frac{1}{2},m,m+M} + \Phi^{M^{(k)}}_{i-\frac{1}{2},m,m+M}\right)\right\} \quad (5.22b)$$

$$m = 1,2,\ldots,M \quad i = I, I-1,\ldots,1$$

For $\zeta_{x_m} < 0$ and $\zeta_{y_m} < 0$:

$$Y^{(k+1/2)}_{i+\frac{1}{2},m+M,m+M} = \frac{1}{(1-T0)}\left\{(1+T0)Y^{(k+1/2)}_{i-\frac{1}{2},m+M,m+M} - T0\left(Y^{M^{(k)}}_{i+\frac{1}{2},m+M,m+M} + Y^{M^{(k)}}_{i-\frac{1}{2},m+M,m+M}\right)\right\} \quad (5.23a)$$

$$\Phi^{(k+1/2)}_{i+\frac{1}{2},m+M,m+M} = \frac{1}{(1-T0)}\left\{(1+T0)\Phi^{(k+1/2)}_{i-\frac{1}{2},m+M,m+M} - T0\left(\Phi^{M^{(k)}}_{i+\frac{1}{2},m+M,m+M} + \Phi^{M^{(k)}}_{i-\frac{1}{2},m+M,m+M}\right)\right\} \quad (5.23b)$$

$$m = 1,2,\ldots,M \quad i = I, I-1,\ldots,1$$

It is noted that Eqs. (5.20) and (5.21) are identical as well as Eqs. (5.22) and (5.23). This is easily explained due to the absence of the axial component of the molecular velocity c_x in the equations. In equations (5.22a,b) and (5.23a,b) where $\zeta_{y_m} < 0$, if we define

$$T0 = \frac{h\delta_0}{8\left|\zeta_{y_m}\right|}\left(\rho_{i+\frac{1}{2}} + \rho_{i-\frac{1}{2}}\right)^{(k)}\left(\tau_{i+\frac{1}{2}} + \tau_{i-\frac{1}{2}}\right)^{1-\omega^{(k)}} \quad (5.24)$$

then they can be rewritten as follows:

For $\zeta_{x_m} > 0$ and $\zeta_{y_m} < 0$:

$$Y^{(k+1/2)}_{i+\frac{1}{2},m,m+M} = \frac{1}{(1+T0)}\left\{(1-T0)Y^{(k+1/2)}_{i-\frac{1}{2},m,m+M} + T0\left(Y^{M^{(k)}}_{i+\frac{1}{2},m,m+M} + Y^{M^{(k)}}_{i-\frac{1}{2},m,m+M}\right)\right\} \quad (5.25a)$$

$$\Phi^{(k+1/2)}_{i+\frac{1}{2},m,m+M} = \frac{1}{(1+T0)}\left\{(1-T0)\Phi^{(k+1/2)}_{i-\frac{1}{2},m,m+M} + T0\left(\Phi^{M^{(k)}}_{i+\frac{1}{2},m,m+M} + \Phi^{M^{(k)}}_{i-\frac{1}{2},m,m+M}\right)\right\} \quad (5.25b)$$

$$m = 1,2,\ldots,M \quad i = I, I-1,\ldots,1$$

For $\zeta_{x_m} < 0$ and $\zeta_{y_m} < 0$:

$$Y^{(k+1/2)}_{i+\frac{1}{2},m+M,m+M} = \frac{1}{(1+T0)}\left\{(1-T0)Y^{(k+1/2)}_{i-\frac{1}{2},m+M,m+M} + T0\left(Y^{M^{(k)}}_{i+\frac{1}{2},m+M,m+M} + Y^{M^{(k)}}_{i-\frac{1}{2},m+M,m+M}\right)\right\} \quad (5.26a)$$

$$\Phi^{(k+1/2)}_{i+\frac{1}{2},m+M,m+M} = \frac{1}{(1+T0)}\left\{(1-T0)\Phi^{(k+1/2)}_{i-\frac{1}{2},m+M,m+M} + T0\left(\Phi^{M^{(k)}}_{i+\frac{1}{2},m+M,m+M} + \Phi^{M^{(k)}}_{i-\frac{1}{2},m+M,m+M}\right)\right\} \quad (5.26b)$$

$$m = 1,2,\ldots,M \quad i = I, I-1,\ldots,1$$

Thus, the explicit expressions (5.20, 5.21), (5.25, 5.26) are the same and only one set of discrete velocities $\zeta_m \in [0,\infty)$ may be used. It is noted that Eqs. (5.21, 5.22) and (5.25, 5.26) are the same but in the first we are moving from bottom to top (or left to right), while in the latter from top to bottom (or right to left). The above two loops with respect to the spatial variable are included into one loop with respect to the molecular velocities. So, for each discrete velocity we march through the spatial grid.

5.4 Discretization in the c_y space

Similarly to the discretization in the (c_x, c_y) molecular velocity space, the discretization in the c_y space is applied. The governing equations are integrated accordingly over the space of the appropriate component of the molecular velocity yielding a reduced set of equations, which do not include the component of the molecular velocity upon which the integration has been performed. Again we choose p_y^m to be the roots of the Legendre polynomials of order M and the transformation

$$\zeta_y = \frac{1+p_y}{1-p_y} \quad \text{with} \quad d\zeta_y = \frac{2dp_y}{(1-p_y)^2} \quad (5.27)$$

is used to convert the initial set to $[0,\infty)$. By letting

$$Y\left(y,c_y\right)\Big|_{i,\zeta_y} = Y\left(y_i,\zeta_{y_m}\right) = Y_{i,m}$$

Eq. (5.14) can be rewritten as follows:

For $\zeta_{y_m} > 0$:

$$Y^{(k+1/2)}_{i+\frac{1}{2},m} = \frac{1}{(1+T0)}\left\{(1-T0)Y^{(k+1/2)}_{i-\frac{1}{2},m} + T0\left(Y^{M\ (k)}_{i+\frac{1}{2},m} + Y^{M\ (k)}_{i-\frac{1}{2},m}\right)\right\} \tag{5.28}$$

$$m = 1,2,\ldots,M \quad i = 1,2,\ldots,I$$

For $\zeta_{y_m} < 0$:

$$Y^{(k+1/2)}_{i-\frac{1}{2},m+M} = \frac{1}{(1-T0)}\left\{(1+T0)Y^{(k+1/2)}_{i+\frac{1}{2},m+M} - T0\left(Y^{M(k)}_{i+\frac{1}{2},m+M} + Y^{M(k)}_{i-\frac{1}{2},m+M}\right)\right\} \tag{5.29}$$

$$m = 1,2,\ldots,M \quad i = I, I-1,\ldots,1$$

In Eq. (11) ($\zeta_{y_m} < 0$), if we define

$$T0 = \frac{h\delta_0}{8|\zeta_m|}\left(\rho_{i+\frac{1}{2}} + \rho_{i-\frac{1}{2}}\right)^{(k)}\left(\tau_{i+\frac{1}{2}} + \tau_{i-\frac{1}{2}}\right)^{1-\omega^{(k)}} \tag{5.30}$$

then it is rewritten as

$$Y^{(k+1/2)}_{i-\frac{1}{2},m} = \frac{1}{(1+T0)}\left\{(1-T0)Y^{(k+1/2)}_{i+\frac{1}{2},m} + T0\left(Y^{M\ (k)}_{i+\frac{1}{2},m} + Y^{M\ (k)}_{i-\frac{1}{2},m}\right)\right\} \tag{5.31}$$

$$m = 1,2,\ldots,M \quad i = I, I-1,\ldots,1$$

Thus, the explicit expressions (5.29) and (5.31) for $\zeta_m > 0$ and $\zeta_m < 0$ respectively are of the same form and the same set of discrete set $\zeta_m \in [0,\infty)$ may be used. It is important to note that, at each iteration, the system of algebraic equations is solved by a marching scheme and no matrix inversion is required. For each discrete velocity the distribution functions are computed at each node explicitly, marching through the physical domain. Following this procedure, supplemented by a reasonable dense grid and an adequate large set of discrete velocities, we are able to obtain grid independent results with modest computational effort.

5.5 Evaluation of macroscopic quantities

Finally, having the values of Y and Φ it is necessary to integrate over ζ to obtain the macroscopic quantities needed for the next iteration namely, density, velocity and temperature as described in Eqs. (5.5a,b,c). We apply a double Gauss – Legendre quadrature scheme and for the density we have

$$\rho(y)=\int_{-\infty}^{\infty}\int_{-\infty}^{\infty}Y\left(y,\zeta_x,\zeta_y\right)d\zeta_x d\zeta_y=$$

$$\int_{0}^{\infty}\int_{0}^{\infty}Y\left(y,\zeta_x,\zeta_y\right)d\zeta_x d\zeta_y+\int_{0}^{\infty}\int_{-\infty}^{0}Y\left(y,-\zeta_x,\zeta_y\right)d\zeta_x d\zeta_y+$$

$$+\int_{-\infty}^{0}\int_{0}^{\infty}Y\left(y,\zeta_x,-\zeta_y\right)d\zeta_x d\zeta_y+\int_{-\infty}^{0}\int_{-\infty}^{0}Y\left(y,-\zeta_x,-\zeta_y\right)d\zeta_x d\zeta_y=$$

$$\int_{0}^{\infty}\int_{0}^{\infty}Y\left(y,\zeta_x,\zeta_y\right)d\zeta_x d\zeta_y+\int_{0}^{\infty}\int_{0}^{\infty}Y\left(y,-\zeta_x,\zeta_y\right)d\zeta_x d\zeta_y+$$

$$+\int_{0}^{\infty}\int_{0}^{\infty}Y\left(y,\zeta_x,-\zeta_y\right)d\zeta_x d\zeta_y+\int_{0}^{\infty}\int_{0}^{\infty}Y\left(y,-\zeta_x,-\zeta_y\right)d\zeta_x d\zeta_y=$$

$$=\sum_{m=1}^{M}\sum_{m=1}^{M}Y(y,\zeta_{x_m},\zeta_{y_m})w'_{x_m}w'_{y_m}+\sum_{m=M}^{2M}\sum_{m=1}^{M}Y(y,-\zeta_{x_m},\zeta_{y_m})w'_{x_m}w'_{y_m}+$$

$$+\sum_{m=1}^{M}\sum_{m=M}^{2M}Y(y,\zeta_{x_m},-\zeta_{y_m})w'_{x_m}w'_{y_m}+\sum_{m=M}^{2M}\sum_{m=M}^{2M}Y(y,-\zeta_{x_m},-\zeta_{y_m})w'_{x_m}w'_{y_m}=$$

$$=\sum_{m=1}^{M}\sum_{m=1}^{M}Y(y,\zeta_{x_m},\zeta_{y_m})w'_{x_m}w'_{y_m}+\sum_{m=M}^{2M}\sum_{m=1}^{M}Y(y,|\zeta_{x_m}|,\zeta_{y_m})w'_{x_m}w'_{y_m}+$$

$$+\sum_{m=1}^{M}\sum_{m=M}^{2M}Y(y,\zeta_{x_m},|\zeta_{y_m}|)w'_{x_m}w'_{y_m}+\sum_{m=M}^{2M}\sum_{m=M}^{2M}Y(y,|\zeta_{x_m}|,|\zeta_{y_m}|)w'_{x_m}w'_{y_m}$$

Here, as mentioned above, ζ_{x_m} and ζ_{y_m}, $m=1,2,\ldots,M$ are the roots of the Legendre polynomials of order M and $w_{x_m}=w_{y_m}$ the corresponding weights. It is noted that weights w'_{x_m}, w'_{y_m} and w_{x_m}, w_{y_m} related by

$$w'_{x_m}=\frac{2w_{x_m}}{\left(1-c_{x_m}\right)^2},\ w'_{y_m}=\frac{2w_{y_m}}{\left(1-c_{y_m}\right)^2} \tag{5.32}$$

The other macroscopic quantities are evaluated in a similar manner.

6

Analytical Solutions and Closed Form Expressions

6.1 Free molecular regime

In the free molecular regime the rarefaction parameter $\delta = 0$ and therefore the governing equations are significantly simplified. It is easily justified that since the problem is one dimensional in space, the distribution functions will be constant between the two plates. In the case of the free molecular flow there are no collisions between molecules. This means that the particles emitted from the boundaries are travelling through the domain without changing their molecular velocity. Then, it is reasonable to expect that the distribution function at any point between the plates is identical to the bottom and top boundary distributions for $c_y > 0$ and $c_y < 0$ respectively.

At the lower wall

$$g^+\left(-\frac{1}{2},\boldsymbol{c}\right) = g_1^+ = \frac{\rho_1}{\left[\pi(1+\beta)\right]^{3/2}} \exp\left(-\frac{\left[(c_x+U_0)^2 + c_y^2 + c_z^2\right]}{(1+\beta)}\right), \qquad c_y > 0 \qquad (6.1)$$

and at the upper wall

$$g^+\left(\frac{1}{2},\boldsymbol{c}\right) = g_2^+ = \frac{\rho_2}{\left[\pi(1-\beta)\right]^{3/2}} \exp\left(-\frac{\left[(c_x-U_0)^2 + c_y^2 + c_z^2\right]}{(1-\beta)}\right), \qquad c_y < 0 \qquad (6.2)$$

In order to compute the macroscopic quantities of practical interest for the flow, we make use of the corresponding moments as they are described in Section 3 (Eqs. 3.22a-j).

For the estimation of density we have

$$\rho_{fm} = \int_{-\infty}^{+\infty}\int_{-\infty}^{+\infty}\int_{-\infty}^{+\infty} g\,dc_x dc_y dc_z = \int_{-\infty}^{+\infty}\int_{-\infty}^{+\infty}\left[\int_{-\infty}^{0} g\,dc_y\right] dc_x dc_z + \int_{-\infty}^{+\infty}\int_{-\infty}^{+\infty}\left[\int_{0}^{+\infty} g\,dc_y\right] dc_x dc_z \Rightarrow$$

$$\rho_{fm}(y) = \frac{1}{2}(\rho_1 + \rho_2) \qquad (6.3)$$

Also using the mean density we write

$$n_0 = \frac{1}{L}\int_{-\frac{L}{2}}^{\frac{L}{2}} n(\hat{y})\,d\hat{y} \Rightarrow Ln_0 = n_0 L\int_{-\frac{1}{2}}^{\frac{1}{2}} \rho_{fm}(y)\,dy \Rightarrow \int_{-\frac{1}{2}}^{\frac{1}{2}} \rho_{fm}(y)\,dy = 1 = \frac{1}{2}(\rho_1 + \rho_2) \qquad (6.4)$$

For the computation of ρ_1 and ρ_2 we make use of the no-penetration condition at the walls in the y direction. According to this condition, the normal component of the velocity vector in both the upper and lower wall equal zero.

$$u_y^{fm} = \frac{1}{\rho}\int_{-\infty}^{+\infty}\int_{-\infty}^{+\infty}\int_{-\infty}^{+\infty} g c_y dc_x dc_y dc_z = \frac{1}{\rho}\int_{-\infty}^{+\infty}\int_{-\infty}^{+\infty}\left[\int_{-\infty}^{0} g c_y dc_y\right] dc_x dc_z + \frac{1}{\rho}\int_{-\infty}^{+\infty}\int_{-\infty}^{+\infty}\left[\int_{0}^{+\infty} g c_y dc_y\right] dc_x dc_z \Rightarrow$$

$$u_y^{fm} = \frac{1}{\rho}\int_{-\infty}^{+\infty}\int_{-\infty}^{+\infty}\int_{-\infty}^{0} \frac{\rho_2}{\left[\pi(1-\beta)\right]^{3/2}} e^{-\frac{\left[(c_x-U_0)^2+c_y^2+c_z^2\right]}{1-\beta}} c_y dc_y dc_x dc_z +$$

$$+\frac{1}{\rho}\int_{-\infty}^{+\infty}\int_{-\infty}^{+\infty}\int_{0}^{+\infty} \frac{\rho_1}{\left[\pi(1+\beta)\right]^{3/2}} e^{-\frac{\left[(c_x+U_0)^2+c_y^2+c_z^2\right]}{1+\beta}} c_y dc_y dc_x dc_z \Rightarrow$$

$$u_y^{fm} = \frac{1}{\rho}\left[-\frac{\rho_2\sqrt{(1-\beta)}}{\pi^{3/2}}\int_{-\infty}^{+\infty}\int_{-\infty}^{+\infty}\int_{0}^{+\infty} e^{-c_x'^2-c_y'^2-c_z'^2} c_y' dc_y' dc_x' dc_z' +\right.$$

$$\left.+\frac{\rho_1\sqrt{(1+\beta)}}{\pi^{3/2}}\int_{-\infty}^{+\infty}\int_{-\infty}^{+\infty}\int_{0}^{+\infty} e^{-c_x'^2-c_y'^2-c_z'^2} c_y' dc_y' dc_x' dc_z'\right] \Rightarrow$$

$$u_y^{fm} = \frac{1}{2\rho\sqrt{\pi}}\left[-\rho_2\sqrt{(1-\beta)}+\rho_1\sqrt{(1+\beta)}\right] = 0 \Rightarrow$$

$$\rho_2^{fm}\sqrt{(1-\beta)} = \rho_1^{fm}\sqrt{(1+\beta)} \qquad (6.5)$$

By combining equations (6.4) and (6.5) we conclude

$$\rho_1^{fm} = \frac{2\sqrt{(1-\beta)}}{\sqrt{(1+\beta)}+\sqrt{(1-\beta)}} \qquad (6.6)$$

and

$$\rho_2^{fm} = \frac{2\sqrt{(1+\beta)}}{\sqrt{(1+\beta)}+\sqrt{(1-\beta)}} \qquad (6.7)$$

Table 6.1: *Free molecular analytical solution for the density parameters* ρ_1^{fm} *and* ρ_2^{fm}

β	U_0							
	0		0.1		0.3		0.5	
0	-	-	1.0000	1.0000	1.0000	1.0000	1.0000	1.0000
0.1	0.9499	1.0501	0.9499	1.0501	0.9499	1.0501	0.9499	1.0501
0.5	0.7321	1.2679	0.7321	1.2679	0.7321	1.2679	0.7321	1.2679
0.9	0.3732	1.6268	0.3732	1.6268	0.3732	1.6268	0.3732	1.6268

The behavior of ρ_1^{fm}, ρ_2^{fm} in terms of β and U_0 is shown in Table 6.1. At each β the first column refers to the values of the values of the ρ_1^{fm} parameter, while the second refers to the ρ_2^{fm}. We can see that the increase of the parameter β of the flow increases the density parameter at the upper cold wall and decreases it at the lower hot wall. This can be easily explained since the density parameter is expected to be proportional the inverse of the temperature. At this point we should stress out that the density of the gas inside the flow domain for all the cases in the free molecular regime is constant and equals to one as described already by Eq. (6.4).

For the estimation of the axial velocity we have

$$u_x^{fm} = \frac{1}{\rho}\int_{-\infty}^{+\infty}\int_{-\infty}^{+\infty}\int_{-\infty}^{+\infty} gc_x dc_x dc_y dc_z = \frac{1}{\rho}\int_{-\infty}^{+\infty}\int_{-\infty}^{+\infty}\left[\int_{-\infty}^{0} gc_x dc_y\right] dc_x dc_z + \frac{1}{\rho}\int_{-\infty}^{+\infty}\int_{-\infty}^{+\infty}\left[\int_{0}^{+\infty} gc_x dc_y\right] dc_x dc_z \Rightarrow$$

$$u_x^{fm} = \frac{1}{\rho}\int_{-\infty}^{+\infty}\int_{-\infty}^{+\infty}\int_{-\infty}^{0} \frac{\rho_2}{\left[\pi(1-\beta)\right]^{3/2}} e^{-\frac{\left[(c_x-U_0)^2+c_y^2+c_z^2\right]}{1-\beta}} c_x dc_y dc_x dc_z +$$

$$+\frac{1}{\rho}\int_{-\infty}^{+\infty}\int_{-\infty}^{+\infty}\int_{0}^{+\infty} \frac{\rho_1}{\left[\pi(1+\beta)\right]^{3/2}} e^{-\frac{\left[(c_x+U_0)^2+c_y^2+c_z^2\right]}{1+\beta}} c_x dc_y dc_x dc_z \Rightarrow$$

$$u_x^{fm} = \frac{1}{\rho}\left[\frac{\rho_2\sqrt{(1-\beta)}}{\pi^{3/2}}\int_{-\infty}^{+\infty}\int_{-\infty}^{+\infty}\int_{0}^{+\infty} e^{-c_x'^2-c_y'^2-c_z'^2}\frac{\left(c_x'+U_0\right)}{\sqrt{(1-\beta)}} dc_y' dc_x' dc_z' +\right.$$

$$\left.+\frac{\rho_1\sqrt{(1+\beta)}}{\pi^{3/2}}\int_{-\infty}^{+\infty}\int_{-\infty}^{+\infty}\int_{0}^{+\infty} e^{-c_x'^2-c_y'^2-c_z'^2}\frac{\left(c_x'-U_0\right)}{\sqrt{(1+\beta)}} dc_y' dc_x' dc_z'\right] \Rightarrow$$

$$u_x^{fm} = \frac{1}{2\rho^{fm}}\left[\rho_2^{fm}U_0 - \rho_1^{fm}U_0\right] = \frac{U_0}{2}\left(\rho_2^{fm} - \rho_1^{fm}\right) \tag{6.8}$$

Introducing Eqs. (6.6) and (6.7) for ρ_1^{fm} and ρ_2^{fm} into Eq. (6.8) we find the following closed form expression:

$$u_x^{fm} = U_0 \frac{\sqrt{(1+\beta)} - \sqrt{(1-\beta)}}{\sqrt{(1+\beta)} + \sqrt{(1-\beta)}} \tag{6.9}$$

From Eq. (6.9) it is seen that when the walls are stationary ($U_0 = 0$) or isothermal ($\beta = 0, \pm U_0 = 0$), the axial velocity is zero. The behavior of u_x^{fm} in terms of β and U_0 is seen in Table 6.2. The increase of the temperature difference between the plates also increases the deviation between the velocity of the flow and the equilibrium velocity. We can also see that the increase of the β parameter of the flow increases the velocity of the flow in a non-linear way, while the increase of the velocity at the wall leads to a linear increase at the velocity of the flow.

Following similar mathematical manipulations for the temperature we define

$$\tau^{fm} = \frac{2}{3\rho}\int_{-\infty}^{+\infty}\int_{-\infty}^{+\infty}\int_{-\infty}^{+\infty} g\left(c-u\right)^2 dc_x dc_y dc_z = \frac{2}{3\rho}\int_{-\infty}^{+\infty}\int_{-\infty}^{+\infty}\left[\int_{-\infty}^{0} g\left(c-u\right)^2 dc_y\right] dc_x dc_z +$$

$$+\frac{2}{3\rho}\int_{-\infty}^{+\infty}\int_{-\infty}^{+\infty}\left[\int_{0}^{+\infty} g\left(c-u\right)^2 dc_y\right] dc_x dc_z \Rightarrow$$

Table 6.2: *Free molecular analytical solution for the axial velocity of the flow.*

β	U_0			
	0	0.1	0.3	0.5
0	-	0.000000	0.000000	0.000000
0.1	0.000000	0.005012	0.015038	0.025083
0.5	0.000000	0.026795	0.080385	0.133975
0.9	0.000000	0.062679	0.180804	0.313395

$$\tau^{fm}=\frac{2}{3\rho}\int_{-\infty}^{+\infty}\int_{-\infty}^{+\infty}\int_{-\infty}^{0}\frac{\rho_2}{\left[\pi(1-\beta)\right]^{3/2}}e^{\frac{\left[(c_x-U_0)^2+c_y^2+c_z^2\right]}{1-\beta}}\left[\left(c_x-u_{x_{fm}}\right)^2+c_y^2+c_z^2\right]dc_y dc_x dc_z+$$

$$+\frac{2}{3\rho}\int_{-\infty}^{+\infty}\int_{-\infty}^{+\infty}\int_{0}^{+\infty}\frac{\rho_1}{\left[\pi(1+\beta)\right]^{3/2}}e^{\frac{\left[(c_x+U_0)^2+c_y^2+c_z^2\right]}{1+\beta}}\left[\left(c_x-u_{x_{fm}}\right)^2+c_y^2+c_z^2\right]dc_y dc_x dc_z \Rightarrow$$

$$\tau^{fm}=\frac{2}{3\rho}\left[\frac{\rho_2^{fm}}{4}\left(3(1-\beta)+2\left(U_0-u_x^{fm}\right)^2\right)+\frac{\rho_1^{fm}}{4}\left(3(1+\beta)+2\left(U_0+u_x^{fm}\right)^2\right)\right]. \qquad (6.10)$$

Introducing Eqs. (6.6), (6.7) for ρ_1^{fm} and ρ_2^{fm} and Eq. (6.9) for u_x^{fm} into Eq. (6.10) we find the following closed form expression:

$$\tau^{fm}=\sqrt{(1-\beta)}\sqrt{(1+\beta)}\left(1+\frac{8U_0^2}{3\left(\sqrt{(1-\beta)}+\sqrt{(1+\beta)}\right)^2}\right) \qquad (6.11)$$

From the form of the equation it is easily concluded that for the cases where there walls are isothermal ($\beta=0$), the temperature distribution equals $1+8U_0^2/3$. For the cases where the parameter β does not change, the increase of the velocity at the plates introduces more compressibility in the flow and this phenomenon is expressed via the increase of deviation between the temperature of the flow and the reference temperature. The detailed behaviour of τ^{fm} in terms of β and U_0 is seen in Table 6.3. For the cases that $U_0=0$ and $U_0=0.1$, for the same value of β, there is a small change in the temperature. The increase of the temperature ratio between the plates, decreases the values of the temperature distributions computed. For these small velocities imposed at the wall, the flow can be treated as incompressible.

Table 6.3: *Free molecular analytical solution for the temperature of the flow.*

β	U_0			
	0	0.1	0.3	0.5
0	-	1.000067	1.060000	1.666667
0.1	0.994987	1.001637	1.054837	1.161235
0.5	0.866025	0.872213	0.921718	1.020726
0.9	0.435890	0.439937	0.472318	0.537079

.By using the suitable moments, the axial heat flux is found to be

$$q_x^{fm} = \int_{-\infty}^{+\infty}\int_{-\infty}^{+\infty}\int_{-\infty}^{+\infty} g(c-u)^2 (c_x-u_x)\,dc_x dc_y dc_z = \int_{-\infty}^{+\infty}\int_{-\infty}^{+\infty}\left[\int_{-\infty}^{0} g(c-u)^2 (c_x-u_x)\,dc_y\right] dc_x dc_z +$$

$$+\int_{-\infty}^{+\infty}\int_{-\infty}^{+\infty}\left[\int_{0}^{+\infty} g(c-u)^2 (c_x-u_x)\,dc_y\right] dc_x dc_z \Rightarrow$$

$$q_x^{fm} = \int_{-\infty}^{+\infty}\int_{-\infty}^{+\infty}\int_{-\infty}^{0} \frac{\rho_2}{\left[\pi(1-\beta)\right]^{3/2}} e^{-\frac{\left[(c_x-U_0)^2+c_y^2+c_z^2\right]}{1-\beta}} \left[\left(c_x-u_{x_{fm}}\right)^2 + c_y^2 + c_z^2\right]\left(c_x-u_{x_{fm}}\right) dc_y dc_x dc_z +$$

$$+\int_{-\infty}^{+\infty}\int_{-\infty}^{+\infty}\int_{0}^{+\infty} \frac{\rho_1}{\left[\pi(1+\beta)\right]^{3/2}} e^{-\frac{\left[(c_x+U_0)^2+c_y^2+c_z^2\right]}{1+\beta}} \left[\left(c_x-u_{x_{fm}}\right)^2 + c_y^2 + c_z^2\right]\left(c_x-u_{x_{fm}}\right) dc_y dc_x dc_z \Rightarrow$$

$$q_x^{fm} = \left[\frac{\rho_2^{fm}}{4}\left(U_0-u_x^{fm}\right)\left(5(1-\beta)+2\left(U_0-u_x^{fm}\right)^2\right) - \frac{\rho_1^{fm}}{4}\left(U_0+u_x^{fm}\right)\left(5(1+\beta)+2\left(U_0+u_x^{fm}\right)^2\right)\right] \tag{6.12}$$

Introducing Eqs. (6.6), (6.7) for ρ_1^{fm} and ρ_2^{fm} and Eq. (6.9) for u_x^{fm} into Eq. (6.12) we yield

$$q_x^{fm} = -\frac{2U_0\left[\left(\sqrt{(1-\beta)}-\sqrt{(1+\beta)}\right)\left(5\beta^2+4U_0^2\right)+\beta\left(\sqrt{(1-\beta)}+\sqrt{(1+\beta)}\right)\left(5+4U_0^2\right)\right]}{\left(\sqrt{(1-\beta)}+\sqrt{(1+\beta)}\right)^3} \tag{6.13}$$

From the form of the equation it is easily concluded that for the cases where the walls are stationary ($U_0 = 0$) or isothermal ($\beta = 0$), the axial heat flux is zero. The detailed behaviour of q_x^{fm} in terms of β and U_0 is shown in Table 6.4. When the parameter β does not change, the increase of the velocity at the plates leads to an increase of the axial heat flux. Also, as β is increased, the absolute value of the axial heat flux increased. This means that, the unexpected horizontal heat flux is increased as the temperature and the velocity gradients between the plates are increased, provided that the flow is sufficiently rarefied. The heat flux computed is always negative, i.e. opposite to the direction of the cold (upper) moving plate. Further more, the increase of the temperature ratio at the plates also decreases the heat flux. The quantitative behavior of the axial heat flux in the flow can be seen in Table 6.4.

For the case of the normal heat flux of the flow, similar procedure is followed. Making use of the corresponding moment and introducing similar mathematical manipulations we find

$$q_y^{fm} = \int_{-\infty}^{+\infty}\int_{-\infty}^{+\infty}\int_{-\infty}^{+\infty} g\left(c-u\right)^2 c_y dc_x dc_y dc_z = \int_{-\infty}^{+\infty}\int_{-\infty}^{+\infty}\left[\int_{-\infty}^{0} g\left(c-u\right)^2 c_y dc_y\right] dc_x dc_z +$$

$$+ \int_{-\infty}^{+\infty}\int_{-\infty}^{+\infty}\left[\int_{0}^{+\infty} g\left(c-u\right)^2 c_y dc_y\right] dc_x dc_z \Rightarrow$$

$$q_y^{fm} = \int_{-\infty}^{+\infty}\int_{-\infty}^{+\infty}\int_{-\infty}^{0} \frac{\rho_2}{\left[\pi\left(1-\beta\right)\right]^{3/2}} e^{-\frac{\left[\left(c_x-U_0\right)^2+c_y^2+c_z^2\right]}{1-\beta}} \left[\left(c_x-u_{x_{fm}}\right)^2 + c_y^2 + c_z^2\right] c_y dc_y dc_x dc_z +$$

$$+ \int_{-\infty}^{+\infty}\int_{-\infty}^{+\infty}\int_{0}^{+\infty} \frac{\rho_1}{\left[\pi\left(1+\beta\right)\right]^{3/2}} e^{-\frac{\left[\left(c_x+U_0\right)^2+c_y^2+c_z^2\right]}{1+\beta}} \left[\left(c_x-u_{x_{fm}}\right)^2 + c_y^2 + c_z^2\right] c_y dc_y dc_x dc_z \Rightarrow$$

$$q_y^{fm} = \left[-\frac{\rho_2^{fm}\sqrt{(1-\beta)}}{2\sqrt{\pi}}\left(2(1-\beta)+\left(U_0-u_x^{fm}\right)^2\right) + \frac{\rho_1^{fm}\sqrt{(1+\beta)}}{2\sqrt{\pi}}\left(2(1+\beta)+\left(U_0+u_x^{fm}\right)^2\right)\right] \tag{6.14}$$

Introducing Eqs. (6.6), (6.7) for ρ_1^{fm} and ρ_2^{fm} and Eq. (6.9) for u_x^{fm} into Eq. (6.14) we find the following closed form expression:

$$q_y^{fm} = \frac{2\left[\left(\sqrt{(1-\beta)}-\sqrt{(1+\beta)}\right)\left(\beta^2+U_0^2\right)+\beta\left(\sqrt{(1-\beta)}+\sqrt{(1+\beta)}\right)\left(1+U_0^2\right)\right]}{\sqrt{\pi}\left(1+\sqrt{1-\beta^2}\right)} \tag{6.15}$$

Table 6.4: *Free molecular analytical solution for axial heat flux (q_x^{fm}).*

β	U_0			
	0	0.1	0.3	0.5
0	-	0.000000	0.000000	0.000000
0.1	0.000000	-0.025037	-0.077512	-0.137186
0.5	0.000000	-0.116523	-0.361507	-0.642305
0.9	0.000000	-0.137367	-0.430366	-0.778164

From the form of the equation it is easily concluded that for the cases where there walls are isothermal ($\beta = 0$), the normal heat flux equals zero. The detailed behaviour of q_y^{fm} in terms of β and U_0 is shown in Table 6.5. For the cases where the parameter β does not change, the increase of the velocity at the plates introduces an increase in the corresponding values of the heat flux, while, on the other hand, the increase of the temperature ratio between the plates, increases the normal heat flux in a more drastic way.

Moreover, macroscopic quantities of major importance for the flow are the stresses (normal and shear). The evaluation of the normal stress in the x direction is

$$\sigma_{xx}^{fm} = \int_{-\infty}^{+\infty}\int_{-\infty}^{+\infty}\int_{-\infty}^{+\infty} g\left(c_x - u_x\right)^2 dc_x dc_y dc_z = \int_{-\infty}^{+\infty}\int_{-\infty}^{+\infty}\left[\int_{-\infty}^{0} g\left(c_x - u_x\right)^2 c_y dc_y\right] dc_x dc_z +$$

$$+ \int_{-\infty}^{+\infty}\int_{-\infty}^{+\infty}\left[\int_{0}^{+\infty} g\left(c_x - u_x\right)^2 c_y dc_y\right] dc_x dc_z \Rightarrow$$

$$\sigma_{xx}^{fm} = \int_{-\infty}^{+\infty}\int_{-\infty}^{+\infty}\int_{-\infty}^{0} \frac{\rho_2}{\left[\pi\left(1-\beta\right)\right]^{3/2}} e^{-\frac{\left[\left(c_x - U_0\right)^2 + c_y^2 + c_z^2\right]}{1-\beta}} \left(c_x - u_x^{fm}\right)^2 dc_y dc_x dc_z +$$

$$+ \int_{-\infty}^{+\infty}\int_{-\infty}^{+\infty}\int_{0}^{+\infty} \frac{\rho_1}{\left[\pi\left(1+\beta\right)\right]^{3/2}} e^{-\frac{\left[\left(c_x + U_0\right)^2 + c_y^2 + c_z^2\right]}{1+\beta}} \left(c_x - u_x^{fm}\right)^2 dc_y dc_x dc_z \Rightarrow$$

$$\sigma_{xx}^{fm} = \left[\frac{\rho_2}{4}\left(\sqrt{(1-\beta)} + 2\left(U_0 + u_x^{fm}\right)^2\right) + \frac{\rho_1}{4}\left(\sqrt{(1+\beta)} + 2\left(U_0 - u_x^{fm}\right)^2\right)\right]. \qquad (6.16)$$

Table 6.5: *Free molecular analytical solution for normal heat flux (q_y^{fm}).*

β	U_0			
	0	0.1	0.3	0.5
0	-	0.000000	0.000000	0.000000
0.1	0.112413	0.112977	0.117485	0.126500
0.5	0.505839	0.508549	0.530236	0.573608
0.9	0.522431	0.526069	0.555176	0.613390

Introducing Eqs. (6.6) and (6.7) for ρ_1^{fm} and ρ_2^{fm} into Eq. (6.16) we yield:

$$\sigma_{xx}^{fm} = \frac{1-\beta^2+\left(\sqrt{1-\beta^2}\right)\left(1+4U_0^2\right)}{\left(\sqrt{(1-\beta)}+\sqrt{(1+\beta)}\right)^2} \tag{6.17}$$

The quantitative behavior of the x-normal stress can be seen in Table 6.6. The increase of the velocity at the walls leads to a significant increase of the computed stress. On the other hand, the increase of the temperature difference between the plates decreases the normal stress of the flow but only when parameter β acquires high values. In small velocities, the computed stress remains quite the same.

In a similar manner we have

$$\sigma_{yy}^{fm} = \int_{-\infty}^{+\infty}\int_{-\infty}^{+\infty}\int_{-\infty}^{+\infty} g\left(c_y-u_y\right)^2 dc_x dc_y dc_z = \int_{-\infty}^{+\infty}\int_{-\infty}^{+\infty}\left[\int_{-\infty}^{0} gc_y^2 dc_y\right] dc_x dc_z +$$

$$+\int_{-\infty}^{+\infty}\int_{-\infty}^{+\infty}\left[\int_{0}^{+\infty} gc_y^2 dc_y\right] dc_x dc_z \Rightarrow$$

$$\sigma_{yy}^{fm} = \int_{-\infty}^{+\infty}\int_{-\infty}^{+\infty}\int_{-\infty}^{0} \frac{\rho_2}{\left[\pi(1-\beta)\right]^{3/2}} e^{-\frac{\left[(c_x-U_0)^2+c_y^2+c_z^2\right]}{1-\beta}} c_y^2 dc_y dc_x dc_z +$$

$$+\int_{-\infty}^{+\infty}\int_{-\infty}^{+\infty}\int_{0}^{+\infty} \frac{\rho_1}{\left[\pi(1+\beta)\right]^{3/2}} e^{-\frac{\left[(c_x+U_0)^2+c_y^2+c_z^2\right]}{1+\beta}} c_y^2 dc_y dc_x dc_z \Rightarrow$$

$$\sigma_{yy}^{fm} = \frac{1}{4}\left[\rho_2^{fm}(1-\beta)+\rho_1^{fm}(1+\beta)\right]. \tag{6.18}$$

Table 6.6: *Free molecular analytical solution for normal stress* σ_{xx}.

β	U_0			
	0	0.1	0.3	0.5
0	-	0.510000	0.590000	0.750000
0.1	0.497494	0.507469	0.587268	0.746866
0.5	0.433013	0.442295	0.516551	0.665064
0.9	0.217945	0.224016	0.272587	0.369729

Introducing Eqs. (6.6) and (6.7) for ρ_1^{fm} and ρ_2^{fm} into Eq. (6.18) we find the following closed form expression:

$$\sigma_{yy}^{fm} = \frac{\sqrt{1-\beta^2}}{2} \quad . \tag{6.19}$$

The values of the y-normal stress are independent of U_0. The detailed behaviour of σ_{yy}^{fm} in terms of β and U_0 is shown in Table 6.7. The increase of the temperature difference between the plates decreases the stress of the flow, especially for the cases where parameter β acquires high values. In large temperature differences, the evaluated stress is less than the half computed in small values of the β parameter.

Finally, the normal stress in the z direction of the flow is found

$$\sigma_{zz}^{fm} = \int_{-\infty}^{+\infty}\int_{-\infty}^{+\infty}\int_{-\infty}^{+\infty} g\left(c_z - u_z\right)^2 dc_x dc_y dc_z = \int_{-\infty}^{+\infty}\int_{-\infty}^{+\infty}\left[\int_{-\infty}^{0} gc_z^2 dc_y\right] dc_x dc_z +$$

$$+\int_{-\infty}^{+\infty}\int_{-\infty}^{+\infty}\left[\int_{0}^{+\infty} gc_z^2 dc_y\right] dc_x dc_z \Rightarrow$$

$$\sigma_{zz}^{fm} = \int_{-\infty}^{+\infty}\int_{-\infty}^{+\infty}\int_{-\infty}^{0} \frac{\rho_2}{\left[\pi\left(1-\beta\right)\right]^{3/2}} e^{-\frac{\left[\left(c_x-U_0\right)^2+c_y^2+c_z^2\right]}{1-\beta}} c_z^2 dc_y dc_x dc_z +$$

$$+\int_{-\infty}^{+\infty}\int_{-\infty}^{+\infty}\int_{0}^{+\infty} \frac{\rho_1}{\left[\pi\left(1+\beta\right)\right]^{3/2}} e^{-\frac{\left[\left(c_x+U_0\right)^2+c_y^2+c_z^2\right]}{1+\beta}} c_z^2 dc_y dc_x dc_z \Rightarrow$$

$$\sigma_{zz}^{fm} = \frac{1}{4}\left[\rho_2^{fm}(1-\beta) + \rho_1^{fm}(1+\beta)\right]. \tag{6.20}$$

Introducing Eqs. (6.6) and (6.7) for ρ_1^{fm} and ρ_2^{fm} into Eq. (6.20) we find the following closed form expression:

$$\sigma_{zz}^{fm} = \frac{\sqrt{1-\beta^2}}{2} = \sigma_{yy}^{fm} \tag{6.21}$$

In this case as expected the behaviour of σ_{zz}^{fm} in terms of β and U_0 is identical to the one of σ_{yy}^{fm}.

Table 6.7: *Free molecular analytical solution for normal stresses* σ_{yy}= σ_{zz}.

β	U_0			
	0	0.1	0.3	0.5
0	-	0.500000	0.500000	0.500000
0.1	0.497494	0.497494	0.497494	0.497494
0.5	0.433013	0.433013	0.433013	0.433013
0.9	0.217945	0.217945	0.217945	0.217945

Probably the most important macroscopic quantity in this problem is the shear stress:

$$\sigma_{xy_{fm}} = \int_{-\infty}^{+\infty}\int_{-\infty}^{+\infty}\int_{-\infty}^{+\infty} f\left(c_x-u_x\right)\left(c_y-u_y\right)dc_x dc_y dc_z = \int_{-\infty}^{+\infty}\int_{-\infty}^{+\infty}\left[\int_{-\infty}^{0} f\left(c_x-u_x\right)c_y dc_y\right]dc_x dc_z +$$

$$+\int_{-\infty}^{+\infty}\int_{-\infty}^{+\infty}\left[\int_{0}^{+\infty} f\left(c_x-u_x\right)c_y dc_y\right]dc_x dc_z \Rightarrow$$

$$\sigma_{xy_{fm}} = \int_{-\infty}^{+\infty}\int_{-\infty}^{+\infty}\int_{-\infty}^{0}\frac{\rho_2}{\left[\pi\left(1-\beta\right)\right]^{3/2}} e^{-\frac{\left[\left(c_x-U_0\right)^2+c_y^2+c_z^2\right]}{1-\beta}}\left(c_x-u_{x_{fm}}\right)c_y dc_y dc_x dc_z +$$

$$+\int_{-\infty}^{+\infty}\int_{-\infty}^{+\infty}\int_{0}^{+\infty}\frac{\rho_1}{\left[\pi\left(1+\beta\right)\right]^{3/2}} e^{-\frac{\left[\left(c_x+U_0\right)^2+c_y^2+c_z^2\right]}{1+\beta}}\left(c_x-u_{x_{fm}}\right)c_y dc_y dc_x dc_z \Rightarrow$$

$$\sigma_{xy_{fm}} = \left[-\frac{\rho_2\sqrt{(1-\beta)}}{2\sqrt{\pi}}\left(U_0-u_{x_{fm}}\right)-\frac{\rho_1\sqrt{(1+\beta)}}{2\sqrt{\pi}}\left(U_0+u_{x_{fm}}\right)\right]. \tag{6.22}$$

Introducing Eqs. (6.6), (6.7) for ρ_1^{fm} and ρ_2^{fm} and Eq. (6.9) for u_x^{fm} into Eq. (6.22) we find the following closed form expression:

$$\sigma_{xy}^{fm} = -\frac{2U_0\sqrt{1-\beta^2}}{\sqrt{\pi}\left(\sqrt{(1-\beta)}+\sqrt{(1+\beta)}\right)}. \tag{6.23}$$

The quantitative behavior of the shear stress can be seen in Table 6.8. As it can be noted from the equation above, the influence of both U_0 and β imposed at the plates of the flow geometry is of great importance. In general, the shear stress computed is always

Table 6.8: *Free molecular analytical solution for shear stress (σ_{xy}^{fm}).*

β	U_0			
	0	0.1	0.3	0.5
0	-	-0.056419	-0.169257	-0.282095
0.1	0.000000	-0.056207	-0.168620	-0.281033
0.5	0.000000	-0.050584	-0.151752	-0.252919
0.9	0.000000	-0.029024	-0.087072	-0.145120

negative, opposite to the direction of the cold (upper) moving plate, behaving in a similar manner with the axial heat flux. The increase of the velocity at the walls leads to a significant increase of the absolute computed stress. However, the increase of the temperature difference between the plates decreases the absolute shear stress.

6.2 Hydrodynamic regime

In order to verify the validity of the proposed method and the computed results, a comparison between the analytical results via the implementation of the Navier Stokes equations and the corresponding numerical ones at the hydrodynamic limit is presented [Liu, 1962]. In obtaining such a solution, the medium is assumed to be a perfect gas with a viscosity μ directly proportional to the absolute temperature. This behaviour is the one of a Maxwell molecule. It is noted that although $\mu = \mu(T)$ and $k = k(T)$, the Prandtl number $\left(\mathrm{Pr} = \mu \cdot c_p / k\right)$ remains constant.

The Navier Stokes equations that describe the physics of the problem are

$$\frac{d}{dy}\left(\mu \frac{du}{dy}\right) = 0 \tag{6.24}$$

$$\frac{dP}{dy} = 0 \tag{6.25}$$

and

$$\frac{d}{dy}\left(\frac{k}{c_p}\frac{d}{dy}\left(c_pT\right)\right)+\mu\left(\frac{du}{dy}\right)^2=0 \tag{6.26}$$

Equations (6.24) and (6.25) are the momentum equations and Eq. (6.26) is the energy equation. For the closure of the problem we have to define the boundary conditions that characterize the flow domain. At $y=H/2$, $u=U_0$ and $T=T_1$, while at $y=-H/2$, $u=-U_0$ and $T=T_2$.

Integration of Eq. (6.24) and (6.26) yields

$$\mu\frac{du}{dy}=b_1 \tag{6.27}$$

and

$$c_pT+\left(\frac{\mathrm{Pr}}{2}\right)u^2-\left(\frac{b_2}{b_1}\right)u=b_3 \tag{6.28}$$

respectively, where b_1, b_2, b_3 are the unknown constants. At the present, we introduce the quantity μ_2 which denotes the viscosity coefficient evaluated at the temperature T_2. By integrating Eq. (6.27) for one more time we conclude

$$\int\frac{\mu}{\mu_2}du=\frac{b_1y+b_4}{\mu_2} \tag{6.29}$$

where b_4 is another unknown constant. Since we are implementing Maxwell intermolecular model ($\omega=1$) the viscosity is proportional to temperature according to

$$\frac{\mu}{\mu_2}=\frac{T}{T_2} \tag{6.30}$$

By using Eq. (6.30) and integrating Eq. (6.23) we finally obtain

$$\frac{1}{c_pT_2}\left[b_3u+\frac{b_2}{b_1}u^2-\frac{\mathrm{Pr}}{6}u^3\right]=\frac{b_1}{\mu_2}y+\frac{b_4}{\mu_2} \tag{6.31}$$

The four unknown constants that appear in Eq. (6.28) and (6.31) are defined by the four boundary conditions. The solution of the system yields

$$b_1=\frac{\mu_2U_0\left[3c_p\left(T_1+T_2\right)+2\,\mathrm{Pr}\,U_0^2\right]}{3c_pHT_2} \tag{6.32}$$

$$b_2 = \frac{\mu_2 (T_1 - T_2)\left[3c_p (T_1 + T_2) + 2\,\mathrm{Pr}\, U_0^2\right]}{6HT_2} \tag{6.33}$$

$$b_3 = \frac{c_p (T_1 + T_2) + \mathrm{Pr}\, U_0^2}{2} \tag{6.34}$$

$$b_4 = \frac{\mu_2 (T_1 - T_2) U_0}{4T_2} \tag{6.35}$$

Substituting Eqs. (6.32-6.35) into Eq. (6.31) we find

$$\left(\frac{1}{2}\left(1+\frac{T_1}{T_2}\right)+\frac{\gamma-1}{2}\mathrm{Pr}\, Ma^2\right)\frac{u}{U_0}-\frac{1}{4}\left(1-\frac{T_1}{T_2}\right)\left(\frac{u}{U_0}\right)^2-\frac{\gamma-1}{6}\mathrm{Pr}\, Ma^2\left(\frac{u}{U_0}\right)^3 = \left(1+\frac{T_1}{T_2}+\frac{2(\gamma-1)}{3}\mathrm{Pr}\, Ma^2\right)y-\frac{1}{4}\left(1-\frac{T_1}{T_2}\right) \tag{6.36}$$

where $Ma = U_0 / c_0$ is the Mach number and $\gamma = c_p / \left(c_p - R\right)$ where R is the specific gas constant. Equation (6.36) is solved in an iterative manner by implementing the Newton –Raphson algorithm. Next we substitute Eqs. (6.32-6.35) into Eq. (6.28) to find

$$\frac{T}{T_2}+\frac{\gamma-1}{2}\mathrm{Pr}\, Ma^2\left(\frac{u}{U}\right)^2+\frac{1}{2}\left(1-\frac{T_1}{T_2}\right)\frac{u}{U}=\frac{1}{2}\left(1+\frac{T_1}{T_2}\right)+\frac{\gamma-1}{2}\mathrm{Pr}\, Ma^2. \tag{6.37}$$

This equation can be easily solved for $T(y)$ provided that the velocity $u(y)$ is known from Eq. (6.36). Equation (6.36) and (6.37) are used to compare with the kinetic solution at $\delta = 100$. This is possible by setting $\gamma = 5/3$, $\mathrm{Pr} = 2/3$ and $Ma = U_0\sqrt{2/\gamma}$.

6.3 Conservation Principles

In this section, conservation principles through the moments of the reduced kinetic equations are presented. The macroscopic quantities of the axial and normal velocities, the temperature, the heat fluxes and the shear stress are used in order to produce these principals. As it has already been mentioned in previous chapters, the corresponding expressions described by Eqs. (4.43a-g) are valid for both the BGK and the S models.

For the conservation of mass flow we take the zeroth moment of Eq. (4.28):

$$\frac{\partial}{\partial y}\int_{-\infty}^{+\infty} c_y Y dc_y + \delta_0 \rho \tau^{1-\omega}\int_{-\infty}^{+\infty} Y dc_y = \delta_0 \rho \tau^{1-\omega}\int_{-\infty}^{+\infty} Y^M dc_y \Rightarrow$$

$$\frac{\partial}{\partial y}\int_{-\infty}^{+\infty} c_y Y dc_y + \delta_0 \rho \tau^{1-\omega}\rho = \delta_0 \rho \tau^{1-\omega}\rho\frac{\sqrt{\pi\tau}}{\sqrt{\pi\tau}} \Rightarrow$$

$$\frac{\partial}{\partial y}\int_{-\infty}^{+\infty} c_y Y dc_y = 0 \Rightarrow \frac{\partial}{\partial y}\left(u_y \rho\right) = 0 \tag{6.38}$$

Also by taking the zeroth moment of Eq. (4.29) we find:

$$\frac{\partial}{\partial y}\int_{-\infty}^{+\infty} c_y \Phi dc_y + \delta_0 \rho \tau^{1-\omega}\int_{-\infty}^{+\infty}\Phi dc_y = \delta_0 \rho \tau^{1-\omega}\int_{-\infty}^{+\infty}\Phi^M dc_y \Rightarrow$$

$$\frac{\partial}{\partial y}\int_{-\infty}^{+\infty} c_y \Phi dc_y + \delta_0 \rho \tau^{1-\omega}\rho u_x = \delta_0 \rho \tau^{1-\omega}u_x\rho\frac{\sqrt{\pi\tau}}{\sqrt{\pi\tau}} \Rightarrow$$

$$\frac{\partial}{\partial y}\int_{-\infty}^{+\infty} c_y \Phi dc_y = 0 \tag{6.39}$$

To yield the conservation of energy flux principal we take the second moment of Eq. (4.28) and the zeroth moment of Eq. (4.30) and we add the resulting equations to yield:

$$\frac{\partial}{\partial y}\int_{-\infty}^{+\infty} c_y\left[Yc_y^2 + X\right]dc_y + \delta_0 \rho \tau^{1-\omega}\int_{-\infty}^{+\infty}\left[Yc_y^2 + X\right]dc_y = \delta_0 \rho \tau^{1-\omega}\int_{-\infty}^{+\infty}\left[Y^M c_y^2 + X^M\right]dc_y \Rightarrow$$

$$\frac{\partial}{\partial y}\int_{-\infty}^{+\infty} c_y\left[Yc_y^2 + X\right]dc_y + \delta_0 \rho \tau^{1-\omega}\left[u_x^2\rho + \frac{3\rho\tau}{2}\right] = \delta_0 \rho \tau^{1-\omega}\frac{\rho}{2}\left[2u_x^2 + 3\tau\right] \Rightarrow$$

$$\frac{\partial}{\partial y}\int_{-\infty}^{+\infty} c_y\left[Yc_y^2 + X\right]dc_y = 0 \tag{6.40}$$

Another equivalent energy conservation principal may be obtained if the integral expression for the y-component of the heat flux vector is used as a guideline. In particular, we take the first moment of Eqs. (4.28), (4.30) and (4.29) after the latter one is multiplied by $\left(-2u_x c_y \Phi\right)$. The resulting equations are added to find:

$$\frac{\partial}{\partial y}\int_{-\infty}^{+\infty}\left[c_y^3 Y + c_y X - 2u_x c_y \Phi\right]dc_y + 2\left[\frac{\partial u_x}{\partial y}\right]\left[\int_{-\infty}^{+\infty} c_y \Phi dc_y\right] + \delta_0 \rho \tau^{1-\omega}\int_{-\infty}^{+\infty}\left[c_y^2 Y + X - 2u_x\Phi\right]dc_y =$$

$$= \delta_0 \rho \tau^{1-\omega}\int_{-\infty}^{+\infty}\left[c_y^2 Y^M + X^M - 2u_x\Phi^M\right]dc_y \Rightarrow$$

$$\frac{\partial}{\partial y}\int_{-\infty}^{+\infty}\left[c_y^3 Y + c_y X - 2u_x c_y \Phi\right]dc_y + 2\left[\frac{\partial u_x}{\partial y}\right]\left[\sigma_{xy}\right] + \delta_0\rho\tau^{1-\omega}\int_{-\infty}^{+\infty}\left[c_y^2 Y + X - 2u_x\Phi\right]dc_y =$$

$$= \delta_0\rho\tau^{1-\omega}\int_{-\infty}^{+\infty}\left[c_y^2 + \left(u_x^2 + \tau\right) - 2u_x^2\right]\exp\left(-\frac{c_y^2}{\tau}\right)dc_y \Rightarrow$$

$$\frac{\partial}{\partial y}\int_{-\infty}^{+\infty}\left[c_y^3 Y + c_y X - 2u_x c_y \Phi\right]dc_y + 2\left[\frac{\partial u_x}{\partial y}\right]\left[\sigma_{xy}\right] + \delta_0\rho\tau^{1-\omega}\left[\left(\frac{2}{3}u_x^2 + \tau\right)\frac{3\rho}{2} - 2u_x^2\rho\right] =$$

$$= \delta_0\rho\tau^{1-\omega}\rho\left[\frac{3\tau}{2} - u_x^2\right] \Rightarrow$$

$$\frac{\partial}{\partial y}\int_{-\infty}^{+\infty}\left[c_y^3 Y + c_y X - 2u_x c_y \Phi\right]dc_y + 2\left[\frac{\partial u_x}{\partial y}\right]\left[\sigma_{xy}\right] = 0 \Rightarrow$$

$$\frac{\partial}{\partial y}\left(q_y\right) + 2\sigma_{xy}\frac{\partial u_x}{\partial y} = 0 \tag{6.41}$$

To deduce and expression for the conservation of momentum flux principal we take the first moment of Eqs. (4.28) and (4.29) after the former one is multiplied by $\left(-u_x\right)$. Then, we add the resulting equations to yield:

$$c_y\frac{\partial}{\partial y}\left[\Phi - u_x Y\right] + \delta_0\rho\tau^{1-\omega}\left[\Phi - u_x Y\right] = \delta_0\rho\tau^{1-\omega}\left[\Phi^M - u_x Y^M\right] \Rightarrow$$

$$c_y\frac{\partial}{\partial y}\left[\Phi - u_x Y\right] + \delta_0\rho\tau^{1-\omega}\left[\Phi - u_x Y\right] = \delta_0\rho\tau^{1-\omega}\left[0\right] \Rightarrow$$

$$\frac{\partial}{\partial y}\int_{-\infty}^{+\infty}\left[\Phi - u_x Y\right]c_y dc_y + \delta_0\rho\tau^{1-\omega}\int_{-\infty}^{+\infty}\left[\Phi - u_x Y\right]dc_y = 0 \Rightarrow$$

$$\frac{\partial}{\partial y}\left(\sigma_{xy}\right) + \delta_0\rho\tau^{1-\omega}\left[u_x\rho - u_x\rho\right] = 0 \Rightarrow$$

$$\frac{\partial}{\partial y}\left(\sigma_{xy}\right) = 0 \tag{6.44}$$

Following similar principals we obtain that

$$\frac{\partial}{\partial y}\left(\sigma_{yy}\right) = 0$$

It is also important to note that in non-equilibrium flows, in general $\sigma_{xx} \neq \sigma_{yy} \neq \sigma_{zz}$, which will result in a non-uniform pressure across the channel.

7

Results

7.1 Computational Parameters

The numerical results presented here have been obtained using the double projected kinetic equations for both the BGK and the S model as they were described in Chapter 4. The two different implementations with regard to the projection method return, as it should, the same results. Therefore, the one with the least computational effort is adopted. In order to achieve a good accuracy for the numerical results, the computational algorithm makes use of $I = 401$ nodes for the spatial discretization and $M = 96$ roots of the Legendre polynomials for the molecular velocity components. The termination criterion for the iterative process has been set as the sum of the maximum relatives errors between the macroscopic quantities of the flow and equal to 10^{-6}. Results are presented in the whole range of rarefaction ($0 \le \delta_0 \le 10^2$), with $U_0 = 0,\ 0.1,\ 0.3$ and 0.5, $\beta = 0$, 0.1, 0.5 and 0.9 and $\omega = 1/2$. Also in some cases results for $\omega = 1$ are presented.

7.2 Comparison with existing results

In order to validate the accuracy of the numerical results extensive comparisons have been performed with analytical and computational results available in the literature.

As it has been shown in Section 6.1 analytical results have been derived for all macroscopic quantities at the free molecular limit (δ=0). The numerical results obtained by the nonlinear kinetic code for δ=0 have been compared with the corresponding analytical ones and in all cases excellent agreement has been found.

Also, in Section 6.2, it has been shown that semi-analytical results may be deduced at the hydrodynamic limit ($\delta \to \infty$). Corresponding results for $\delta = 100$ with the BGK model have been obtained and a comparison is presented in Figures 7.1-7.4. In general, the agreement is very good. Actually at small values of U_0 and β the agreement is excellent, while as these two parameters are increased there are some discrepancies, which are small and they can be easily justified by the fact that the BGK solution is based on the hard sphere model, while the Navier-Stokes solution on the assumption of Maxwell molecules.

Finally, a comparison is made with some results solving the same problem based on the DSMC method [Marques, Kremer and Sharipov, 2000]. First we analyze the profile of the velocity field as a function of the distance between the plates. In Fig. 7.5 the velocity profile for Kn=0.25, $\beta = 0$ and $V = 0.1(kT_0/m)^{1/2}$ is in excellent agreement with the corresponding DSMC solution. Also, in Figure 7.6 the ratio P_{xy}/p_0, with $p_0 = n_0 kT_0$ denoting the equilibrium pressure, is plotted as a function of the Knudsen number when the velocity of the plates is $V = 0.1(kT_0/m)^{1/2}$. The comparison between the DSMC and the kinetic results yields very good agreement in the whole range of the Kn number. In all cases computed, the relative error between the kinetic and the corresponding DSMC results is from 8% for the free molecular regime, reaching a maximum of 13% at the continuum regime. In Figures 7.7 and 7.8 the vertical and horizontal heat fluxes estimated by the DSMC method are plotted for Kn=0.25 and $V = (kT_0/m)^{1/2}$. The kinetic solution is in excellent agreement with the DSMC. The bigger discrepancies compared to the DSMC results appear at the walls where the kinetic approach overestimates the values of the heat flux vector.

7.3 Pure Heat Transfer $\left(\pm U_0 = 0\right)$

In Figures 7.9-7.11 the pure heat transfer problem is presented for $\delta_0 = 0,\ 0.1,\ 1,\ 10$ and 10^2 with $\beta = 0.1,\ 0.5,\ 0.9$ respectively. The velocity profiles for all cases are equal to zero. The deviation of the temperature profiles from the isothermal profile $\tau = 1$ is increased as β is increased. Also as the temperature ratio between the walls is increased,

the temperature jump at the hot plate is larger than the corresponding jump at the cold plate. The normal heat flux is always positive, denoting as expected, that heat is moving from the lower cold plate towards the cold upper plate. The vertical heat flux is increasing as the temperature difference between the plates is increased. The horizontal heat flux $q_x(y)$ parallel to the flow is zero, something which is expected, since the axial heat flux is related to the velocity as it is shown from the analytical solutions for the free molecular regime. The density distributions change significantly as β is increased. The deviation from the average value $\rho = 1$ is increased with the parameter β. It is seen that the density jump at the cold upper wall is significantly larger than the one at the lower hot plate. Finally, the pressure distribution $\mathrm{P}(y)$ is constant for $\delta_0 = 0$ and 10^2, while for the intermediate values of δ_0 depends on y and in particular it is decreased as we are moving from the lower towards the upper plate. Also, it is decreasing as the temperature gradient is increased.

7.4 Coupled Couette flow with heat transfer

In the present section, some results for non-isothermal walls for various values of parameter β are presented. The selected values of $\beta = 0.1,\ 0.5,\ 0.9$ correspond to wall temperature ratios equal to 1.2, 3 and 19 respectively. In Figures 7.12-7.23, a detailed quantitative description of the flow quantities is presented. In particular, distributions of velocity $u(y)$, temperature $\tau(y)$, vertical and horizontal heat fluxes $q_y(y)$ and $q_x(y)$, density $\rho(y)$ and pressure $P(y)$ are presented for $\delta_0 = 0,\ 0.1,\ 1,\ 10$ and 10^2 with $U_0 = 0$, 0.1, 0.3 and 0.5 and $\beta = 0.1,\ 0.5,\ 0.9$.

7.4.1 Isothermal plates

First, results are provided for the case of isothermal plates ($\beta = 0$) via the BGK model kinetic equation. In Figures 7.12-7.14, distributions for the velocity $u(y)$, the

temperature $\tau(y)$,the heat fluxes $q_y(y)$ and $q_x(y)$, the density $\rho(y)$ and the pressure $\mathrm{P}(y)$ are presented for $\delta_0 = 0$, 0.1, 1, 10 and 10^2 with $U_0 = 0.1$, 0.3 and 0.5 respectively. At $\delta_0 = 10^2$ (very close to the hydrodynamic limit) the velocity profiles are straight lines. As δ_0 is decreased, the profiles have the well known s-shape and finally, at $\delta_0 = 0$, $u(y)$ is constant and equal to zero. In all cases the velocity profiles are anti-symmetric and there is very good quantitative agreement with the corresponding results obtained by using linear kinetic theory.

Quite more interesting are the temperature distributions. It is seen that although the walls are isothermal the flow is not. The temperature distribution is symmetric about the axis $y = 0$ and reaches a maximum at $y = 0$. This maximum value is increased as U_0 is increased. For example in the specific case of $\delta_0 = 1$ the temperature at the center compared to the wall temperature is increased less than 1% when $U_0 = 0.1$, more than 5% when $U_0 = 0.3$ and more than 12% when $U_0 = 0.5$. Also, as δ_0 is decreased the shape of the temperature distribution is changed from parabolic to flat. Actually, at $\delta_0 = 0$ the temperature is a straight line equal to $1 + 8U_0^2/3$. It is also evident that as δ_0 is decreased the temperature variation from the isothermal conditions, at each point between the plates, including the temperature jump at the walls and the maximum value of the temperature at the center, is increased.

The heat flux distributions, shown in Figures 7.9-7.11, for the pure heat transfer problem, compared to the corresponding ones in Figures 7.12-7.14 for $\beta = 0$ are qualitatively different. The normal heat fluxes are anti-symmetric (positive at the upper half and negative at the lower half) and almost linear in terms of y. For the specific case of $\delta_0 = 0$ we have $q_y(y) = 0$. The axial heat flux $q_x(y)$, which is parallel to the flow is also shown. It is seen that these fluxes appear even for isothermal walls. They are anti-symmetric (negative at the upper half and positive at the lower half) having an s-shape at intermediate values of δ_0. It is important to note that the behavior of both heat fluxes in terms of δ_0, as it is shown in Figures 7.12-7.14, is typical only for isothermal walls.

Moreover, the density and pressure distributions of the flow are also presented. Both macroscopic quantities appear to have a symmetric distribution about the axis $y=0$, where the density has its minimum value and the pressure its maximum. Also, as δ_0 is decreased the shape of the density distribution is changed from parabolic to flat. Actually, at $\delta_0=0$ the density is a straight line equal to unity and therefore the pressure distribution matches the temperature one, since in general $P=\rho\times\tau$. It is also noted that in the free molecular and hydrodynamic regimes the pressure distribution is flat, while in the transition regime is a function of y.

7.4.2 Coupled flow

In Figures 7.15-7.23 all macroscopic distributions of some practical interest are shown for $U_0=0.1$, 0.3. 0.5 and $\beta=0.1$, 0.3, 0.5 in the whole range of the rarefaction parameter δ_0 from the free molecular through the transition up to the hydrodynamic limit. Studying these figures it is possible to investigate the effects of the velocity and temperature of the walls on the flow characteristics and properties. A general comment is that the well known anti-symmetric profiles of the velocity and temperature distributions in the case of the linear Couette and heat transfer problems are not present anymore. Due to the coupling of the problem and the implemented nonlinear kinetic solvers the solutions are not anti-symmetric.

Starting with the velocity profiles it is seen that when $\delta_0=0$ the velocity profile is flat (there is dependency on y) and different than zero. At the other end, when $\delta_0=10^2$ for small values of U_0 is almost linear but as U_0 is increased becomes nonlinear. The velocity distributions in the transition regime lay between the velocity distributions corresponding between these two limiting cases. In all cases the velocity slip at the lower hot walls are larger than the corresponding slips at the upper cold walls. Also, as expected the slip is increased as δ_0 is decreased (the atmosphere becomes more rarefied).

The dependency of the temperature profiles, in terms of all flow parameters can be also studied. The temperature jump at the hot walls is always larger than the corresponding ones at the cold wall and it is increased as δ_0 is decreased. At large wall velocities and small temperature differences the temperature of the gas inside the channel may be larger than the temperature of the hot wall. In contrary, at large wall temperature differences even at large values of the wall velocity the temperature of the gas is always decreasing as we are moving from the lower towards the upper plate. In general, as U_0 is increased its effect on the temperature distribution becomes more significant it becomes more prominent as δ_0 is decreased (more rarefied atmospheres).

Both the vertical and horizontal heat fluxes are also presented in Figures 7.15-7.23. The vertical heat flux is always positive indicating a heat flow from the lower hot towards the cold upper plate. The heat flux is increased as the temperature difference and the relative velocity of the walls are increased. Also they are increased as δ_0 is decreased. For $\delta_0 = 0$ and 100 the vertical heat flux profiles are almost constant, while at the intermediate values of δ_0 they are a monotonic increasing function of y.

The existence of an horizontal flux it is a non-expected phenomenon, which may have several useful heat transfer applications. Its presence is due to non-equilibrium (rarefied) conditions. The sign of these heat fluxes is always negative indicating that the flow is from right to left and its absolute values are increased as δ_0 is decreased. It is also noted that at $\delta_0 = 10^2$ the horizontal heat fluxes become almost zero. It is important to note that in addition to the rarefied atmosphere the horizontal heat fluxes are present only when both velocity and temperature gradients exist in the flow and they are increased as these gradients are increased.

Finally, the density and pressure distributions across the plates are also shown. In general, the density profiles have an opposite variation in terms of y, compared to the corresponding one of the temperature profiles. That means that when the temperature is increased the velocity is decreased and vice versa. In that sense the density jump is larger at the cold wall compared to the density jump at the hot walls, while the temperature

jumps are the other way around. This behaviour is well justified by the relation $P = \rho \times \tau$, where the pressure distribution has small variation in terms of y. It is important however to note that the pressure is a function of y. Again this is a non-equilibrium effect. It is also noted that $\sigma_{zz} \neq \sigma_{yy} \neq \sigma_{zz}$. This non-equilibrium behaviour is clear at intermediate values of δ_0 in the transition regime. At $\delta_0 = 10^2$, when the flow is dominated by intermolecular collisions and at $\delta_0 = 0$, when there are no intermolecular collisions at all, the pressure distributions are constant.

7.5 Comparison between the BGK and Sakhov models

A systematic comparison between the results obtained by the BGK and Sakhov models are presented in Figures 7.24-7.26 for a wide set of flow parameters. The comparison is made by using the hard sphere model (w=0.5). The macroscopic distributions for $\delta_0 = 0$ are not shown since in this case the flow is collisionless and does not depend on the intermolecular potential. In Figure 7.24, where U_0=0.1 and β=0.1 there is an excellent agreement between the results of the two models. As both β and U_0 are increased there are some discrepancies between the results, which however in general remain small. This behavior is expected since the BGK model is not the appropriate model to study nonisothermal model since it does not produce the correct Prandtl number. From the other hand the Shakhov model, which produces the correct Prandtl number is considered as more reliable. The discrepancies become more evident in Figure 7.26, where U_0=0.5 and β=0.9 particularly when the temperature and heat flux profiles are compared. Figure 7.25, corresponds to the moderate values of U_0=0.3 and β=0.5. In general, the two models follow the same trend in all macroscopic quantities, having an excellent agreement is free molecular and hydrodynamic regimes and having good agreement in the transition regime. So overall, if the BGK model is implemented due to its simplicity instead of the Shakhov model, the expected error should not be more than 20%.

7.6 Comparison between intermolecular collision models

The hard sphere and the Maxwell intermolecular potential models are the two limiting cases of the so-called inverse power law (IPL) models. As it has been pointed out in previous chapters by setting the parameter w=0.5 we obtain the hard sphere model, while by setting w=1 we obtain the Maxwell model. In this paragraph results are presented, in Figures 7.26-7.28, for all macroscopic quantities for different set of flow parameters for these two limiting intermolecular collision cases. The results are for $\delta_0 = 0.1$, 1, 10 and 10^2 with $\beta = 0.1$ and $U_0 = 0.1$ in Figure 7.27, $\beta = 0.5$ and $U_0 = 0.3$ in Figure 7.28 and $\beta = 0.9$ and $U_0 = 0.5$ in Figure 7.29. Again, the distributions for $\delta_0 = 0$ are not shown since the results are irrespective of the collision model being used. The agreement between the results is very good clearly indicating that this specific flow configuration does not, at least significantly, on the implemented intermolecular model. In general the agreement between the results obtained by the two models vary from 1% for small values of U_0 and β up to 10% for large values U_0 and β. In terms of the rarefaction parameter the results are almost identical for small and large values of delta, with the largest differences at intermediate values of δ_0 inside the transition regime.

7.7 Estimation of shear stress

One macroscopic quantity of great importance for the problem in question is the shear stress. As it has been shown theoretically the distribution of the shear stress, in all cases, irrespective of δ_0, β and U_0 is flat and independent of the spatial variable y. Here, we present, as reference, tabulated results of the shear stresses for all parameters involved in the calculations. In Tables 7.1 and 7.2 the values of the shear stress are computed via the BGK and Shakhov kinetic model equations respectively using the hard sphere model. In Table 7.3 the BGK results for the shear stresses are shown for the Maxwell molecular model.

The shear stress is always negative. It depends both on β and U_0. The absolute value of the shear stress is increased as δ_0 is decreased, as U_0 is increased and as β is

decreased. The maximum absolute values occur at $\beta = 0$, $U_0 = \pm 0.5$ and $\delta_0 = 0$. The results are considered as accurate up to three significant figures.

Table 7.1: *Shear stress based on the BGK equation and hard sphere model*

β	U_0	δ_0				
		0	0.1	1	10	100
0	0.1	-0.0564	-0.0522	-0.0339	-0.0083	-0.0010
	0.3	-0.1693	-0.1570	-0.1023	-0.0253	-0.0030
	0.5	-0.2821	-0.2625	-0.1723	-0.0431	-0.0051
0.1	0	0.0000	0.0000	0.0000.	0.0000	0.0000
	0.1	-0.0562	-0.0521	-0.0338	-0.0083	-0.0010
	0.3	-0.1686	-0.1565	-0.1020	-0.0252	-0.0030
	0.5	-0.2810	-0.2616	-0.1719	-0.0430	-0.0051
0.5	0	0.0000	0.0000	0.0000.	0.0000	0.0000
	0.1	-0.0506	-0.0472	-0.0313	-0.0081	-0.0010
	0.3	-0.1518	-0.1418	-0.0946	-0.0246	-0.0029
	0.5	-0.2529	-0.2373	-0.1596	-0.0420	-0.0050
0.9	0	0.0000	0.0000	0.0000.	0.0000	0.0000
	0.1	-0.0290	-0.0283	-0.0218	-0.0074	-0.0009
	0.3	-0.0871	-0.0851	-0.0662	-0.0224	-0.0028
	0.5	-0.1451	-0.1428	-0.1131	-0.0386	-0.0048

Table 7.2: *Shear stress based on the Shakhov equation and hard sphere model*

β	U_0	δ_0				
		0	0.1	1	10	100
0	0.1	-0.0564	-0.0522	-0.0339	-0.0083	-0.0010
	0.3	-0.1693	-0.1570	-0.1022	-0.0252	-0.0030
	0.5	-0.2821	-0.2625	-0.1719	-0.0427	-0.0050
0.1	0	0.0000	0.0000	0.0000.	0.0000	0.0000
	0.1	-0.0562	-0.0521	-0.0338	-0.0083	-0.0010
	0.3	-0.1686	-0.1565	-0.1019	-0.0252	-0.0030
	0.5	-0.2810	-0.2616	-0.1714	-0.0427	-0.0050
0.5	0	0.0000	0.0000	0.0000.	0.0000	0.0000
	0.1	-0.0506	-0.0473	-0.0314	-0.0081	-0.0010
	0.3	-0.1518	-0.1420	-0.0947	-0.0244	-0.0029
	0.5	-0.2529	-0.2376	-0.1595	-0.0415	-0.0050
0.9	0	0.0000	0.0000	0.0000.	0.0000	0.0000
	0.1	-0.0290	-0.0286	-0.0222	-0.0072	-0.0009
	0.3	-0.0871	-0.0862	-0.0673	-0.0220	-0.0028
	0.5	-0.1451	-0.1445	-0.1146	-0.0375	-0.0048

Table 7.3: *Shear stress based on the BGK equation and Maxwell model*

β	U_0	δ_0				
		0	0.1	1	10	100
0	0.1	-0.0564	-0.0523	-0.0339	-0.0083	-0.0010
	0.3	-0.1693	-0.1573	-0.1032	-0.0256	-0.0030
	0.5	-0.2821	-0.2638	-0.1762	-0.0446	-0.0052
0.1	0	0.0000	0.0000	0.0000	0.0000	0.0000
	0.1	-0.0562	-0.0521	-0.0338	-0.0083	-0.0010
	0.3	-0.1686	-0.1567	-0.1029	-0.0256	-0.0030
	0.5	-0.2810	-0.2629	-0.1756	-0.0445	-0.0052
0.5	0	0.0000	0.0000	0.0000	0.0000	0.0000
	0.1	-0.0506	-0.0470	-0.0310	-0.0081	-0.0010
	0.3	-0.1518	-0.1416	-0.0944	-0.0249	-0.0030
	0.5	-0.2529	-0.2377	-0.1617	-0.0435	-0.0052
0.9	0	0.0000	0.0000	0.0000	0.0000	0.0000
	0.1	-0.0290	-0.0280	-0.0219	-0.0075	-0.0010
	0.3	-0.0871	-0.0846	-0.0672	-0.0232	-0.0030
	0.5	-0.1451	-0.1426	-0.1167	-0.0406	-0.0052

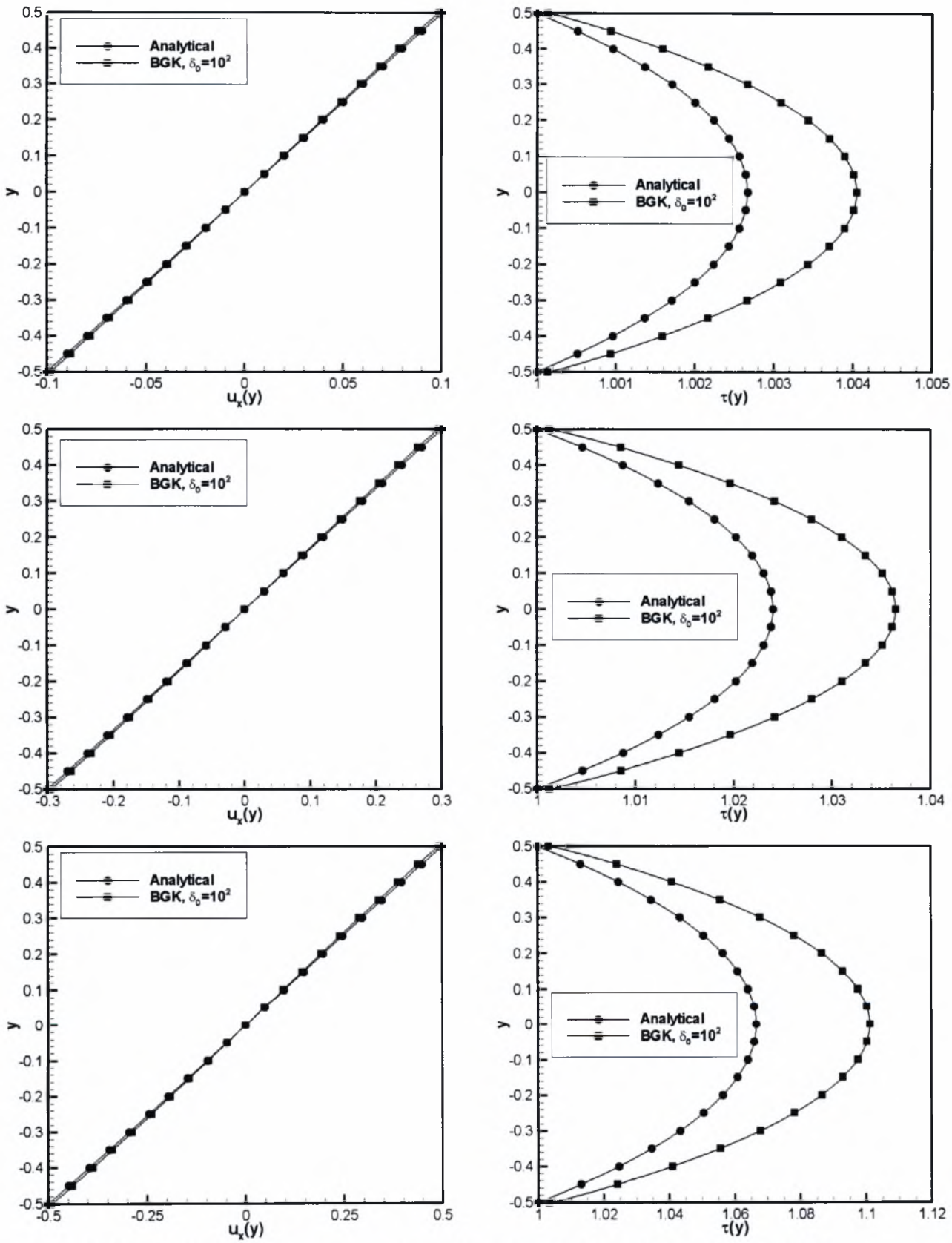

Figure 7.1: *Distributions of macroscopic quantities for $\beta = 0$ and $U = 0.1, 0.3$ and 0.5*

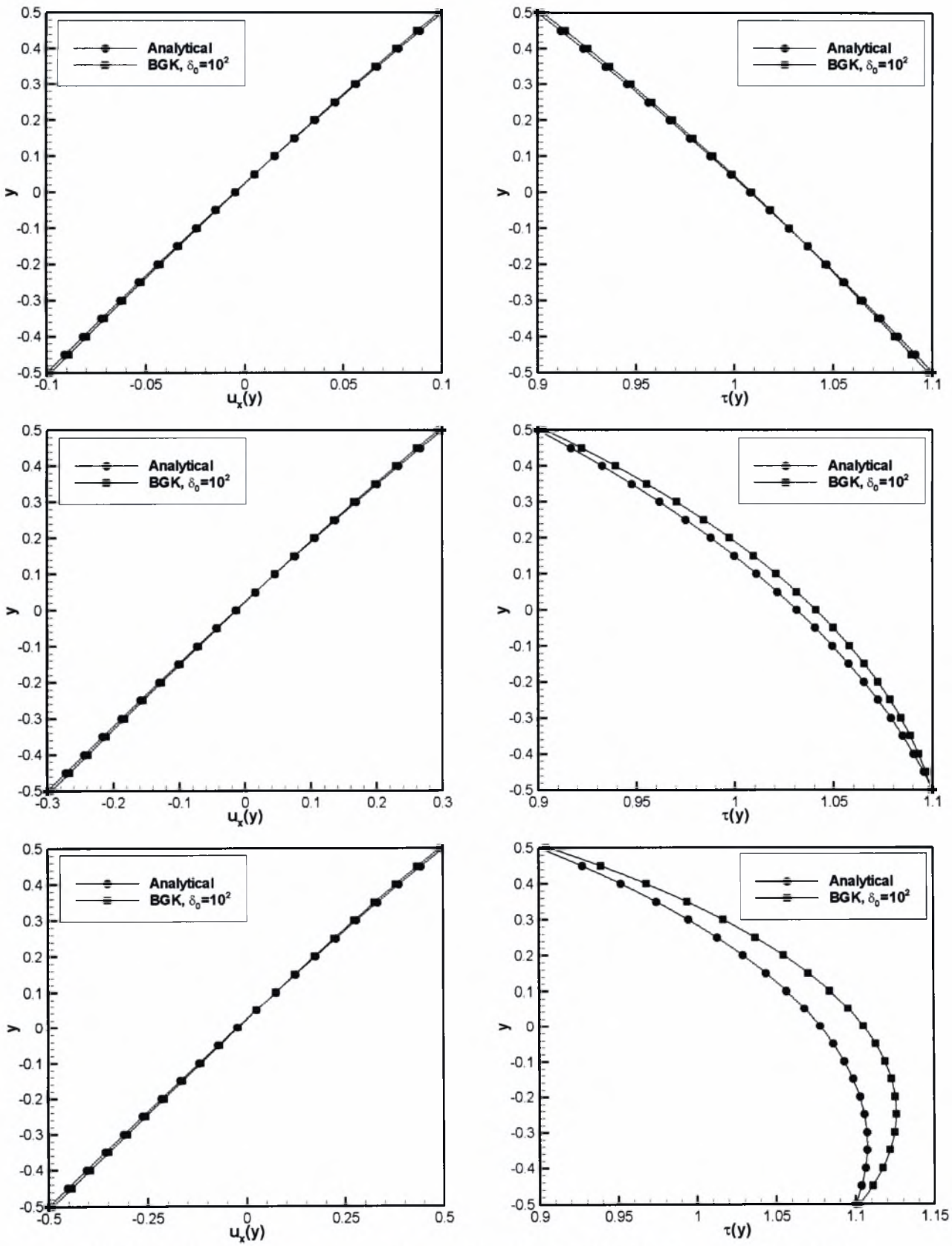

Figure 7.2: *Distributions of macroscopic quantities for $\beta = 0.1$ and $U = 0.1, 0.3$ and 0.5*

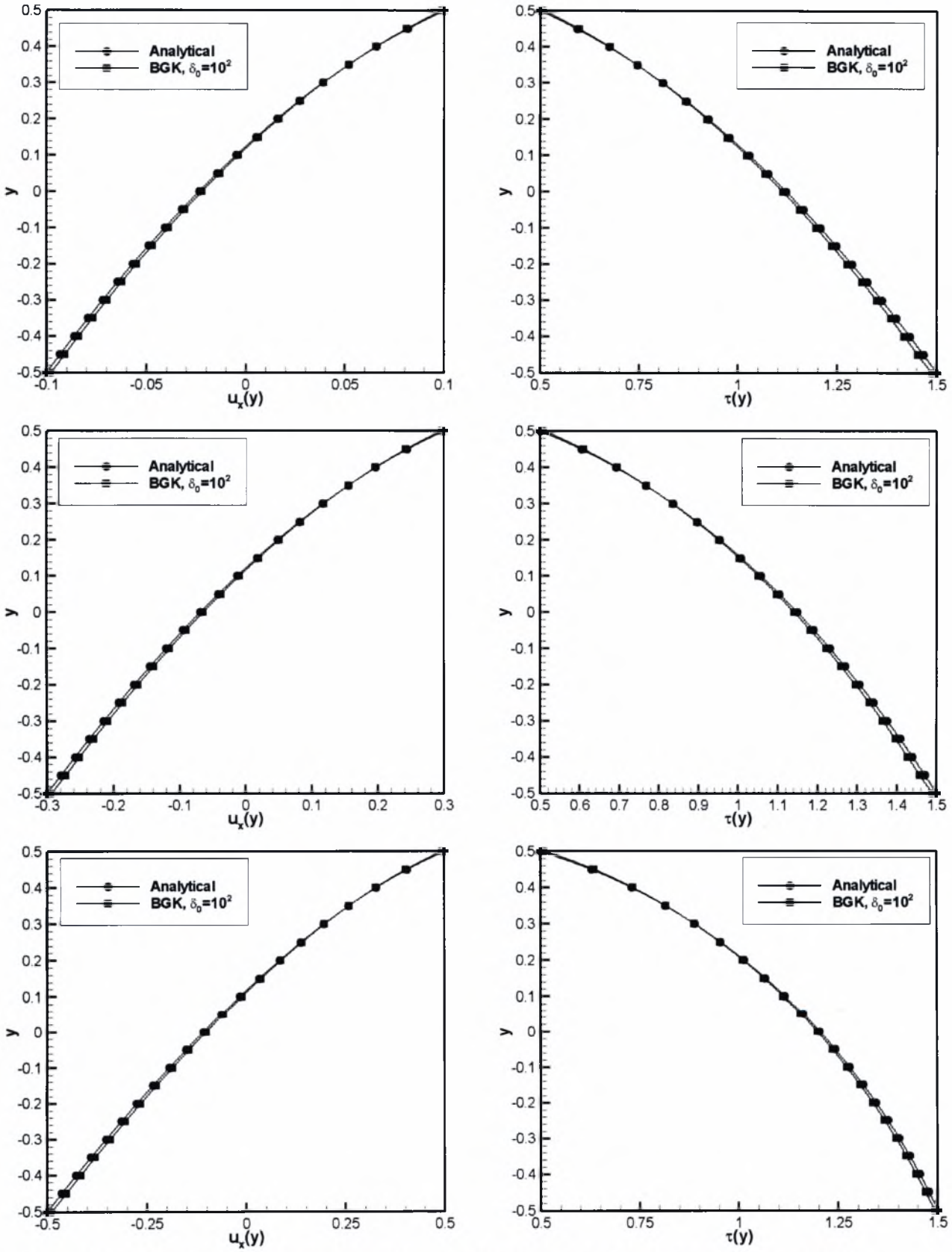

Figure 7.3: *Distributions of macroscopic quantities for $\beta = 0.5$ and $U = 0.1, 0.3$ and 0.5*

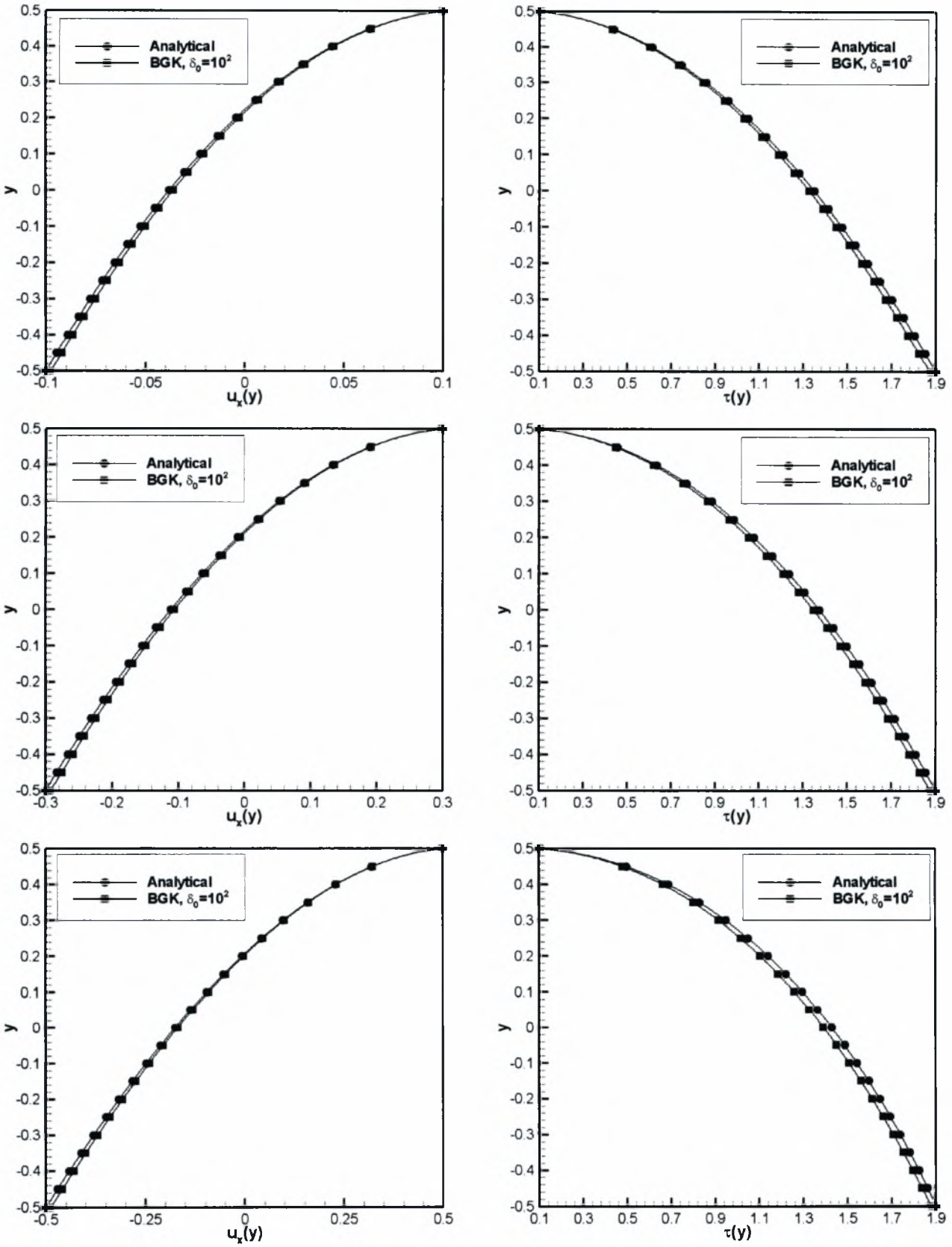

Figure 7.4: *Distributions of macroscopic quantities for $\beta = 0.9$ and $U = 0.1, 0.3$ and 0.5*

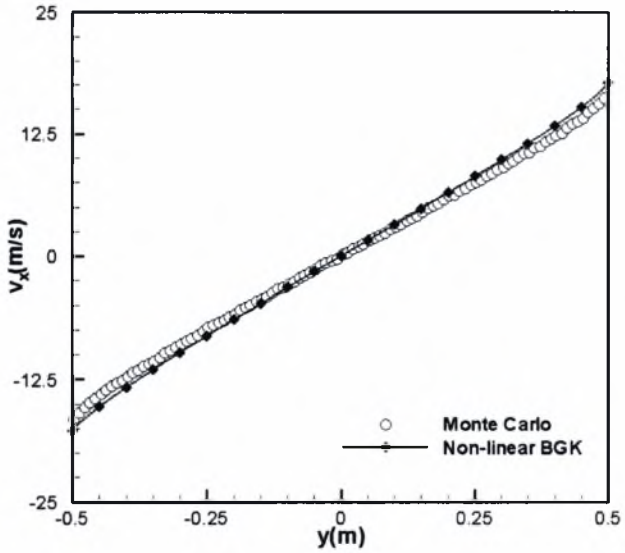

Figure 7.5: *Velocity profile for Kn=0.25 $\beta = 0$ and $V = 0.1\left(kT_0 / m\right)^{1/2}$*

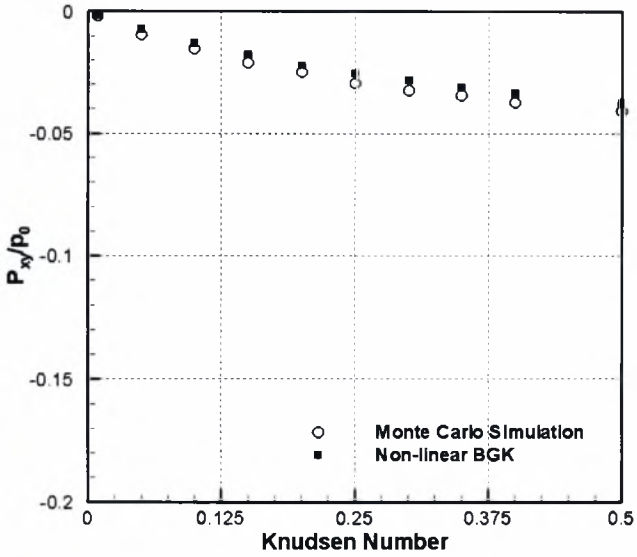

Figure 7.6: *Distributions of macroscopic quantities for $\beta = 0$ and $V = 0.1\left(kT_0 / m\right)^{1/2}$*

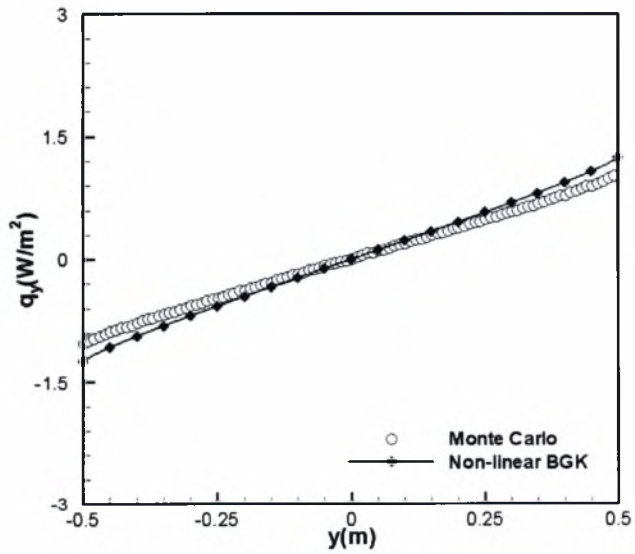

Figure 7.7: *Heat flux perpendicular to the plates for Kn=0.25, $\beta = 0$ and $V = \left(kT_0 / m\right)^{1/2}$*

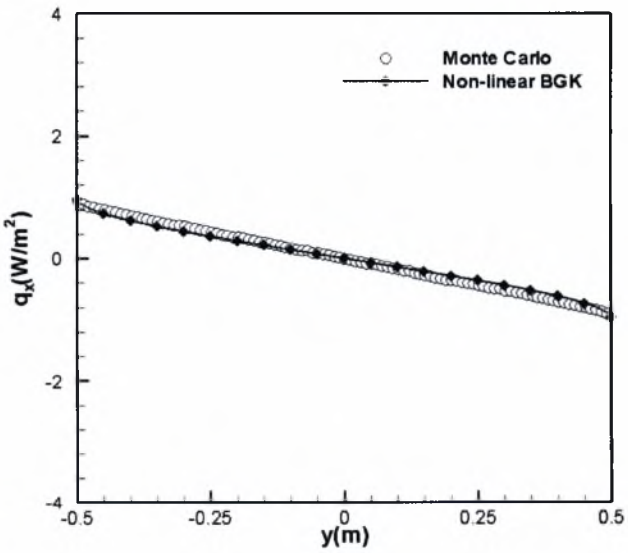

Figure 7.8: *Heat flux parallel to the plates for Kn=0.25, $\beta = 0$ and $V = \left(kT_0 / m\right)^{1/2}$*

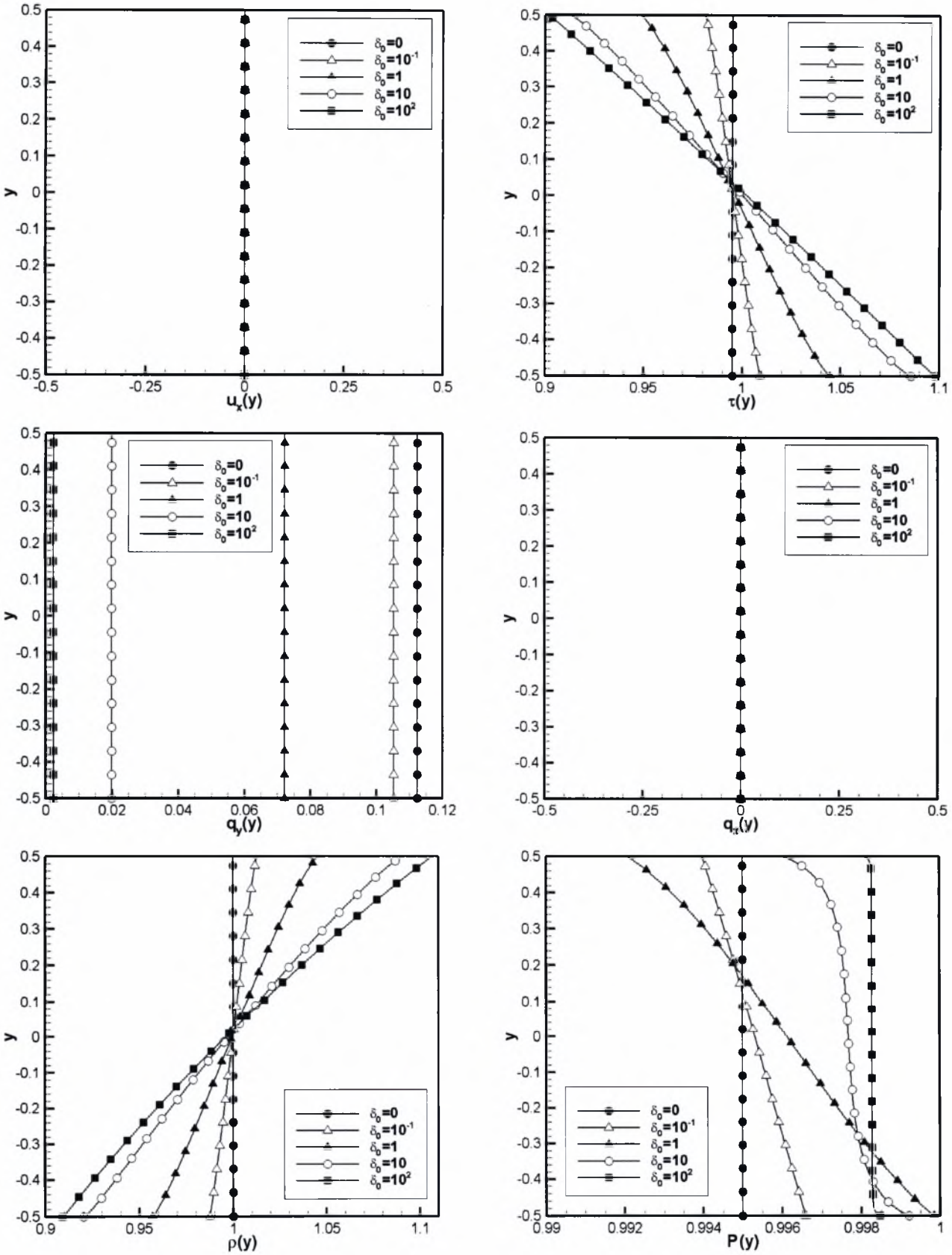

Figure 7.9: *Distributions of macroscopic quantities for* $\beta = 0.1$ *and* $U = 0$

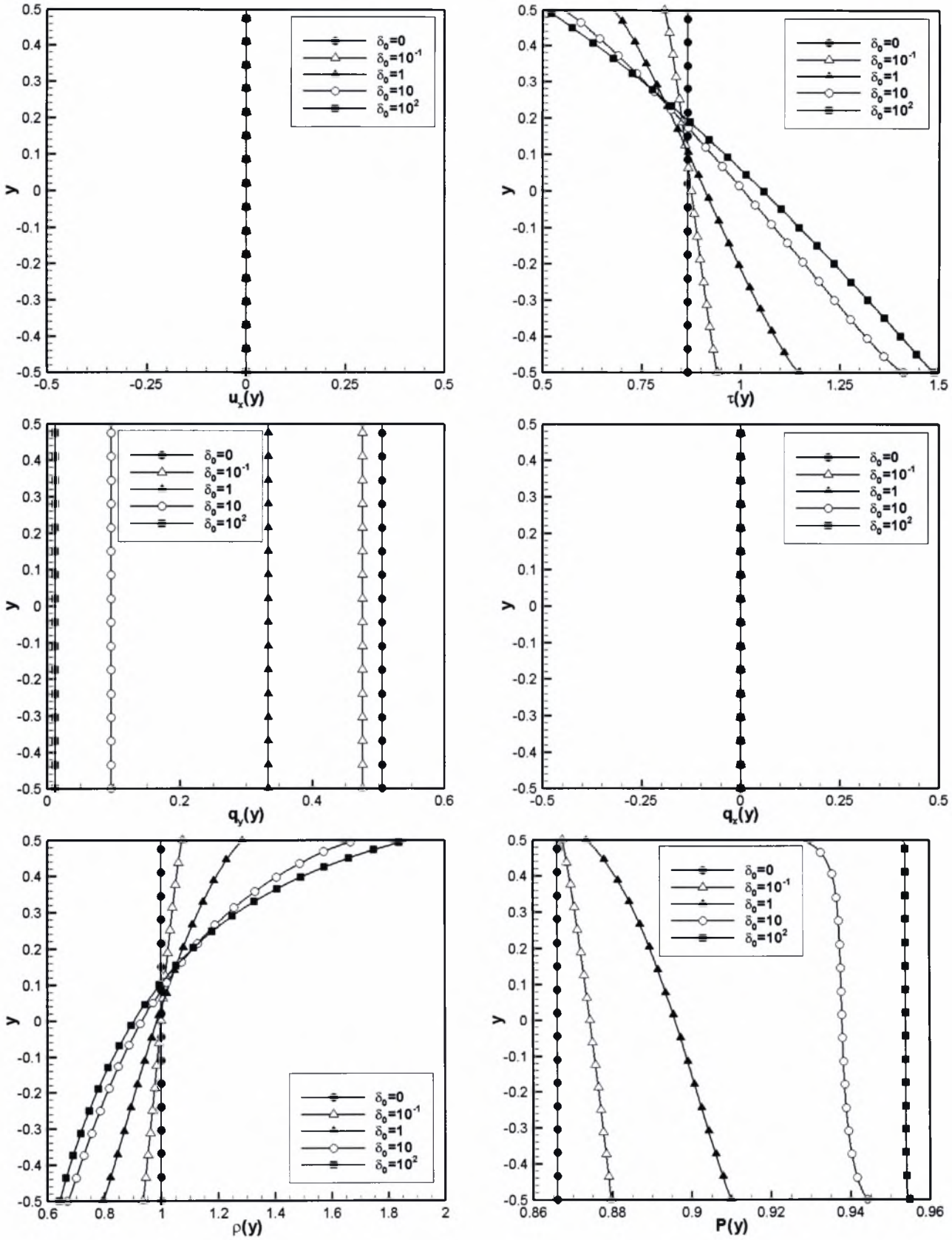

Figure 7.10: *Distributions of macroscopic quantities for* $\beta = 0.5$ *and* $U = 0$

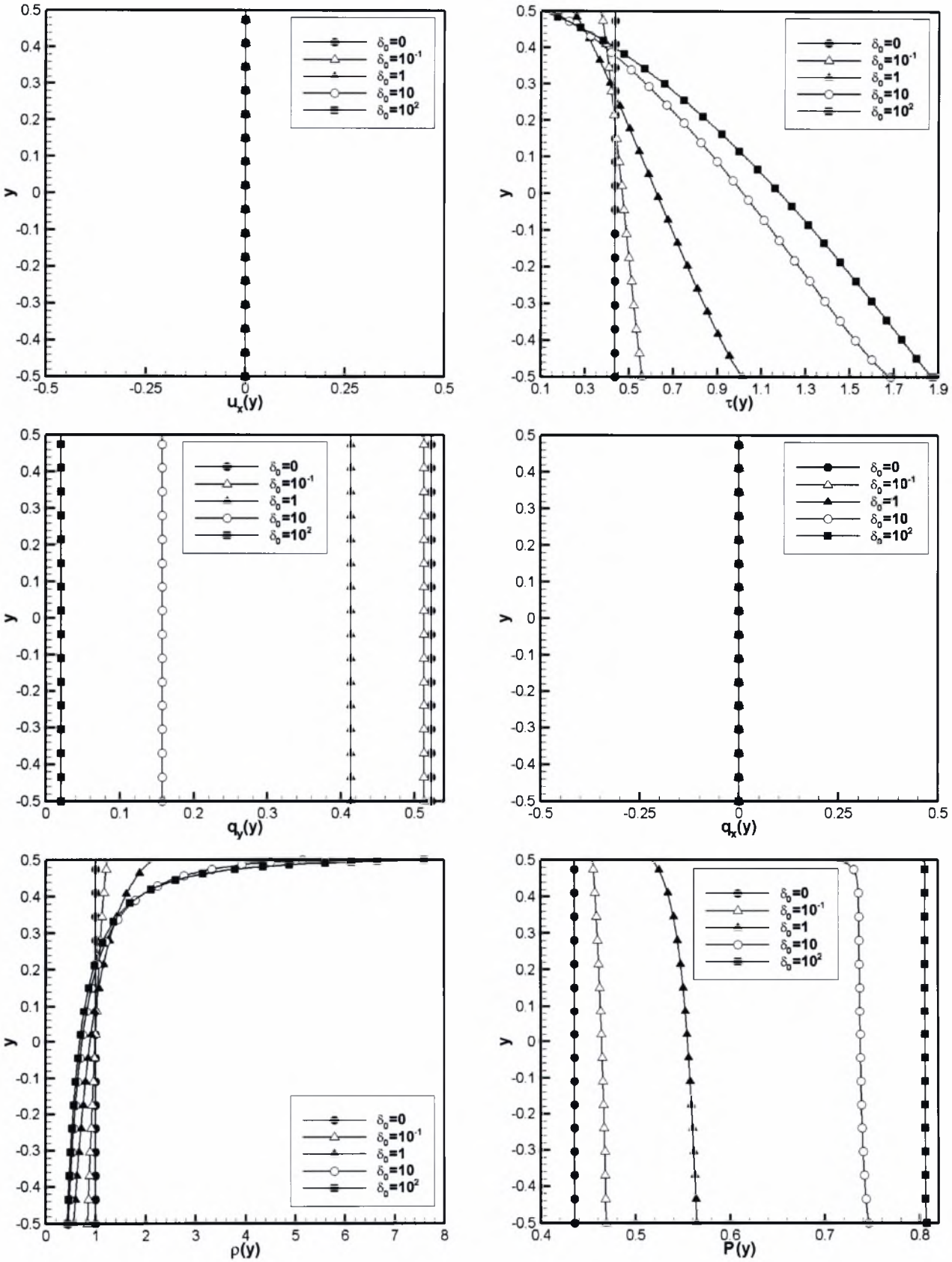

Figure 7.11: *Distributions of macroscopic quantities for* $\beta = 0.9$ *and* $U = 0$

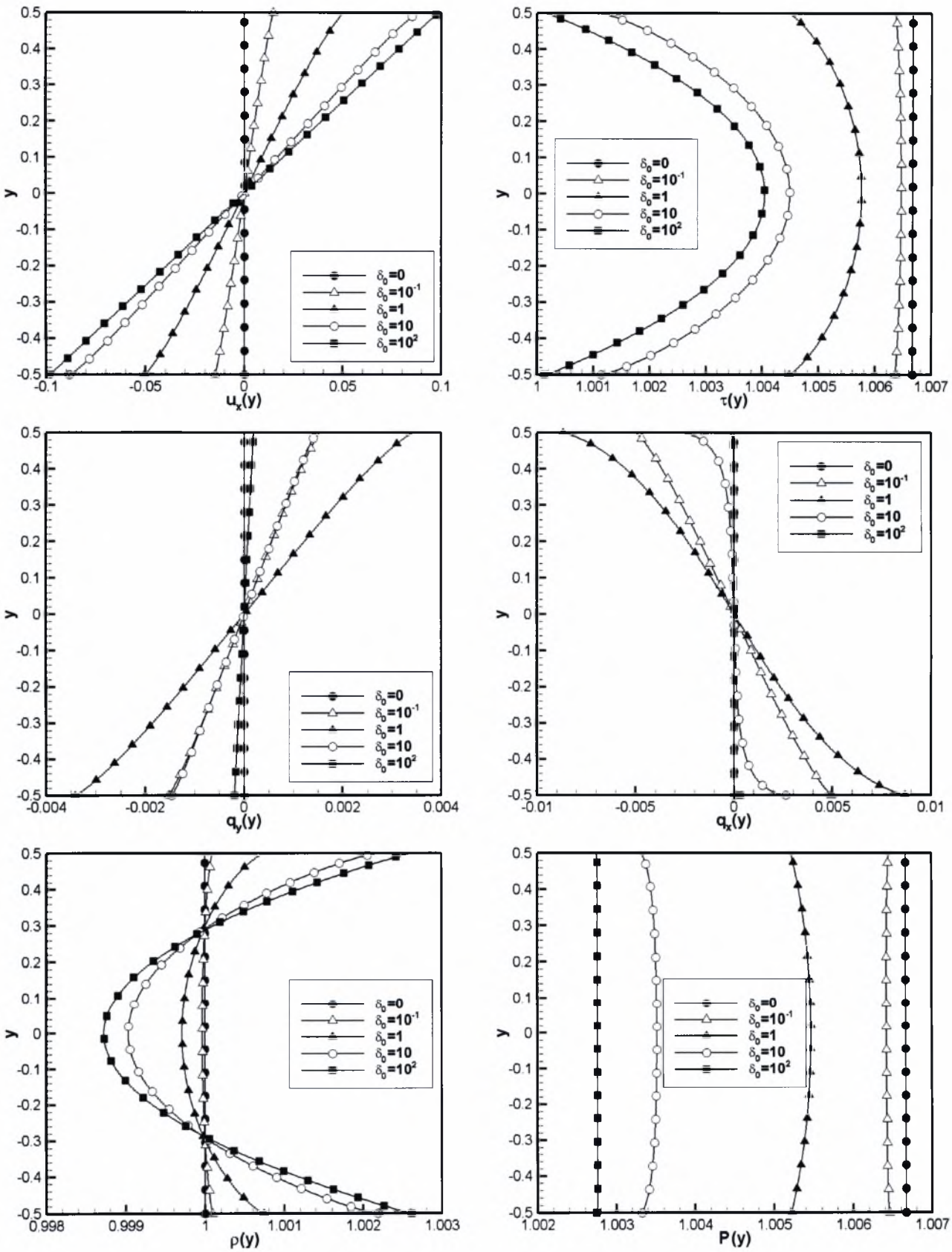

Figure 7.12: *Distributions of macroscopic quantities for* $\beta = 0$ *and* $U = 0.1$

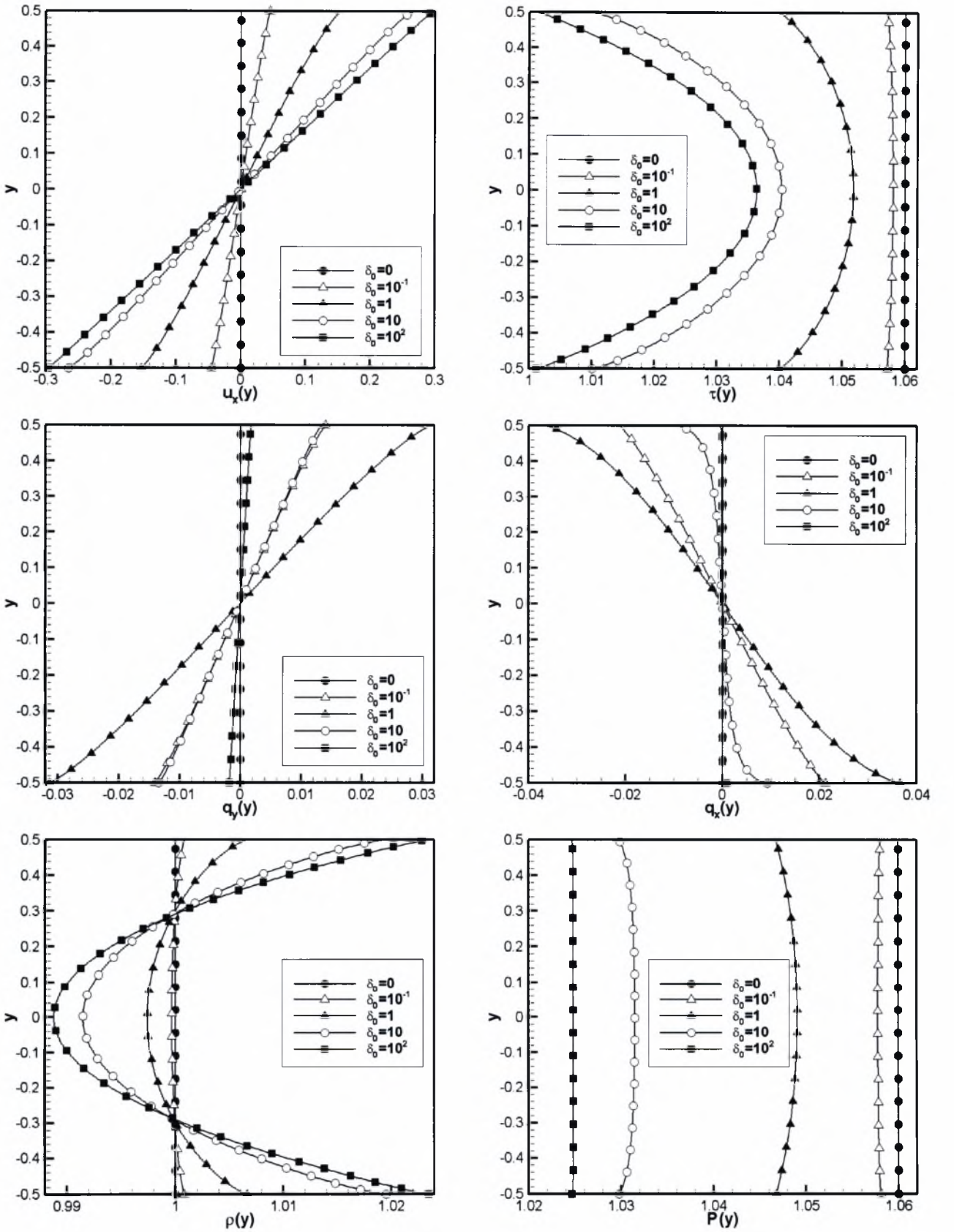

Figure 7.13: *Distributions of macroscopic quantities for* $\beta = 0$ *and* $U = 0.3$

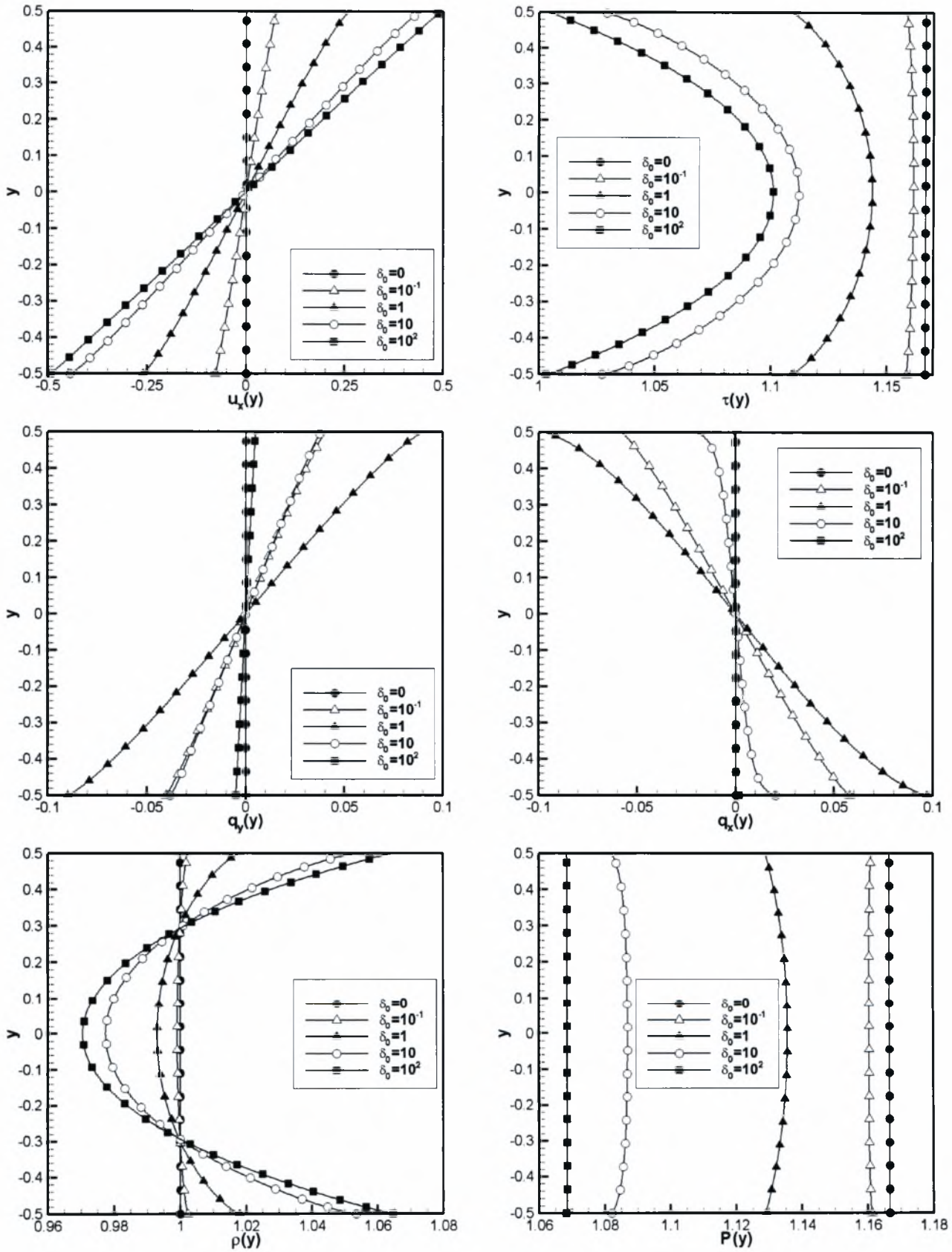

Figure 7.14: *Distributions of macroscopic quantities for* $\beta = 0$ *and* $U = 0.5$

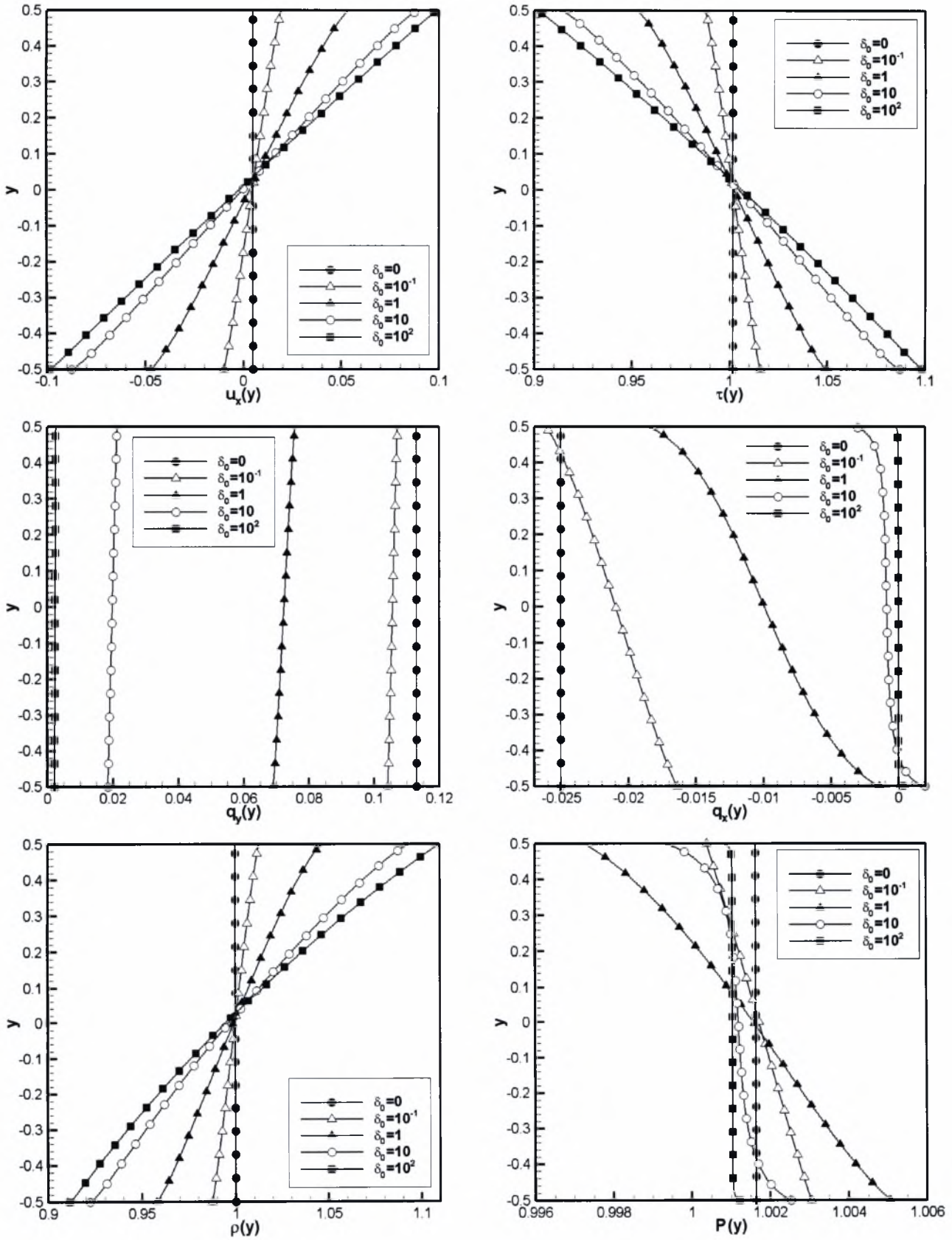

Figure 7.15: *Distributions of macroscopic quantities for* $\beta = 0.1$ *and* $U = 0.1$

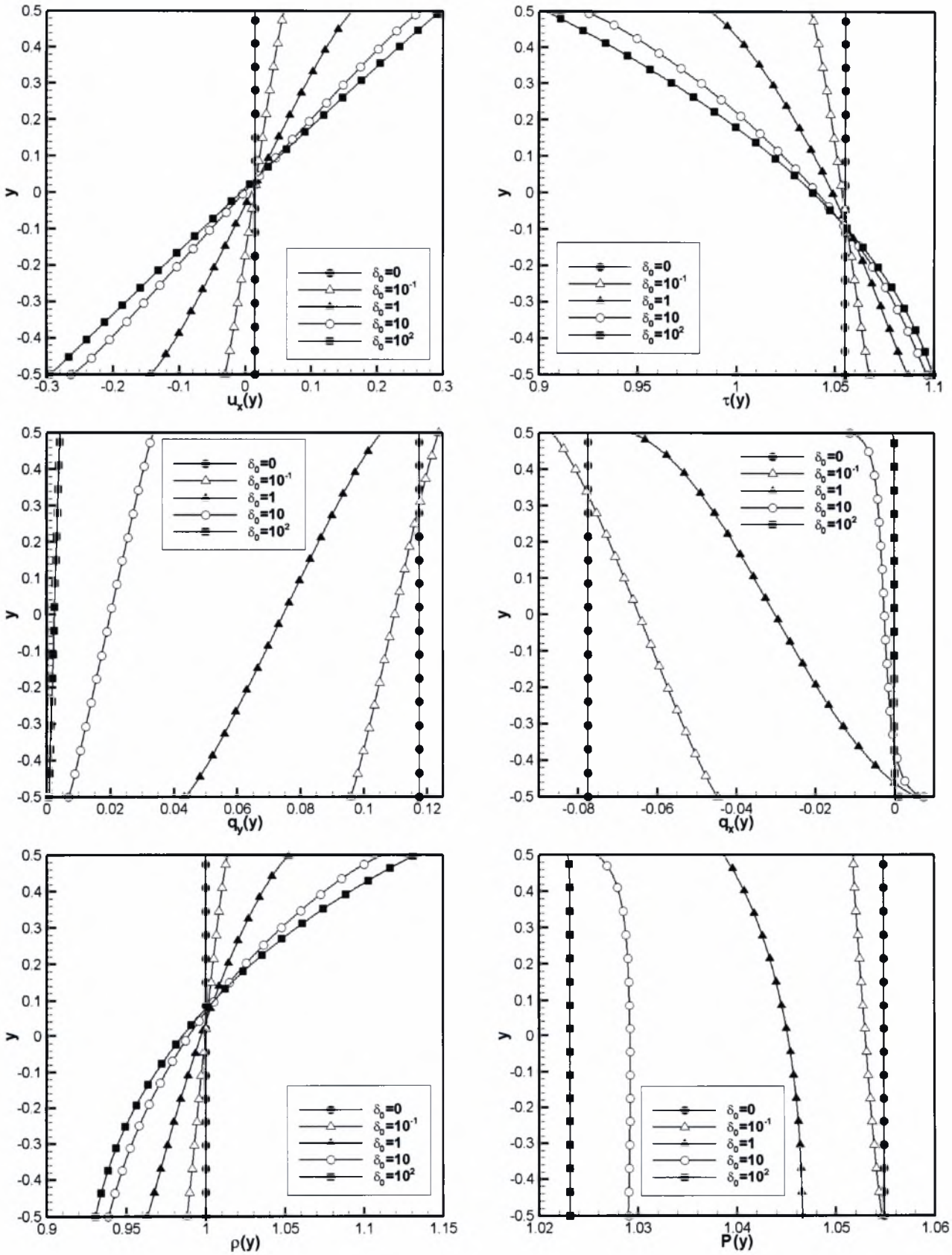

Figure 7.16: *Distributions of macroscopic quantities for* $\beta = 0.1$ *and* $U = 0.3$

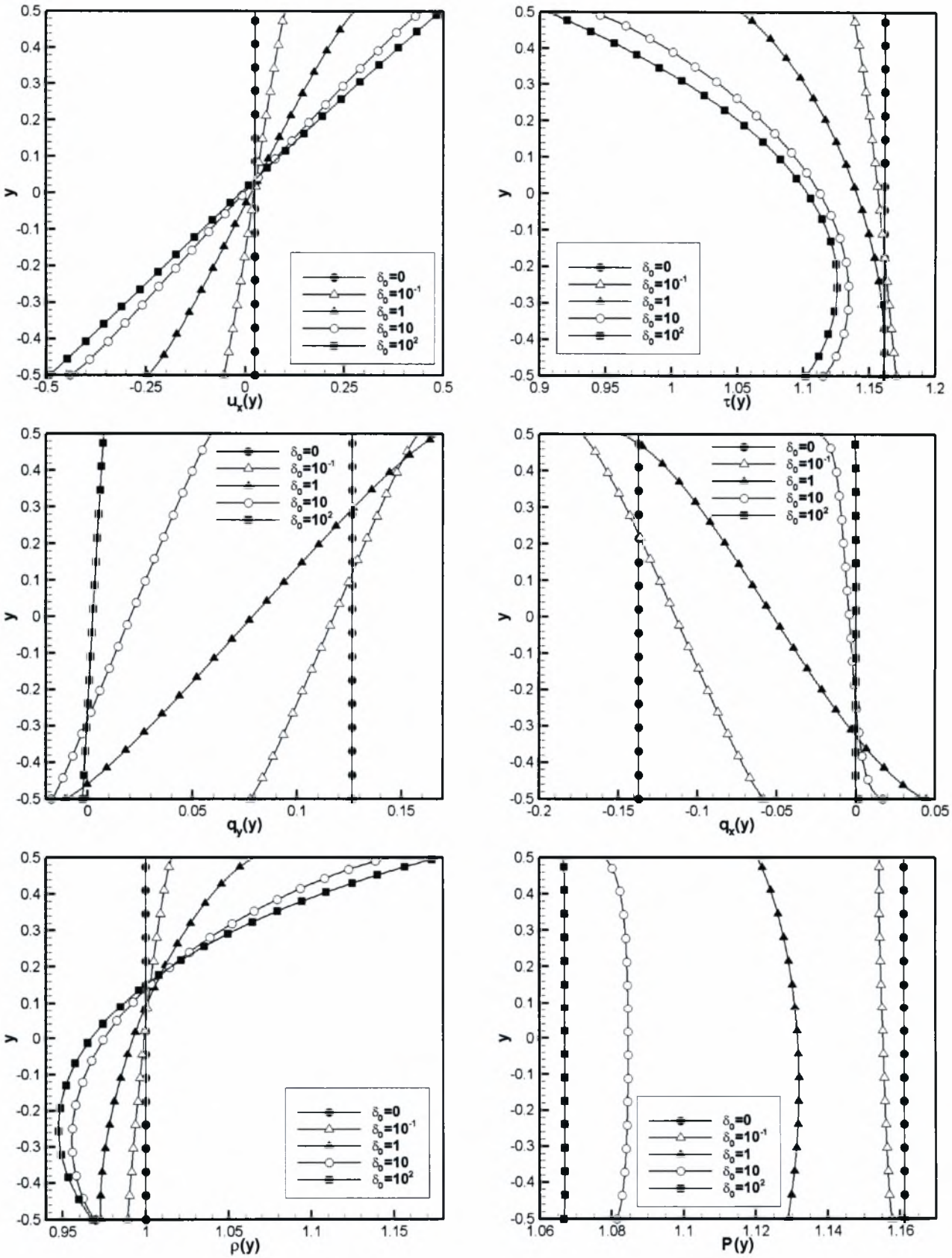

Figure 7.17: *Distributions of macroscopic quantities for* $\beta = 0.1$ *and* $U = 0.5$

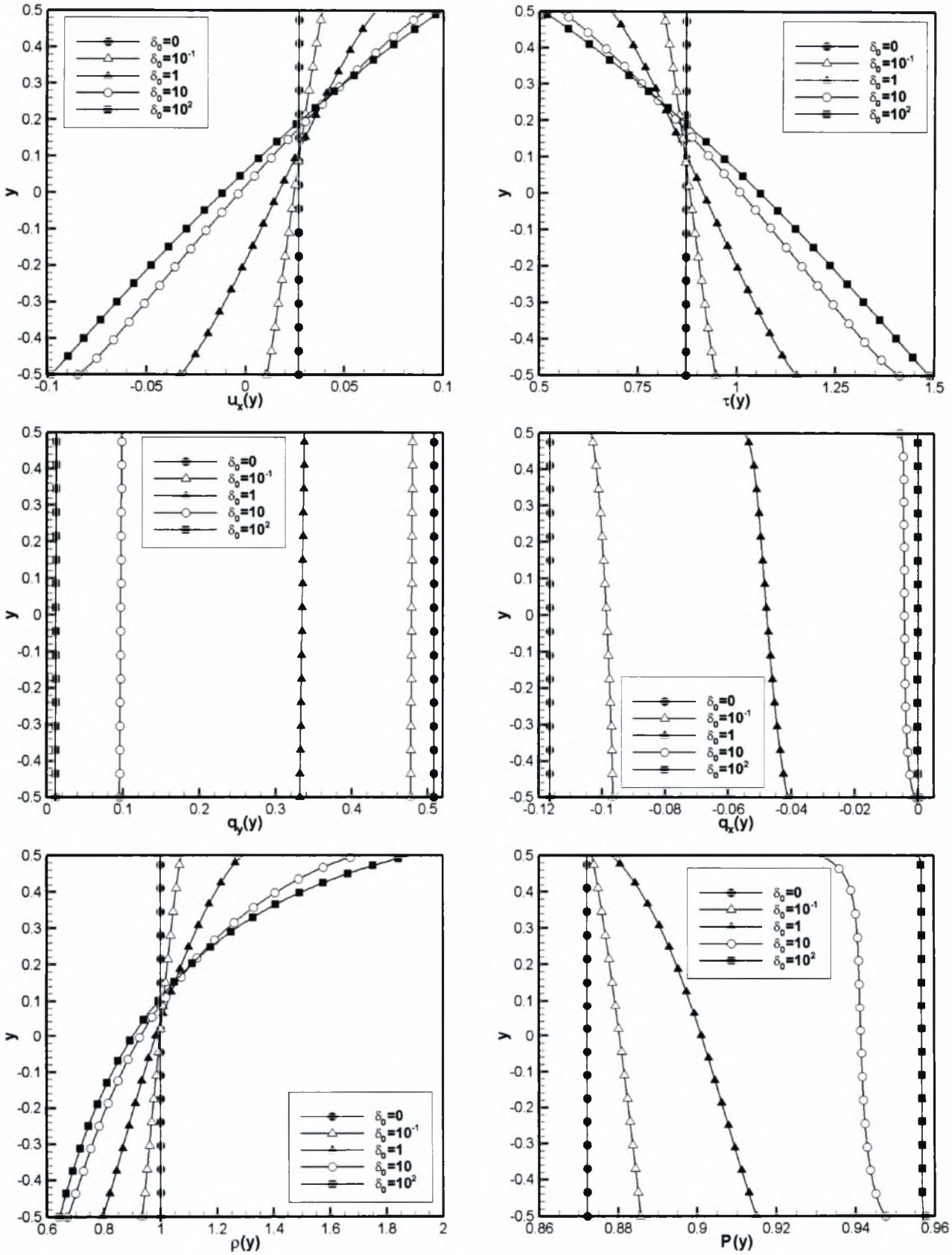

Figure 7.18: *Distributions of macroscopic quantities for* $\beta = 0.5$ *and* $U = 0.1$

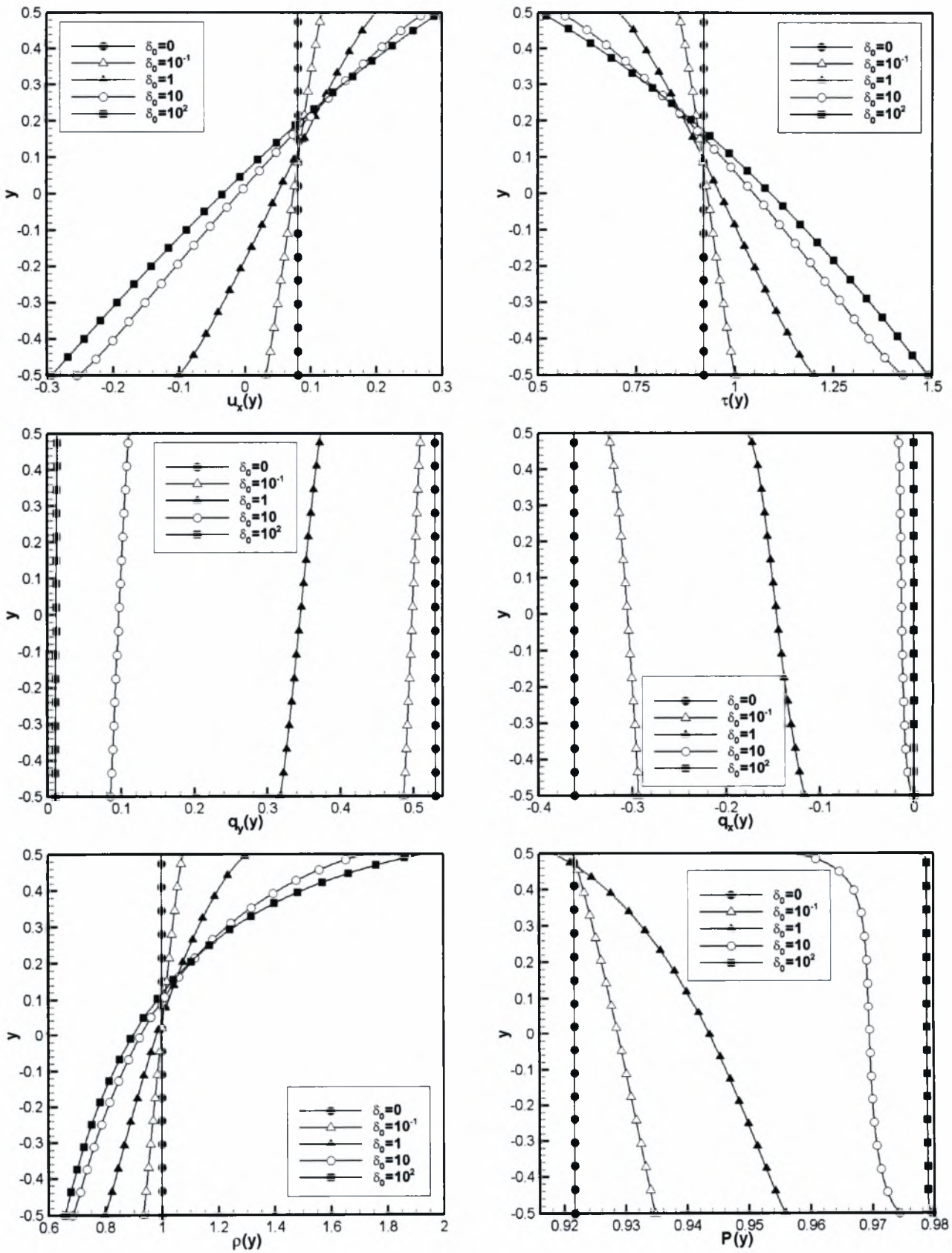

Figure 7.19: *Distributions of macroscopic quantities for* $\beta = 0.5$ *and* $U = 0.3$

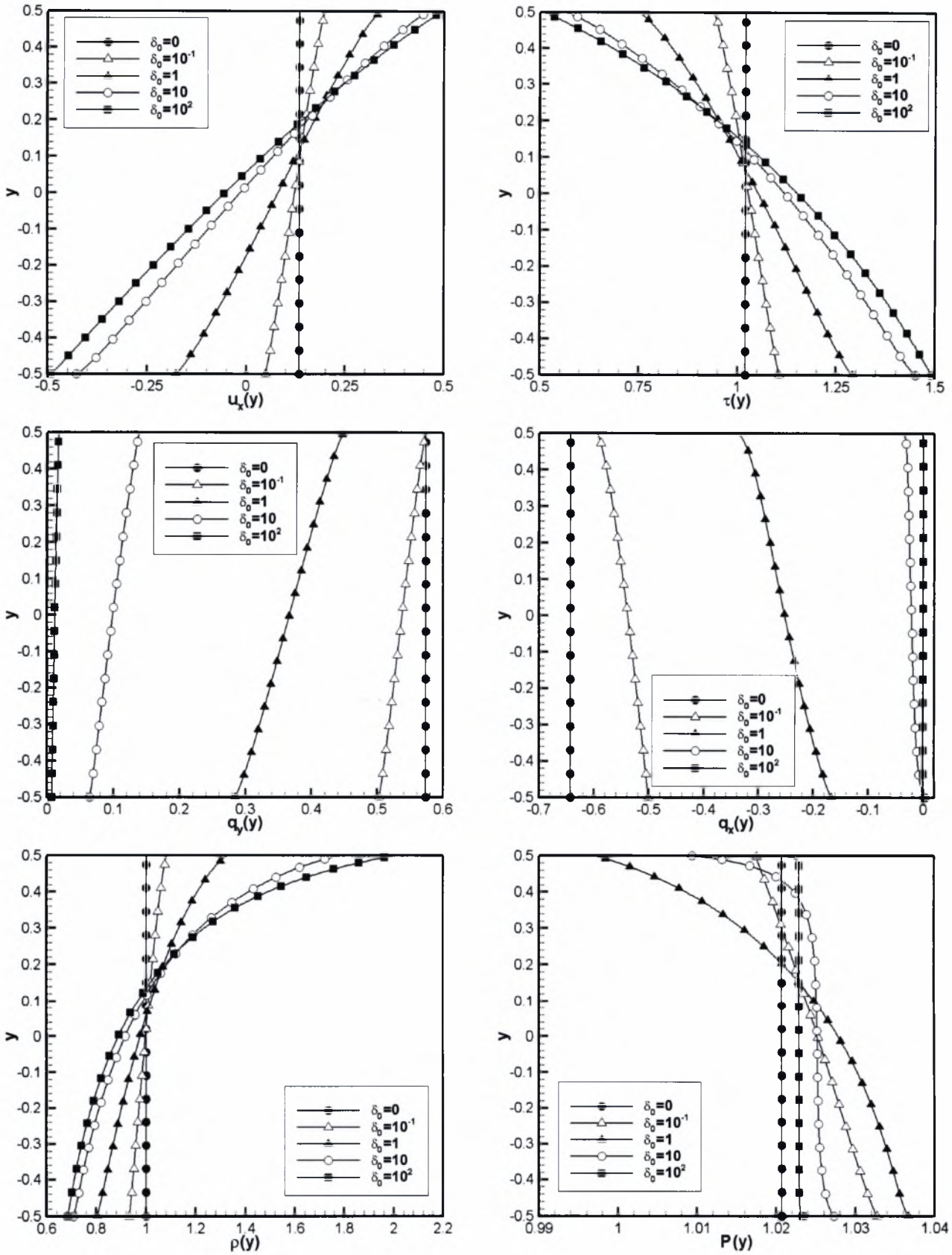

Figure 7.20: *Distributions of macroscopic quantities for* $\beta = 0.5$ *and* $U = 0.5$

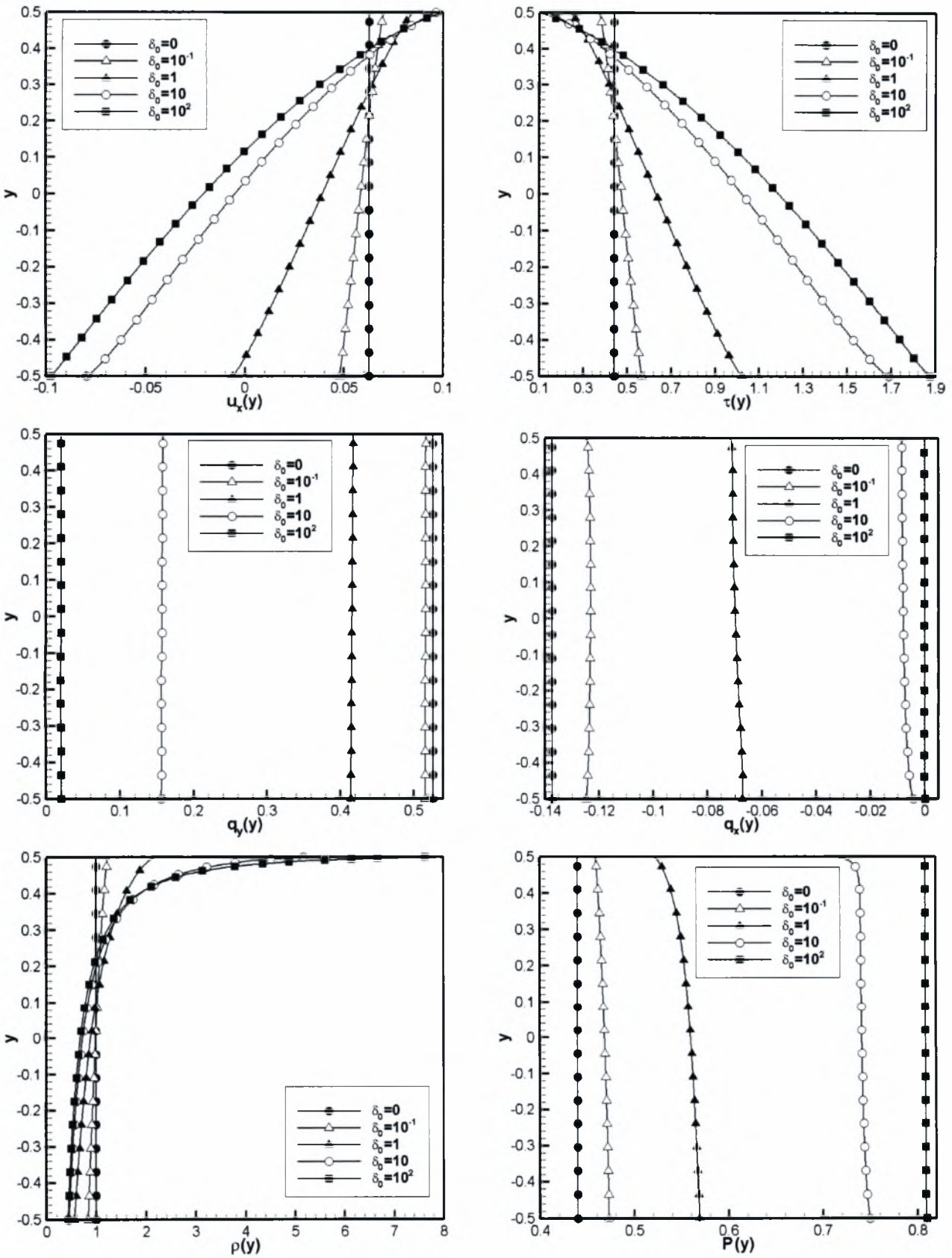

Figure 7.21: *Distributions of macroscopic quantities for* $\beta = 0.9$ *and* $U = 0.1$

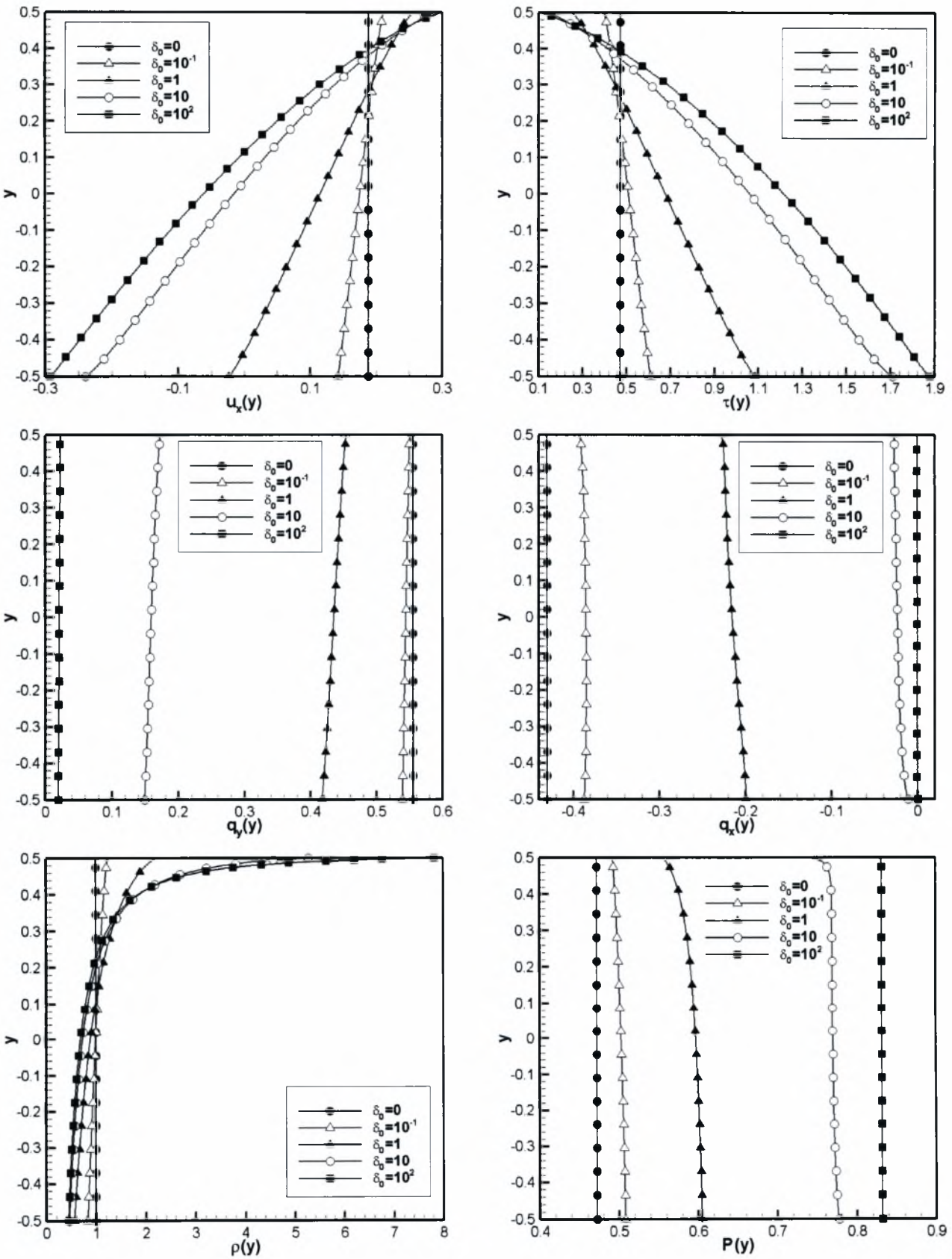

Figure 7.22: *Distributions of macroscopic quantities for* $\beta = 0.9$ *and* $U = 0.3$

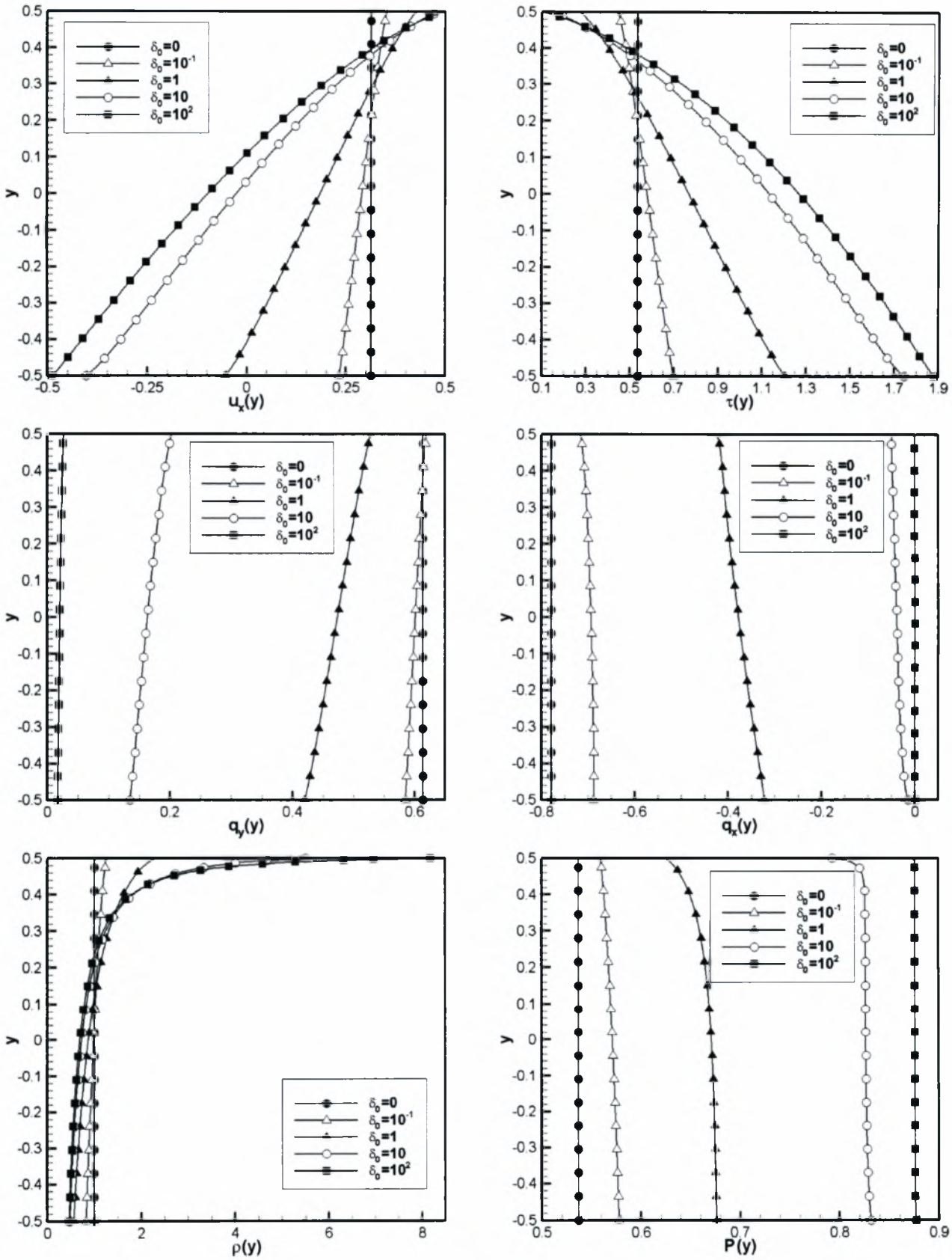

Figure 7.23: *Distributions of macroscopic quantities for* $\beta = 0.9$ *and* $U = 0.5$

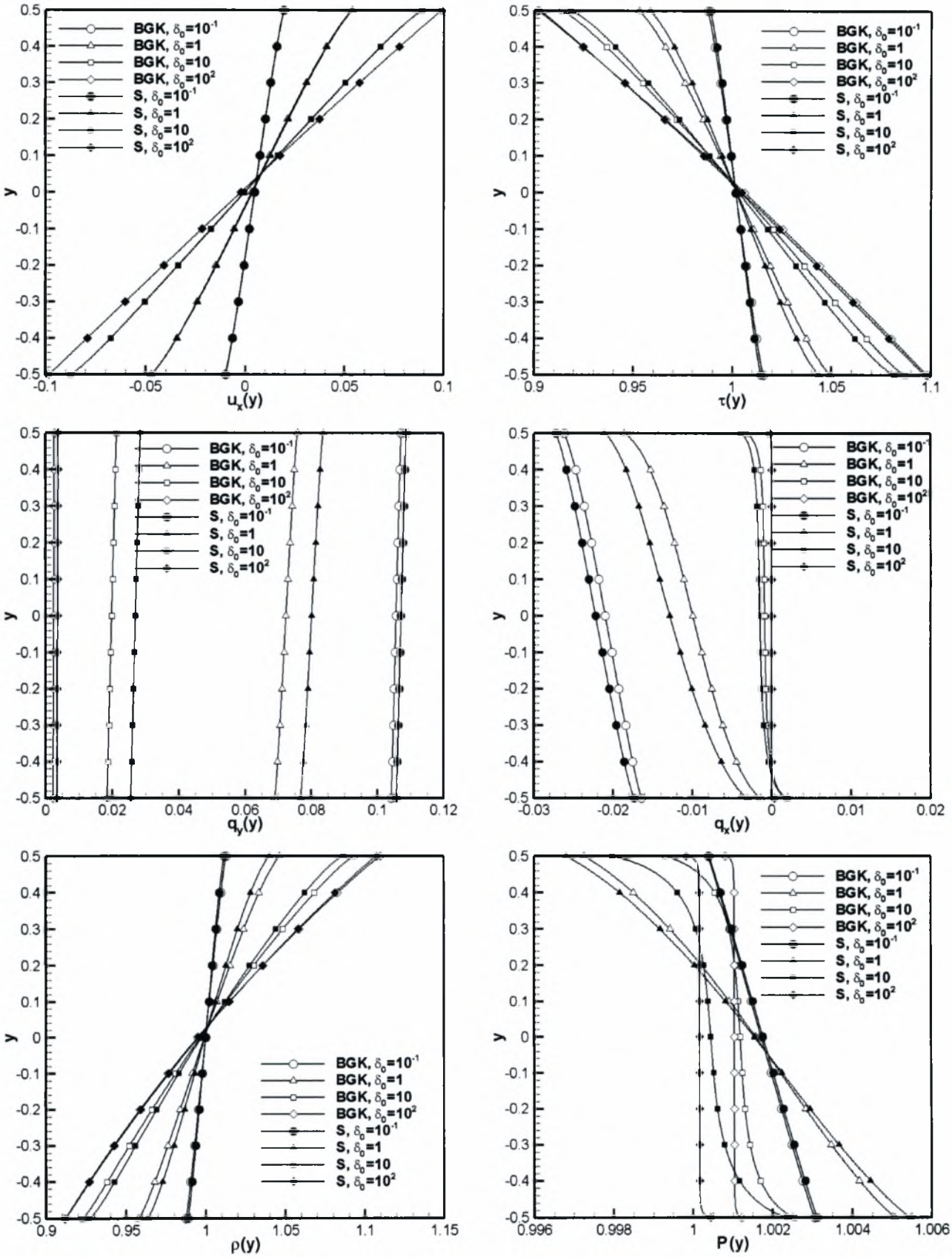

Figure 7.24: *Comparison of macroscopic quantities for $\beta = 0.1$ and $U = 0.1$*

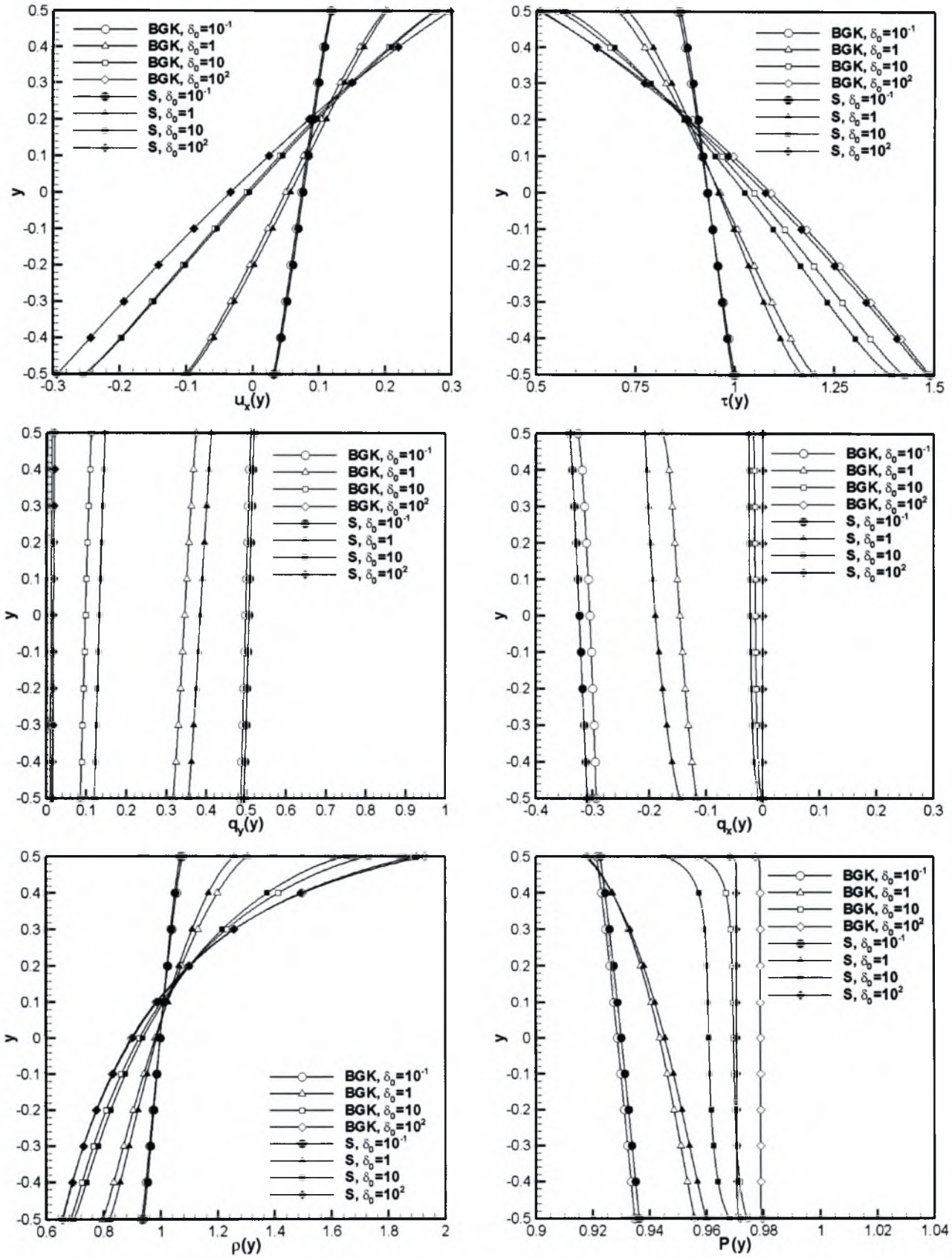

Figure 7.25: *Comparison of macroscopic quantities for $\beta = 0.5$ and $U = 0.3$*

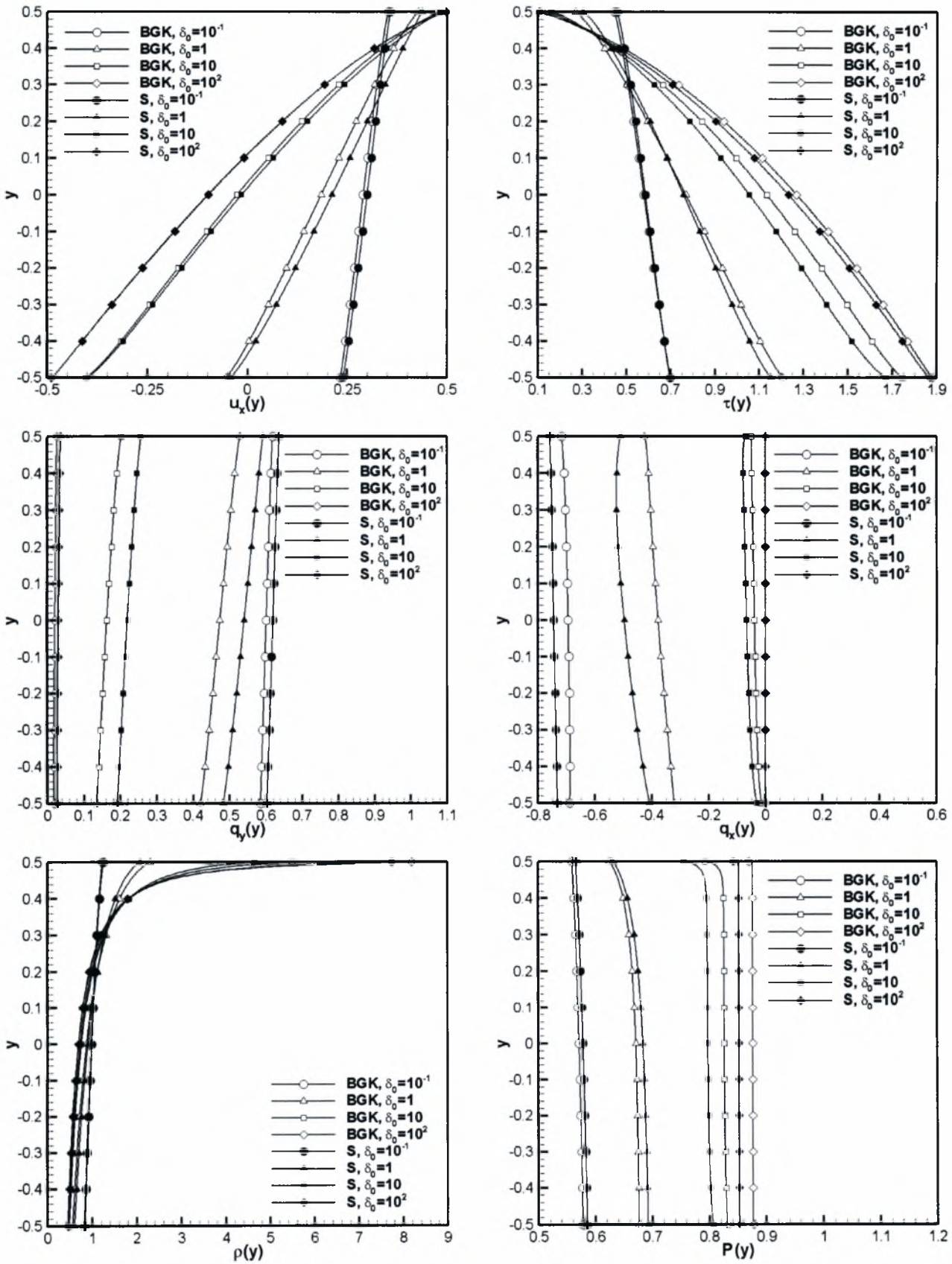

Figure 7.26: *Comparison of macroscopic quantities for* $\beta = 0.9$ *and* $U = 0.5$

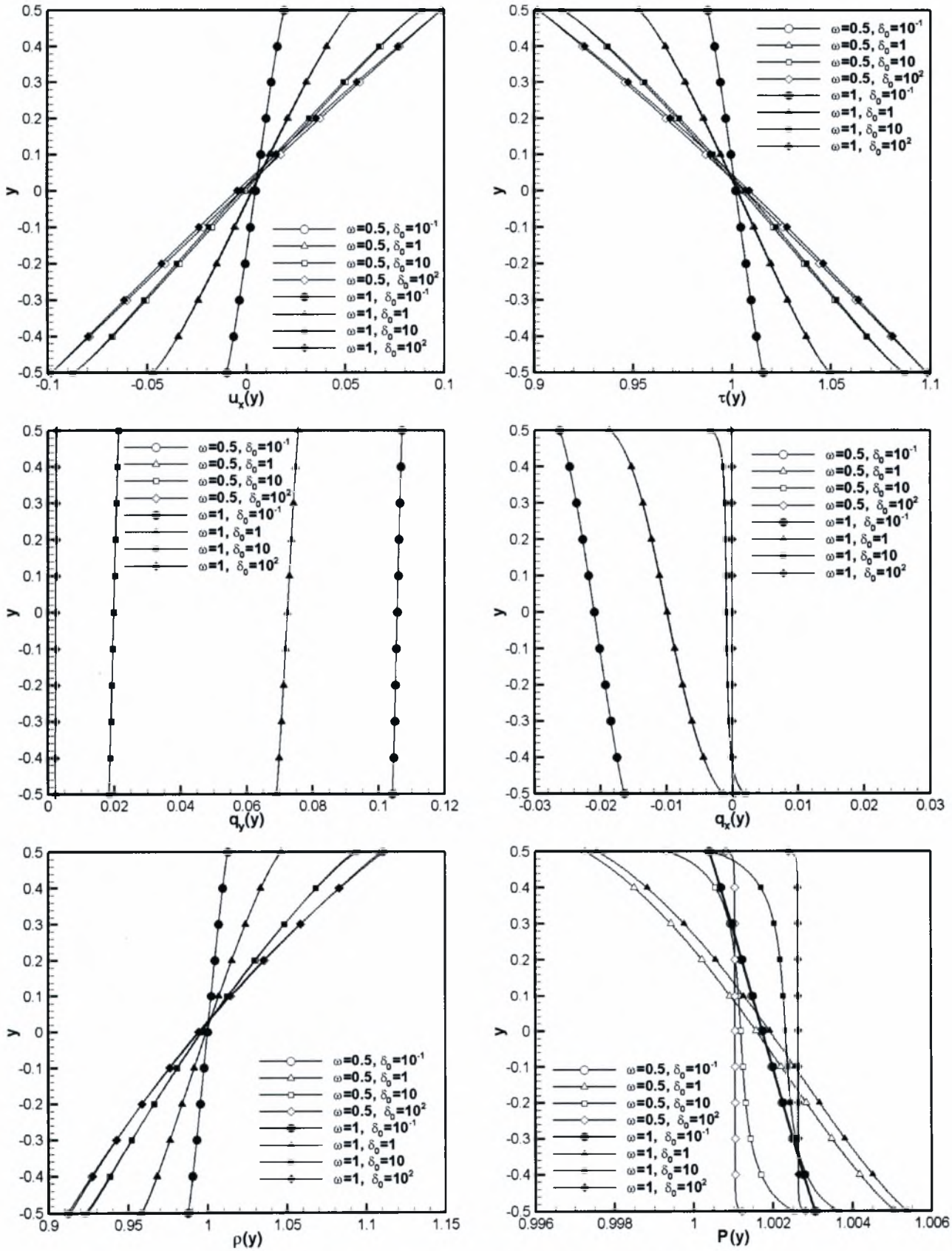

Figure 7.27: *Comparison of macroscopic quantities for* $\beta = 0.1$ *and* $U = 0.1$

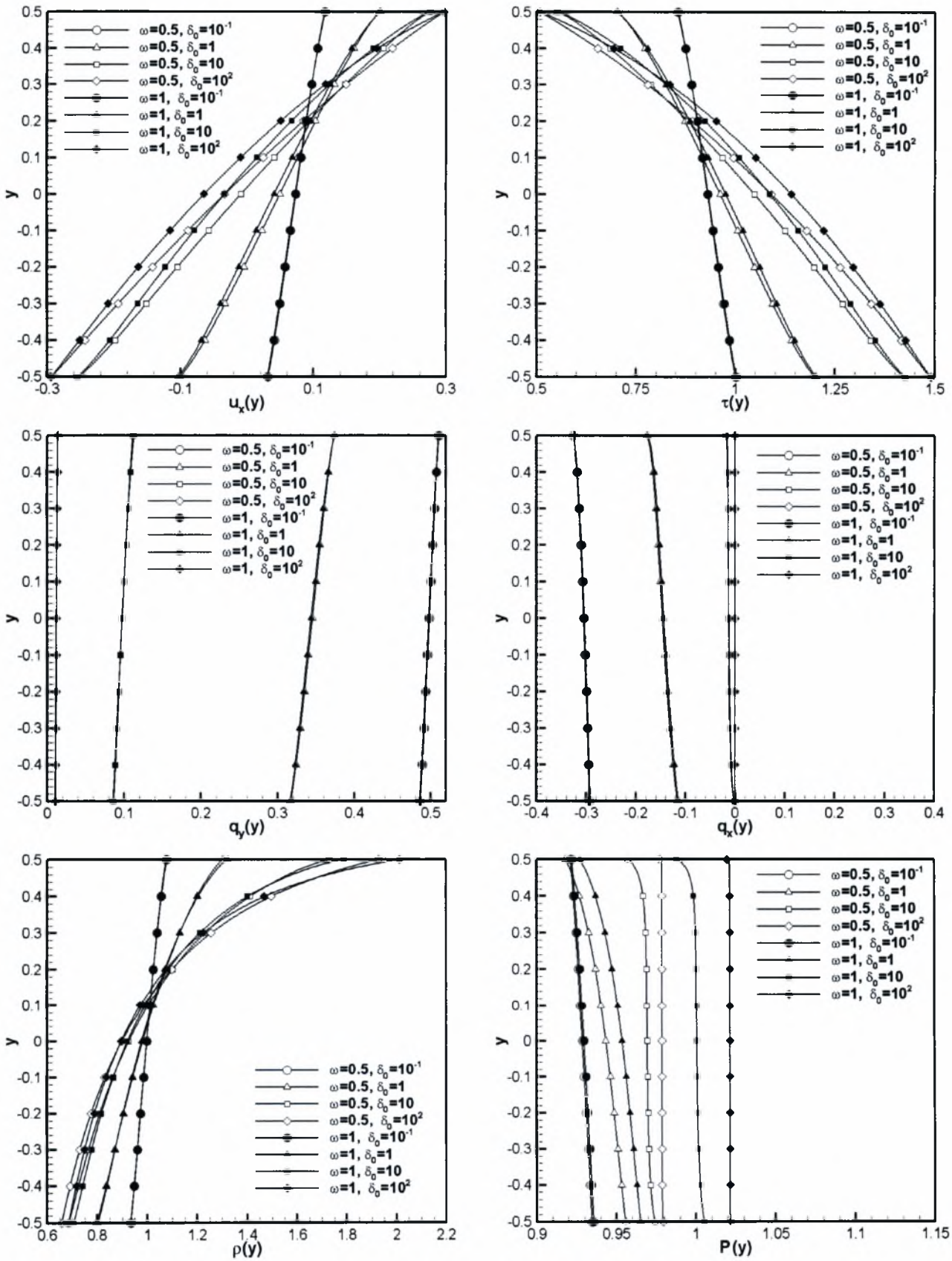

Figure 7.28: *Comparison of macroscopic quantities for* $\beta = 0.5$ *and* $U = 0.3$

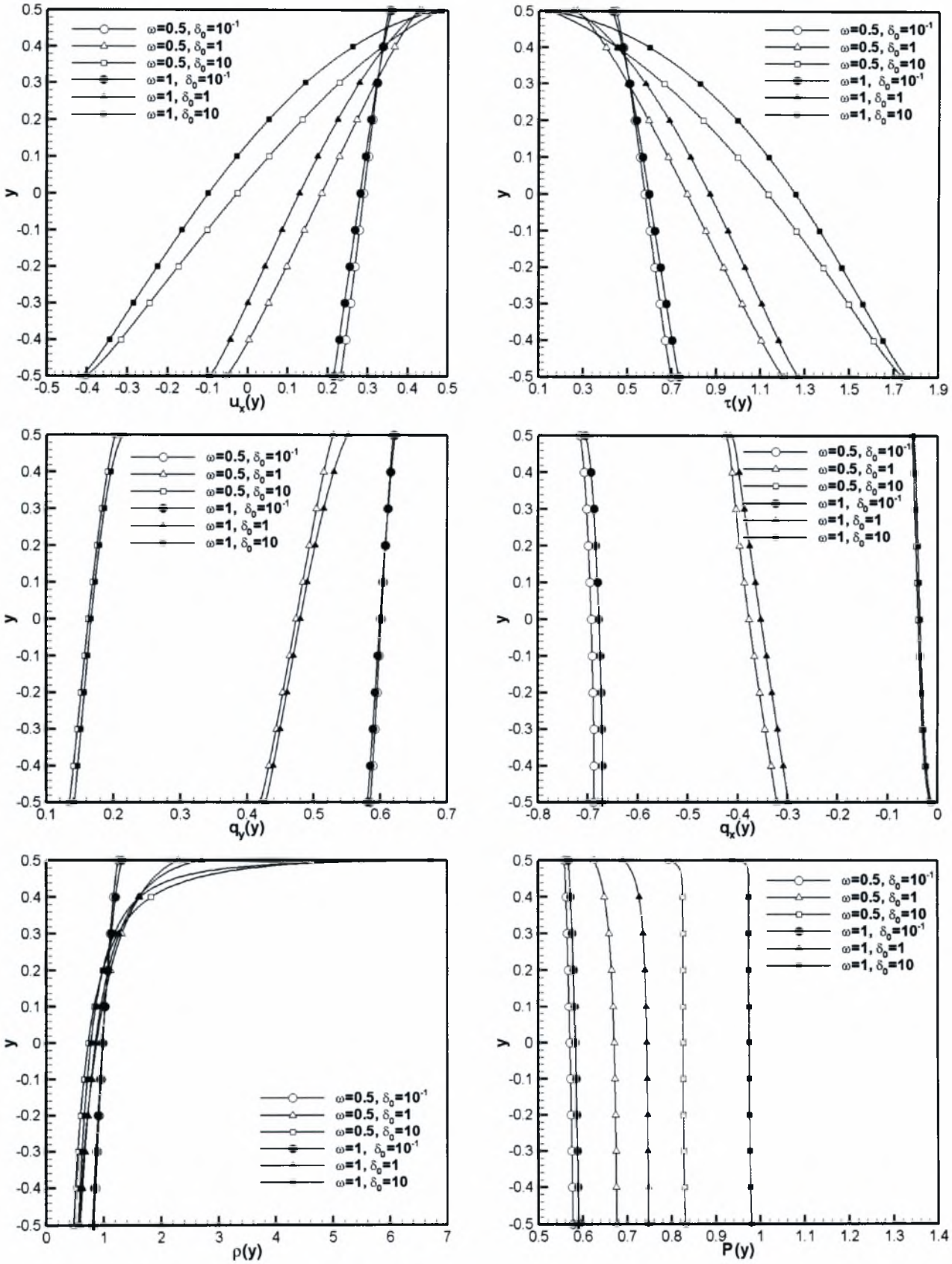

Figure 7.29: *Comparison of macroscopic quantities for* $\beta = 0.9$ *and* $U = 0.5$

8

Concluding Remarks

The scope of the present work is the investigation of the rarefied gas flow between two moving plates maintained at different temperatures. This problem has been attracted a lot of attention over the years. Here we study this problem as a test bed in order to validate the accuracy of our recently developed nonlinear kinetic codes and also due to the fact that still there are some interesting non-equilibrium phenomena which require further investigation.

In order to model the flow, we use both the nonlinear BGK and Shakhov equations coupled to Maxwell diffuse boundary conditions. The numerical solution is based on the discrete velocity method. The results include all macroscopic distributions of practical interest (velocity, temperature, normal and shear stresses, vertical and horizontal heat flux, density and pressure) in the whole range of the Knudsen number in terms of the relative velocity and the temperature ratio of the two plates.

In an attempt to evaluate the accuracy of the implemented algorithms, the analytical solutions at the free molecular limit and the hydrodynamic regime have been compared with the corresponding numerical results. In all cases excellent agreement has been demonstrated. In addition, a detailed comparison between the simple BGK with the more sophisticated Shakhov model clearly indicate that the BGK model remains a reliable choice at least for engineering purposes. If very accurate solutions are required then implementation of the Shakhov model is needed. Also, applying the hard sphere and Maxwell molecular models for intermolecular interaction it is deduced that the intermolecular potential model does not significantly influence the flow properties and characteristics.

Several interesting findings have been presented. It has been found that the velocity slip and the temperature jump are larger at the hot plate compared to the ones at the cold plate. Even more the flow is characterized by the presence of an horizontal

axial heat flux, which increases as the rarefaction of the gas is increased and which is present only when both velocity and temperature gradients exist in the flow. This is a non-equilibrium cross effect and it vanishes at the hydrodynamic limit. Also the pressure distribution is a function of the spatial variable in the transition regime. This is also due to the rarefaction of the flow.

In the future, the implementation of the non linear kinetic equations could be extended to solve problems in more complex geometries in two and three spatial dimensions. The use of the Cercignani - Lampis kernel for the simulation of the gas-wall interaction could also be introduced.

References

1. Bhatnagar, P. L., Gross, E. P. and Krook, M. A., A model for collision processes in gases. *Phys. Rev.*, 94:511–525, 1954.
2. Bird, G. A., *Molecular* Gas Dynamics and the Direct Simulation of Gas Flows. *Oxford University Press*, Oxford, 1994.
3. Boltzmann, L., Lectures on Gas Theory. New York: *Dover Publications*, 1995.
4. Brey, J. J., Santos, A. and Dufty, W. J., Heat and momentum transport far from equilibrium. *Phys. Rev. A*, 36, 6, 2842-2849, 1987.
5. Cercignani, C., Mathematical Methods in Kinetic Theory. *Plenum, New York*, 1969.
6. Cercignani, C., Theory and Application of the Boltzmann Equation. *Scottish Academic Press*, Edinburgh, 1975.
7. Cercignani, C., The Boltzmann equation and its applications. *New York: Springer*, 1988.
8. Chapman, S. and Cowling, T. G., The Mathematical Theory of Non-Uniform Gases. *University Press, Cambrige*, 1952.
9. Ferziger, J. H. and Kaper, H. G., Mathematical Theory of Transport Processes in Gases. *North-Holland, Amsterdam*, 1972.
10. Feynman, R. P., The Feynman Lectures on Physics. *Addison-Wesley*, 1977.
11. Gad-el Hak, M., The MEMS Handbook. *CRCPress*, Florida, USA, 2002.
12. Gallis, M. A., Torczynski, J. R., Rader, D. J., Tij, M. and Santos, A., Normal solutions of the Boltzmann equation for highly nonequilibrium Fourier flow and Couette flow, *Phys. Fluids* 18, 017104, 1-15, 2006.
13. Garzo, V. and Lopez de Haro, M., Kinetic model for heat and momentum transport, *Phys. Fluids*, 6, 11, 3787-3794, 1994
14. Ho, C. M. and Tai, Y. C., Micro-electro-mechanical systems (MEMS) and fluid flows. *Ann. Rev. Fluid. Mech.*, 30:579–612, 1998.
15. Huang A. B. and Hartley D. L., Nonlinear rarefied couette flow with heat transfer. *Phys. Fluids*, 11, 6, 1321-1326, 1968

16. Karniadakis, G.E. and Beskok A., Microflows: Fundamentals and Simulations. *Springer-Verlag*, Berlin, 2000.
17. Kim, S. C., Dufty, W. J., Santos, A. and Brey, J. J., Hilbert-class or "normal" solutions for stationary heat flow. *Phys. Rev. A*, 39, 1, 328-338, 1989.
18. Kim, S. C., Dufty, W. J., Santos, A. and Brey, J. J., Analysis of nonlinear transport in Couette flow. *Phys. Rev. A*, 40, 12, 7165-7174, 1989.
19. Kogan, M. N., Rarefied Gas Dynamics. Plenum, *New York*, 1969.
20. Lewis, E. E. and Miller W. F. Jr., Computational Methods of Neutron Transport Theory, *Wiley, New York*, 1984.
21. Liu, Chung-Yen, Kinetic theory description of plane, compressible Couette flow, *PhD thesis*, California Institute of Technology, Pasadena, California, 1962.
22. Loyalka, S. K., Kinetic theory of thermal transpiration and mechanocaloric effect. I. *J. Chem. Phys.*, 55(9):4497-4503, 1971.
23. Loyalka, S. K., Kinetic theory of thermal transpiration and mechanocaloric effect. II. *J. Chem. Phys.*, 63(9):4054-4960, 1975.
24. Loyalka, S. K. and Storvick, T. S., Kinetic theory of thermal transpiration and mechanocaloric effect. III. Flow of a polyatomic gas between parallel plates. *J. Chem.Phys.*, 71(1):339–350, 1979.
25. Marques, W. Jr., Kremer, G.M. and Sharipov, F., Couette flow with slip and jump boundary conditions, *J. Continuum Mech. Thermodyn.*, 12, 6, 379-386, 2000.
26. Maxwell, J. C., On stress in rarefied gases arising from inequalities of temperature. *Phil Trans. R. Soc. Lond.*, 1879.
27. Naris, S. and Valougeorgis, D., The driven cavity flow over the whole range of the Knudsen number, *Phys. Fluids*, 17, 9, 907106.1-907106.12, 2005.
28. Naris, S. and Valougeorgis, D., Boundary driven non-equilibrium gas flow in a grooved channel via kinetic theory, *Phys. Fluids*, 19, 6, 067103.1-067103.15, 2007.
29. Reese, J. M., Gallis, M. A. and Lockerby D. A., New directions in fluid dynamics: nonequilibrium aerodynamics and Microsystems flows. *Phil. Trans. R. Soc. Lond.* A361, 2967-2988, 2003.
30. Reitebuch, D. and Wolf W., *J. Continuum Mech. Thermodyn.*, 4, 217-225, 1999.
31. Santos, A., Brey, J. J.Kim and S. C., Dufty, Velocity distributions for a gas with steady heat flow. *Phys. Rev. A*, 39, 1, 32-327, 1989.

32. Shakhov, E. M., Method of Investigation of Rarefied Gas Flows. *Nauka, Moscow*, 1974. [in Russian].
33. Sharipov, F. M., Rarefied gas flow through a long tube at any temperature difference. *J. Vac. Sci. Technol. A*, 14(4):2627-2635, 1996.
34. Sharipov, F. M. and Seleznev, V., Data on internal rarefied gas flows. *J. Phys. Chem. Ref. Data*, 27, 657-706, 1998.
35. Sharipov, F. M., Application of the Cercignani-Lampis scattering kernel to calculations of rarefied gas flows. I. Plane flow between two parallel plates. *Eur. J. Mech. B / Fluids*, 21(1):113-123, 2002.
36. Sharipov, F. M., Application of the Cercignani-Lampis scattering kernel to calculations of rarefied gas flows. II. Slip and jump coefficients. *Eur. J. Mech. B / Fluids*, 22:133-143, 2003.
37. Sharipov, F. M. and Kalempa, D., Velocity slip and temperature jump coefficients for gaseous mixtures. I. Viscous slip coefficient. *Phys. Fluids*, 15(6):1800-1806, 2003.
38. Sharipov, F. M. and Kalempa, D., Velocity slip and temperature jump coefficients for gaseous mixtures. II. Thermal slip coefficient. *Phys. Fluids*, 16(3):759-764, 2004.
39. Sharipov, F. M. and Kalempa, D., Velocity slip and temperature jump coefficients for gaseous mixtures. III. Diffusion slip coefficient. *Phys. Fluids*, 16(10):3779-3785, 2004.
40. Srivastava, M. P. and Jagdish, J. R., Non-linear coquette flow with heat transfer using the BGK model, *ZAMP*, 22, 3, 542-551, 1971.
41. Tij, M. and Santos, A., Combined heat and momentum transport in a dilute gas, *Phys. Fluids*, 7, 11, 2858-2866, 1995.
42. Umrath, W., *Fundamentals of Vacuum Technology*, Leybold Press, 1998.
43. Valougeorgis, D., Couette flow of a binary gas mixture. *Phys. Fluids*, 31(3):521-524, 1988.
44. Valougeorgis, D., An analytical solution of the s-model kinetic equtaion. *Z. Angew. Math. Phys. (ZAMP)*, 54:112-124, 2003.
45. Welander, P., On the temperature jump in a rarefied gas. *Ark. Fys.*7, 507, 1954.
46. White, F., Fluid Mechanics. *McGraw-Hill*, 2002.
47. Ziering S., Shear and heat flow for Maxwellian molecules, *Phys. Fluids*, 3,4, 503-509, 1960.

Appendix: Source Codes

In the attached CD-ROM, the source codes used in the present thesis can be found

A.1 Fortran source codes for Rarefied Gas Flow Between Moving Plates With Heat Tranfer, BGK model

- Projection in z direction: Couette flow with heat transfer (BGK,z).f90
- Projection in x and z directions: Couette flow with heat transfer (BGK,x-z).f90

A.2 Fortran source codes for Rarefied Gas Flow Between Moving Plates With Heat Tranfer, Shakhov model

- Projection in z direction: Couette flow with heat transfer (S,z).f90
- Projection in x and z directions: Couette flow with heat transfer (S,x-z).f90